Inhibition of cathepsin B by ferrocenyl indenes highlights a new pharmacological facet of ferrocifens

Juan Sanz Garcia, Marie Gaschard, Isabelle Navizet, Mehdi Sahihi, Siden Top, Yong Wang, Pascal Pigeon, Anne Vessieres, Michèle Salmain, Gerard Jaouen

Inhibition of cathepsin B by ferrocenyl indenes highlights a new pharmacological facet of ferrocifens

Juan Sanz Garcia,[1] Marie Gaschard,[2] Isabelle Navizet,[1] Mehdi Sahihi,[1] Siden Top,[2] Yong Wang,[2,3] Pascal Pigeon,[2,3] Anne Vessières,[2] Michèle Salmain,[2*] and Gérard Jaouen[2,3*]

[1] Univ Gustave Eiffel, CNRS, Univ Paris-Est Créteil, MSME, F-77454 Marne-la-Vallée Cedex 2, France

[2] Sorbonne Université, CNRS, Institut Parisien de Chimie Moléculaire, 4 place Jussieu 75005 Paris, France

[3] PSL Research University, Chimie ParisTech, 11 rue Pierre et Marie Curie, 75005 Paris, France

Abstract

The family of ferrocifens initially built up from the anti-oestrogen tamoxifen shows a broad antitumor activity both *in vitro* and *in vivo*. Their mechanism of action relies on the presence of the redox motif [ferrocene-ene-phenol] that, under oxidative conditions, generates reactive oxygen species (ROS) and affords electrophilic quinone methides (QMs) having the ability to alkylate biological nucleophiles and in turn elicit a strong antiproliferative activity. In this context, the cysteine protease cathepsin B was initially presumed to be a target for ferrocenyl QMs. *In vitro* enzymatic assays ruled out this hypothesis but unexpectedly revealed that other ferrocifen metabolites, i.e. ferrocenyl indenes, acted as moderate inhibitors of cathepsin B. These experimental results were nicely confirmed by molecular docking calculations, that showed that the monophenol ferrocenyl indene and to a lower extent the diphenol interacted with the active site of cathepsin B, making it an unanticipated target of ferrocifens.

Keywords

antitumor agent; bioorganometallic chemistry; computational chemistry; cysteine protease; docking; ferrocene; inhibitors.

Introduction

The potential use of metallocenes in oncology was first introduced by Köpf-Maier[1] with simple complexes of Ti[2] and Fe[3,4]. Unfortunately, the titanocenes proved to be too unstable to provide a biologically useful formulation. In the ferrocene series, only the ferriceniums possess some cytotoxicity but they show low biological activity and, in any case are not stable in aqueous media. A novel strategy based on multifunctional hybrids of ferrocene was then considered. This approach has recently been the subject of a large number of reviews[5-16] and the results have proved to be, to say the least, mixed. Nonetheless the redox motif [ferrocenyl-ene-phenol] remains the most biologically promising candidate to date, since compounds presenting this motif show remarkable antitumor properties both *in vitro* and *in vivo*.[17] For example, complexes **P5**, **P15**, **P85** and **P722** (Scheme 1) exhibit IC_{50} values in the range 0.035 - 1.5 µM on the triple negative breast cancer cell line MDA-MB-231.[17]

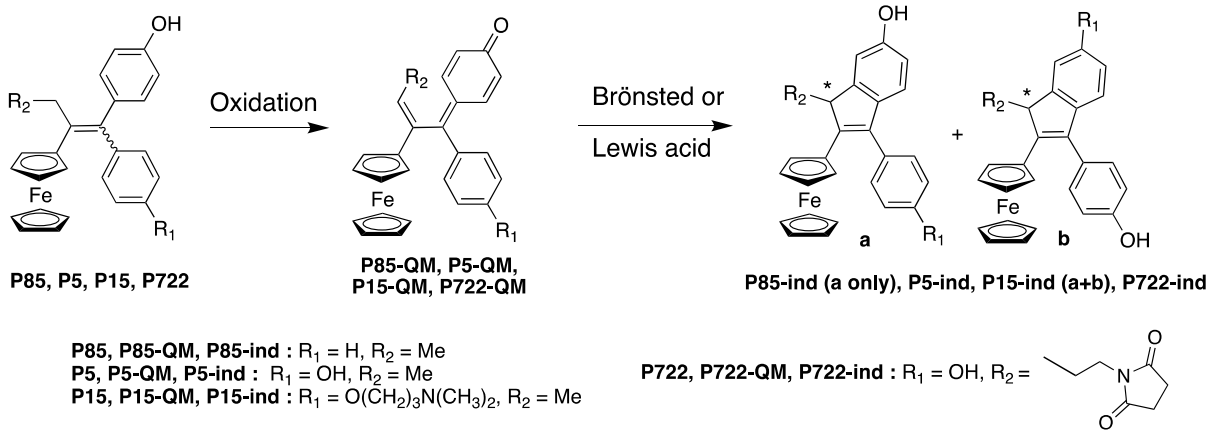

Scheme 1. Sequence of reactions leading to ferrocenyl indenes

Under mild oxidative conditions, this motif evolves to ferrocenyl quinone methide (QM, Scheme 1) via transient oxidation of the ferrocene. These QMs are remarkably electrophilic, allowing the reaction of biologically relevant nucleophiles such as thiolates to take place mainly by 1,8-Michael addition.[18] Quinone methide products generated by chemical or enzymatic oxidation of **P15**, **P5** and **P85** proved to be responsible for inhibition of thioredoxin reductase (TrxR) *in vitro*, one of the enzymes involved in the cellular redox homeostasis. Further investigation showed that inhibition was irreversible and took place by alkylation of the thiol / selenol group in the enzyme's active site.[19,20] Conversely, only **P15-QM** and its precursor **P15** itself were able to inhibit TrxR *in cellulo* while neither **P85** nor its QM did.[19] This discrepancy was explained by the instability of **P85-QM** that readily converts into a cyclic product (indene) in protic medium (Scheme 1) that is devoid of reactivity for thiols. **P85-ind** was indeed shown to be the main metabolite resulting from oxidation of **P85** by liver microsomes.[21]

Cathepsin B (cat.B) is an ubiquitous proteolytic enzyme belonging to the CA clan of cysteine proteases. This enzyme is mostly localized in the lysosomes and is involved in proteins turnover at the cellular level. Interestingly, this enzyme has also been proved to participate in tumor progression by degrading extracellular matrix proteins and is therefore considered as a relevant target for cancer treatment.[22–24] Cat.B shares a common feature with TrxR, that is the presence of a highly nucleophilic thiol in its active site.[25] Unsurprisingly, most of the known organic inhibitors of cat.B are irreversible, acting as alkylating agents.[25] Various metallodrugs are also known to target cysteine proteases[26] including cat.B[27]. For example inorganic gold(I)[28,29] and organometallic gold(III)[30] complexes are good to excellent cat.B inhibitors owing to the aurophilicity of sulfur. Inhibition by the gold(I) complexes is considered as reversible because addition of excess cysteine allows recovery of cat.B activity. Some half-sandwich organometallic complexes of Ru(II)[31–35] and some Pd complexes[36,37] also act as reversible inhibitors of cat.B and two of the ruthenium complexes were effective in impairing tumor invasion as a consequence of cat.B inhibition.

Due to the well-established reactivity of ferrocenyl quinone methides with thiols and their ability to readily convert to indenes,[19] we thought relevant to investigate the possible interaction of these compounds with cat.B in the aim of finding a new target explaining the anti-proliferative activity of the ferrocifen precursors.

Results

Inhibition of cathepsin B by ferrocifen derivatives

P85-QM (Scheme 1) was first chosen to assay its ability to inhibit cat.B since it is reasonably stable and easy to manipulate conversely to **P5-QM**.[17] **P85-QM** was obtained by chemical oxidation of **P85** according to a previously published protocol.[21] In the classical assay conditions used for measuring the catalytic activity of cat.B, no inhibition of the enzyme was induced by **P85-QM** up to 100 µM.

In the presence of Bronsted or Lewis acids, ferrocenyl quinone methides, specially **P85-QM**, are readily converted into indene derivatives.[21] Therefore, we also investigated the ability of **P85-ind** to interfere with the catalytic activity of cat.B. **P85-ind** was synthesized from **P85-QM** by treatment with $ZnCl_2$ (Scheme 1). To our surprise, the esterolytic activity of cat.B on the chromogenic substrate Z-Lys-ONp, measured by monitoring the formation of *p*-nitrophenol at 326 nm**,** was inhibited by **P85-ind** in a concentration-dependent fashion with an IC_{50} of 19 µM (Table 1). Thus, we next investigated whether **P5-ind, P15-ind** or **P722-ind**

shared the same property. Only **P5-ind** was able to inhibit cat.B with an IC_{50} of 38 µM whereas **P15-ind** and **P722-ind** were completely inactive. Let us also notice that **P5**, **P15** or **P85** were also fully inactive with respect to cat.B activity.

Table 1. Cathepsin B inhibition results and docking calculations.

Compound		IC_{50} (µM)		Docking cluster distribution[2]
		substrate = Z-Lys-ONp	substrate = Z-Arg-Arg-AMC[1]	
P85-ind	(*R*)-P85-ind	19.2 ± 1.3 [6]	52.9 ± 0.3 [6]	++[3]
	(*S*)-P85-ind			++[3]
P5-ind	(*R*)-P5-ind	38 ± 12 [6]	86.1 ± 0.3 [6]	+[3]
	(*S*)-P5-ind			+[3]
P15-ind	(*R*)-P15-ind	No inhibition	nd[5]	- [4]
	(*S*)-P15-ind	No inhibition	nd	- [4]
P722-ind	(*R*)-P722-ind	No inhibition	nd	- [4]
	(*S*)-P722-ind	No inhibition	nd	- [4]

[1] at pH 5; [2]++: well clustered distribution, +: intermediate, -:dispersed; [3] in main binding site of cat.B; [4] not inside the main binding site; [5] not determined; [6] inhibition curves can be found in the SI (figures S38 and S39)

These experiments were repeated with the more selective fluorogenic substrate Z-Arg-Arg-AMC classically used for measuring cat.B endoproteolytic activity by monitoring the formation of 7-amino-4-methylcoumarin by fluorimetry.[38] Using phosphate buffer pH 6 for the assay, no inhibition was noticed for any of the tested compounds. However, when the pH was decreased to 5, **P85-ind** was shown to inhibit cat.B, albeit with a lower efficacy since the IC_{50} equalled 53 µM. In the same experimental conditions, only **P5-ind** inhibited cat.B with a modest IC_{50} of 86 µM, whereas **P5** and **P85** were again inactive up to 100 µM. The unexpected behaviour of **P5-ind** and **P85-ind** towards cat.B prompted us to perform a series of docking calculations as follows.

Docking calculations

In order to better understand the analysis of the docking results few points need to be clarified:

1) Docking calculations using a genetic algorithm and random seeds (random starting points) are heuristic and stochastic calculations meaning that at each independent run we may obtain different results. Hence, a large number of calculations need to be performed so

that a representative population of docked conformations can be obtained, and thus, a distribution analysis can be performed.

2) The distribution obtained can be interpreted as a probability of finding a specific conformation as proposed by the developers of AutoDock.[39]
3) As highlighted in ref.[39], tight binding ligands afford well clustered distributions (not dispersed). On the other hand, ligands affording dispersed distributions can be interpreted as non specific binding ligands (see Analysis of the Docking Results Section in the Supporting Information for a detailed description of clustered and dispersed distributions).

For all these reasons and rather than using the "raw" computed binding energies, we focused our attention in the quality of the clustered distribution to discuss the docking results. In order to rationalize how **P85-ind** acts as an inhibitor and where the active site of cat.B is located, a series of blind docking experiments were performed, meaning that no *a priori* information was used to determine the active site of cat.B, the whole enzyme being considered for the docking calculations. It is worth noting that the docked conformation of **P85-ind** was found close to residues His199 and Cys29 (Figure 1) where the active site of the enzyme is known to be located.

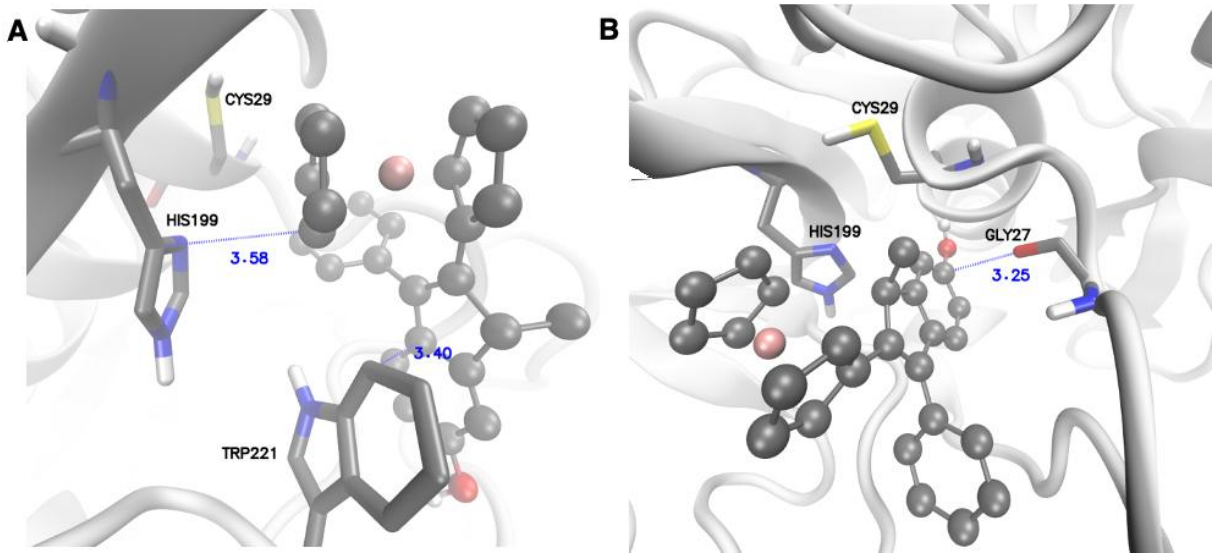

Figure 1. Docked conformations of (**A**) **(*R*)-P85-ind** and (**B**) **(*S*)-P85-ind** in cat.B (the "non-polar" hydrogen atoms are not represented). Relevant residues in the binding site are represented in Licorice while the ligand is represented in CPK.

At this point, it is important to highlight that the inhibition experiments were carried out with racemic complexes (Figure 2). *A priori*, we are not able to determine if only one, or both enantiomers, are responsible for the impairment of the enzymatic activity of cat B. On the one hand, the docked conformation of **(*R*)-P85-ind** exhibits an aromatic interaction

between one of the cyclopentadienyl moieties of the ferrocene and His199 (Figure 1). Aromatic interactions with His199 have already been identified as key factors in the inhibition of cat.B by ferrocene-based compounds.[40] Another important interaction can be found between the indene moiety and Trp221. **(*R*)-P85-ind** also shows hydrophobic interactions with Trp221, Gln23, Ser25, Cys26, Gly27, Cys29, Cys71, Asn72 and Leu181 (Table 2 and Figure S22).

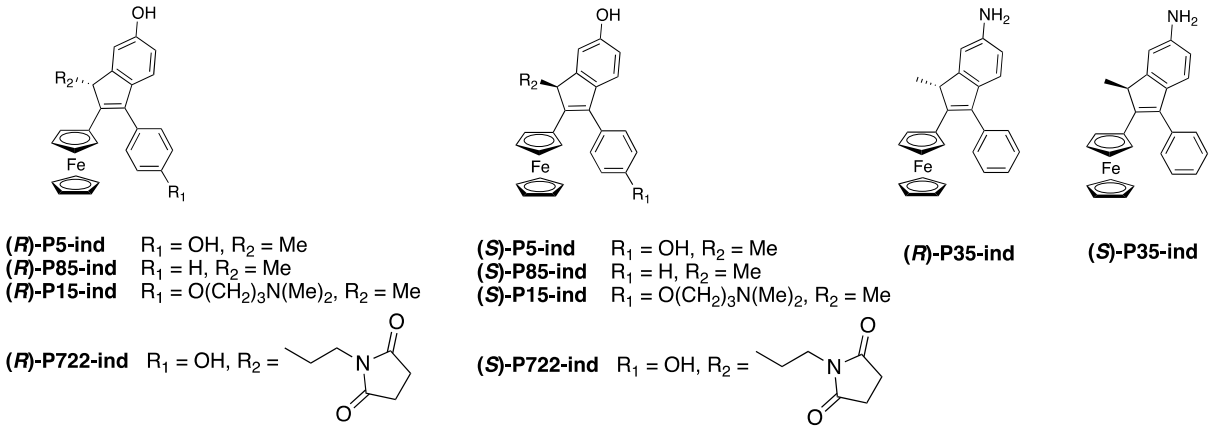

Figure 2. Enantiomers of the different indenes used in this study

It also exhibits one H-bond with Asn222. On the other hand, **(*S*)-P85-ind** displays a lone pair-π (lp-π) interaction between Gly27 residue and the indene moiety (Figure 1). It also shows hydrophobic interactions with Gln23, Gly24, Ser25, Gly27, Phe32, Asn72, His199, Ser220 and Trp221 (Table 2 and Figure S24). **(*S*)-P85-ind** also shows two H-bonds with Cys29 and Gly33.

Table 2. Interactions between active ligands and cathepsin B.

Compound	**Interactions**			
	Hydrophobic Interactions	**H-Bonds**	**π-π stacking**	**Lp-π**
(*R*)-P85-ind	Gln23 Ser25 Cys26 Gly27 Cys29 Cys71 Asn72 Leu181 Trp221	Asn222	Ferrocene-His199 Indene-Trp221	-
(*S*)-P85-ind	Gln23 Gly24 Ser25 Gly27 Phe32 Asn72 His199 Ser220 Trp221	Cys29 Gly33	-	Gly27
(*R*)-P5-ind	Gly24 Ser25 Cys108 Trp221 Asn222	Asp22 Gln23 Leu181	Indene-Trp221	-
(*S*)-P5-ind	Gln23 Ser25 Gly27 Phe32 Asn72 His199 Trp221 Ser220	Gly24 Cys29 Gly33	-	Gly27

Further docking experiments were performed with the two enantiomers of **P5-ind** giving the following results. First, **(*R*)-P5-ind** is also docked in the main binding site of cat.B and exhibits an aromatic interaction between the indene moiety and Trp221 (Figure S15) as for **(*R*)-P85-ind**. In addition, **(*R*)-P5-ind** displays three H-bonds with Asp22, Gln23 and Leu181 which help stabilizing the docked conformation (Table 2). Although the indene and ferrocene moieties of **(*R*)-P5-ind** are "staggered" with respect to the **(*R*)-P85-ind** conformation in the main binding site, both inhibitors have the ferrocene pointing towards His199 and Cys29 and the indene moiety pointing towards the outer edge of the cavity (Figure 3). **(*R*)-P5-ind** also shows hydrophobic interactions with Gly24, Ser25, Cys108, Trp221 and Asn222 (Table 2 and Figure S14). Second, the **(*S*)-P5-ind** docked conformation has the ferrocene and indene moieties oriented towards His199 and Cys29 like **(*S*)-P85-ind**. Indeed, both structures are notably similar, showing a common lp-π interaction between the indene moiety and Gly27 (Figure S17). As for **(*S*)-P85-ind, (*S*)-P5-ind** shows hydrophobic interactions with Gln23, Ser25, Gly27, Phe32, Asn72, His199, Ser220 and Trp221 and three H-bonds with Cys29, Gly24 and Gly33 (Table 2 and Figure S16). However, **(*S*)-P5-ind** forms H-bond with Gly24 via its phenol and whereas **(*S*)-P85-ind** has hydrophobic interaction with this residue.

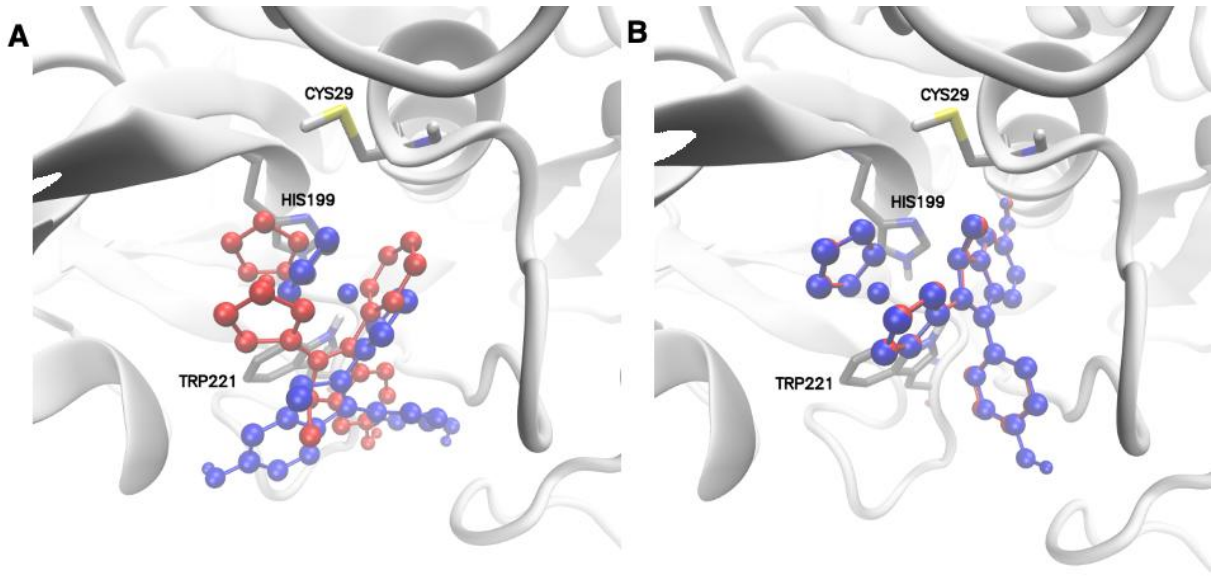

Figure 3. Docked conformations of (**A**) **(*R*)-P5-ind** (in blue) *vs.* **(*R*)-P85-ind** (in red) and (**B**) **(*S*)-P5-ind** (in blue) *vs.* **(*S*)-P85-ind** (in red) inside the cathepsin B main binding site (the "non-polar" hydrogen atoms are not represented). His199, Cys29 and Trp221 are also depicted.

Third, **P722-ind** and **P15-ind** do not reduce the *in vitro* activity of cat.B (Table 1). This experimental result can be easily explained taking a closer look into the docking results. The docked conformation of both **(*R*)-P722-ind** and **(*R*)-P15-ind** (and their enantiomers) are not found inside the main binding site (the active site) of cat.B (Table 1**,** Figures S3-S4 and S7-S8). In addition, the cluster distribution of both enantiomers is dispersed, so that the ligands do not display any specific binding conformation.

Discussion

Cathepsin B is recognized to participate in the development of tumours and its level of activity is high in many types of cancers. As such, it appears as a potentially attractive target to develop anticancer drugs based on its inhibition. In addition to peptide-based inhibitors generally carrying an electrophilic warhead for irreversible inhibition, a number of other non peptidic, reversible inhibitors of cat.B have also been reported.[41–45] While investigating the ability of electrophilic ferrocenyl quinone methides to inhibit cat.B, we serendipitously found out that the indenes derived from **P5** (diphenol) and **P85** (monophenol) resulting from acid-catalysed cyclization of the quinone methide showed moderate IC_{50} (in the micromolar range) as determined by enzymatic assays with two different substrates. In both assay conditions, the monophenol derivative was more active than the diphenol and the inhibition activity was highly pH-dependent. Moreover, compounds having bulky substituents on the aryl group at position 3 or at position 1 of the indene scaffold were inactive. The docking calculations performed with the four different indenes supported the experimental data.

Docking calculations performed on the two enantiomers of **P85-ind** and **P5-ind** localized the molecules in the active site of cat.B, more precisely at the vicinity of Cys29 and His199 that are both involved in peptide bond cleavage by a mechanism typical of cysteine proteases belonging to the papain superfamily (Scheme S1).[46] Such a configuration has previously been reported for ferrocene-tethered ionic liquids.[40] Following the Schechter and Berger nomenclature, the binding site of cat.B contains six subsites (S1 to S3 and S1' to S3'). In contrast to other cysteine proteinases, cat.B displays an unusual peptide segment (Ile105 – Thr 125) called the occluding loop that is flexible and governs the exoproteolytic (peptidyl dipeptidase) and endoproteolytic activities depending on its conformation. In the closed conformation (maintained by salt bridges between Asp22 and His110 and Arg116 and Asp224), the S2' subsite is partially obscured, preventing large substrates to bind and the enzyme to exert its endoproteolytic activity.[47] X-ray structures of bovine cat.B with different

epoxide inhibitors provides a good picture of the active site in the closed form and the individual subsites.[48] The S1' subsite consists of a hydrophobic pocket formed by Val176, Leu181, Met196, His199 and Trp221 while the S1 subsite comprises Gln23, Gly27, Cys29, Gly74 and Gly198. According to these data and the docking calculations, **(*R*)-P85-ind** occupies a space formed by the upper parts of S1' and S1 subsites. **(*S*)-P85-ind** and **(*S*)-P5-ind** occupy the same space with a different relative orientation in the binding pocket, the OH substituent carried by the indene pointing toward the core of the protein. These common orientations may play an important role in the inhibition of cat.B. Interestingly, the two pairs of enantiomers also roughly occupy the same position as nitroxoline in the active site of cat.B.[49] IC_{50}s in the micromolar range are consistent with the occupancy of a single subsite by the inhibitors as pointed out by Wanatabe et al. [48]. The relatively larger IC_{50}s measured with substrate Z-Arg-Arg-AMC (covering the S3 to S1' subsites) might be due to a higher relative affinity of this substrate for cat.B with respect to Z-Lys-ONp.

Docking results also highlight why experimentally, neither **P722-ind** nor **P15-ind** inhibit the enzyme. Apparently, bulky substituents on the indene motif are not suitable for a favourable inhibition of cat.B. Since **P722** exhibits a remarkable anticancer activity with an IC_{50} of 0.035 ± 0.005 µM on triple negative breast cancer cell line MDA-MB231,[50] this work clearly demonstrates that its antiproliferative activity does not originate from cat.B inhibition.

In view of all these results, the indene motif seems to be the key factor conferring the ability to inhibit cat.B but it does not seem to be the only requirement since ferrocenyl indenes with bulky substituents do not. In order to confirm this hypothesis, another docking experiment has been conducted with **(*R*)-P35-ind,** i.e. an indene similar to **(*R*)-P85-ind** where the hydroxyl group was replaced by a primary amino group (Figure 1). Under mildly basic conditions, electrochemical oxidation of **P35,** the potential precursor of **P35-ind**, was assumed to result in the formation of an imino methide via a two-electron, two-proton process analogous to the oxidation of **P85**.[51] Interestingly, **P35** has a lower IC_{50} value (0.8 µM) than **P85** (1.13 µM) on MDA-MB231. This difference extends to other ferrociphenols and even to ferrocenophanes, for which the amino compounds are systematically slightly more cytotoxic than their phenolic equivalents.[52] One could hypothesize that the oxidation product of **P35** also evolves to **P35-ind** and contribute to its biological activity a little more than **P85-ind** contributes to the activity of **P85**. Thus, even though **P35-ind** was not synthesized, it seemed relevant to include it in the docking studies. Once again, we find the **(*R*)-P35-ind** ligand docked inside the main binding site of cat.B. Both docked structures for **(*R*)-P85-ind**

and **(*R*)-P35-ind** are remarkably similar (Figure S37). **(*R*)-P35-ind,** like **(*R*)-P85-ind,** shows two π-π interactions with His199 and Trp221 (Figure S34). **(*R*)-P35-ind** also shows hydrophobic interactions with Gln23, Ser25, Cys26, Gly27, Cys29, Cys71, Asn72, Leu181 and Trp221, and one H-bond with Asn222 (Figure S33). In turn, **(*S*)-P35-ind** shows a similar lp-π interaction with Gly27 (Figure S36) as the one observed for **(*S*)-P85-ind**. Once more, **(*S*)-P35-ind** and **(*S*)-P85-ind** docked conformations are virtually the same (Figure S37). **(*S*)-P35-ind** also shows hydrophobic interactions with Gln23, Gly24, Ser25, Gly27, Phe32, Asn72, His199, Ser220 and Trp221 (Figure S35). **(*S*)-P35-ind** shows two H-bonds with Cys29 and Gly33 residues like **(*S*)-P85-ind**. We anticipate that **P35-ind** should exhibit good cat.B inhibition properties like **P85-ind**.

Conclusion

In summary, we have successfully identified a first biological target for the main indene metabolite of the monophenol and diphenol ferrocifens **P85** and **P5** that may at least partially account for the anticancer activity of these compounds. We have also demonstrated that cathepsin B is not a target of the highly antiproliferative compounds **P15** and **P722**. Further work is now needed to assess the ability of the indene metabolites to prevent extracellular matrix degradation and tumour invasion using for instance wound healing assays.

Experimental section

Materials

All reagents and solvents were obtained from Sigma–Aldrich. Acetone was dried over 4 Å molecular sieves. Thin-layer chromatography (TLC) was performed on silica gel 60 GF254. Column chromatography was performed on Merck silica gel 60 (40–63 μm). All NMR experiments (^{1}H, ^{13}C and COSY) were carried out at room temperature on 400 MHz NMR spectrometer (Bruker), and chemical shifts (δ) are reported in ppm relative to solvent residual peak; s, d, t and q are used to denote singlet, doublet, triplet, and quartet, respectively. UV-visible spectra were recorded on a Cary 50 spectrometer (Varian). HRMS measurements were performed on a Thermo Fischer LTQ-Orbitrap XL apparatus equipped with an electrospray source. Ag_2O was freshly prepared in our laboratory before use. **P5**, **P85**, **P15**, **P722**, **P85-QM**, **P5-ind**, **P15-ind** and **P85-ind** were synthesized according to literature methods.[21,53,54] Bovine spleen cathepsin B was purchased from Sigma-Aldrich (C6286). A stock solution in water was prepared and assayed at 280 nm taking OD_{280nm} = 2.18 for [cat.B]

= 1 mg/mL. Aliquots were stored at -20°C until use. Z-Lys-ONp and Z-Arg-Arg-AMC were purchased from Bachem.

Methods

*Synthesis of the indene derivative of **P722** (**P722-ind**)*

P722 (0.06 g, 0.11 mmol) was dissolved in acetone (3 mL). Ag_2O (0.1 g, 0.43 mmol) was added in one portion as a solid. The mixture was stirred for 10 min at room temperature. The black solid was eliminated by filtration. $ZnCl_2$ (0.06 g, 0.4 mmol) was then added in one portion as a solid. The reaction was complete after 10 min of stirring. The mixture was then filtered over a 1-cm thick pad of silica gel. After solvent evaporation, the crude product was purified by silica gel column chromatography, using petroleum ether/ ethyl acetate (6:1) as eluent. **P722-ind** was isolated as an orange solid (30 mg, 50% yield). ^{1}H NMR (400 MHz; acetone-d_6): δ = 2.10 (m, 1H, CH_2), 2.50 (s, 4H, 2xCH_2; succinimide), 2.74 (m,1H, CH_2), 3.47 (m, 2H, CH_2; CH_2N), 3.82 (m, 1H, CH), 4.03 (s, 5H, C_5H_5), 4.06 (bs, 1H, C_5H_4), 4.15 (bs, 1H, C_5H_4), 4.23 (bs, 1H, C_5H_4), 4.46 (bs, 1H, C_5H_4), 6.72 (m, 2H, 2xCH; C_6H_3), 7.04 (d, *J* = 8.1 Hz, 2H, 2xCH; C_6H_4), 7.11 (s, 1H, CH; C_6H_3), 7.29 (d, *J* = 8.1 Hz, 2H, 2xCH; C_6H_4), 8.20 (bs, 1H; OH), 8.46 (bs, 1H; OH) ppm. ^{13}C NMR (100 MHz; acetone-d_6): δ = 27.8 (CH_2), 29.2 (CH_2), 38.2 (2xCH_2; succinimide), 49.8 (CH), 66.6 (CH; C_5H_4), 67.8 (CH; C_5H_4), 68.3 (CH; C_5H_4), 68.4 (CH; C_5H_4), 69.2 (5xCH; Cp), 81.0 (Cq; C_5H_4), 110.6 (CH; C_6H_3), 113.3 (CH; C_6H_3), 115.4 (2xCH; C_6H_4), 119.6 (CH; C_6H_3), 128.1 (C), 130.6 (2xCH; C_6H_4), 138.4 (C), 139.6 (C), 139.7 (C), 148.3 (C), 155.4 (C), 156.8 (C), 177.2 (2xC; CO-N-CO) ppm. MS (EI) *m/z*: 533 $[M]^+$. HRMS calcd for $C_{31}H_{27}FeNO_4$: 533.1290, found: 533.1287.

Cathepsin B spectrophotometric inhibition assay

The assay was performed in 20 mM acetate, 1 mM EDTA, 5 mM cysteine pH 5.0 at 20°C. Prior to the assay, cat.B (10 µL of 20 µM solution) was activated for 3 min by addition of assay buffer (0.5 mL). Enzymatic assays were performed with a fixed concentration of cat.B (67 nM) and a fixed concentration of Z-Lys-ONp (87 µM) in the presence of a variable concentration of test compound (3 – 66 µM) in a total volume of 3 mL containing 5% DMSO.[55] Activity was measured by recording OD_{326nm} for 3 min. IC_{50} were determined by applying a 4-parameter logistic equation.

Cathepsin B fluorimetric inhibition assay

Prior to the assay, solutions of **P5**, **P85**, **P5-ind** and **P85-ind** were prepared in DMSO at different concentrations (with a factor 20 compared to the final concentrations). The assay

was performed at pH 5 or 6, using respectively an acetate or a phosphate buffer (37°C) and the solutions should be freshly prepared. The assay consisted in mixing L-cysteine (8 mM, in buffer, 60 µL), Triton X-100 (0.1% v/v, in water, up to 200 µL), cat.B (0.75 µM, in Triton X-100 0.1% v/v, 8 µL) and the tested compound (variable concentrations in DMSO, 10 µL) in a 96-well black plate. They were incubated 10 min at 37°C.[56] Then, the substrate Z-Arg-Arg-AMC (20 µM, in Triton-100 -initially diluted in a minimal volume of DMSO, 60 µL) was added to the mixture and the plate was directly read with a microplate reader (Fluostar optima, BMG Labtech; ex: 380 nm, em: 470 nm) during 15 min. Negative and positive controls (with or without the specific inhibitor E-64) and the influence of the percentage of DMSO were also tested. The initial rates were determined and the IC_{50} were calculated using Prism 8.01 for windows (GraphPad software).

Computational methods

Before performing the docking calculations, models of all the ligands (optimized structures can be found in the Supporting Information (Tables S1-S13) and the target (cat.B) were built (see Supporting Information for further details). All docking calculations were carried out with a locally modified version (the only parameter that has been changed in the source code of AutoDock 4.2.6 is the MAX_RUNS variable) of AutoDock 4.2.6 software.[57] All the optimized ligands were docked to the prepared cathepsin B model. For both, ligand and protein, Gasteiger[58] charges were assigned and non-polar hydrogen atoms were merged using the AutoDockTools[57]. All the ligands contain an iron atom and atomic charges for metals need to be carefully assigned by the user. Computing the iron charge in this family of ligands with several schemes[59–64] leads to results close to zero. Hence, the charge of the metallic centre has been set to zero, affording a neutral organometallic compound. Flexible ligand docking was performed using the Lamarckian Genetic Algorithm[65] as implemented in the original AutoDock package. The grid used in all the calculations was centred at the protein's centre of mass with 160 lattice points in all three space directions with a point spacing of 0.375 Å. In order to have a very large distribution for each docking experiment, 10,000 runs were carried out for each ligand with 5,000,000 energy evaluations performed for each run. Figures S1 to S13 (in the Supporting Information) show the cluster distributions obtained after the docking experiments performed for each ligand. Information on the interactions found between each ligand and cathepsin B can be found further in this Supporting Information (Figures S14-S36).

Acknowledgement

The Agence Nationale de la Recherche (NaTeMOc project, grant number ANR-19-CE18-00022-01) and Feroscan are gratefully acknowledged for financial support. Valentin Barrandard is acknowledged for his technical assistance.

References

[1] P. Köpf-Maier, H. Köpf, E. W. Neuse, *J. Cancer Res. Clin. Oncol.* **1984**, *108*, 336–340.

[2] K. Strohfeldt, M. Tacke, *Chem. Soc. Rev.* **2008**, *37*, 1174–1187.

[3] G. Jaouen, S. Top, A. Vessières, G. Leclercq, M. J. McGlinchey, *Curr. Med. Chem.* **2004**, *11*, 2505–2517.

[4] D. Osella, M. Ferrali, P. Zanello, F. Laschi, M. Fontani, C. Nervi, G. Cavigiolio, *Inorg. Chim. Acta* **2000**, *306*, 42–48.

[5] I. Montes-Gonzalez, A. M. Alsina-Sanchez, J. C. Aponte-Santini, S. M. Delgado-Rivera, G. L. Duran-Camacho, *Pure Appl. Chem.* **2019**, *91*, 653–669.

[6] M. Zaki, S. Hairat, E. S. Aazam, *RSC Adv.* **2019**, *9*, 3239–3278.

[7] K. Kowalski, *Coord. Chem. Rev.* **2018**, *366*, 91–108.

[8] S. Peter, B. A. Aderibigbe, *Molecules* **2019**, *24*, e3604.

[9] P. Chellan, P. J. Sadler, *Chem.-Eur. J.* **2020**, *26*, 8676–8688.

[10] A. Singh, I. Lumb, V. Mehra, V. Kumar, *Dalton Trans.* **2019**, *48*, 2840–2860.

[11] R. Wang, H. Chen, W. Yan, M. Zheng, T. Zhang, Y. Zhang, *Eur. J. Med. Chem.* **2020**, *190*, 112109.

[12] G. Jaouen, A. Vessières, S. Top, *Chem. Soc. Rev.* **2015**, *44*, 8802–8817.

[13] B. Sharma, V. Kumar, *J. Med. Chem.* **2021**, DOI 10.1021/acs.jmedchem.1c00390.

[14] J.-L. H. A. Duprey, J. H. R. Tucker, *Chem. Lett.* **2014**, *43*, 157–163.

[15] K. Kowalski, *Coord. Chem. Rev.* **2021**, *432*, 213705.

[16] V. Raičević, N. Radulović, M. Sakač, *Eur. J. Inorg. Chem.* **n.d.**, DOI 10.1002/ejic.202100951.

[17] A. Vessières, Y. Wang, M. J. McGlinchey, G. Jaouen, *Coord. Chem. Rev.* **2021**, *430*, 213658.

[18] Y. Wang, M. A. Richard, S. Top, P. M. Dansette, P. Pigeon, A. Vessieres, D. Mansuy, G. Jaouen, *Angew. Chem. Int. Ed.* **2016**, *55*, 10431–10434.

[19] A. Citta, A. Folda, A. Bindoli, P. Pigeon, S. Top, A. Vessieres, M. Salmain, G. Jaouen, M. P. Rigobello, *J. Med. Chem.* **2014**, *57*, 8849–8859.

[20] V. Scalcon, M. Salmain, A. Folda, S. Top, P. Pigeon, H. Z. S. Lee, G. Jaouen, A. Bindoli, A. Vessieres, M. P. Rigobello, *Metallomics* **2017**, *9*, 949–959.

[21] M.-A. Richard, D. Hamels, P. Pigeon, S. Top, P. M. Dansette, H. Z. S. Lee, A. Vessières, D. Mansuy, G. Jaouen, *ChemMedChem* **2015**, *10*, 981–990.

[22] J. Kos, A. Mitrović, B. Mirković, *Future Med. Chem.* **2014**, *6*, 1355–1371.

[23] C. Jedeszko, B. F. Sloane, *Biol. Chem.* **2004**, *385*, 1017–1027.

[24] A. Bergamo, G. Sava, *Chem. Soc. Rev.* **2015**, *44*, 8818–8835.

[25] S. Gobec, R. Frlan, *Curr. Med. Chem.* **2006**, *13*, 2309–2327.

[26] S. P. Fricker, *Metallomics* **2010**, *2*, 366–377.

[27] A. O. Akinyemi, G. B. S. Pereira, F. V. Rocha, *MRMC* **2021**, *21*, 1612–1624.

[28] S. S. Gunatilleke, A. M. Barrios, *J. Inorg. Biochem.* **2008**, *102*, 555–563.

[29] S. S. Gunatilleke, A. M. Barrios, *J. Med. Chem.* **2006**, *49*, 3933–3937.

[30] Y. Zhu, B. R. Cameron, R. Mosi, V. Anastassov, J. Cox, L. Qin, Z. Santucci, M. Metz, R. T. Skerlj, S. P. Fricker, *J. Inorg. Biochem.* **2011**, *105*, 754–762.

[31] A. Casini, C. Gabbiani, F. Sorrentino, M. P. Rigobello, A. Bindoli, T. J. Geldbach, A. Marrone, N. Re, C. G. Hartinger, P. J. Dyson, L. Messori, *J. Med. Chem.* **2008**, *51*, 6773–6781.

[32] A. Casini, F. Edafe, M. Erlandsson, L. Gonsalvi, A. Ciancetta, N. Re, A. Ienco, L. Messori, M. Peruzzini, P. J. Dyson, *Dalton Trans.* **2010**, *39*, 5556–5563.

[33] L. Oehninger, M. Stefanopoulou, H. Alborzinia, J. Schur, S. Ludewig, K. Namikawa, A. Muñoz-Castro, R. W. Köster, K. Baumann, S. Wölfl, W. S. Sheldrick, I. Ott, *Dalton Trans.* **2013**, *42*, 1657–1666.

[34] A. Mitrović, J. Kljun, I. Sosič, S. Gobec, I. Turel, J. Kos, *Dalton Trans.* **2016**, *45*, 16913–16921.

[35] A. Mitrović, J. Kljun, I. Sosič, M. Uršič, A. Meden, S. Gobec, J. Kos, I. Turel, *Inorg. Chem.* **2019**, *58*, 12334–12347.

[36] J. Spencer, A. Casini, O. Zava, R. P. Rathnam, S. K. Velhanda, M. Pfeffer, S. K. Callear, M. B. Hursthouse, P. J. Dyson, *Dalton Trans.* **2009**, 10731–10735.

[37] C. Bincoletto, I. L. S. Tersariol, C. R. Oliveira, S. Dreher, D. M. Fausto, M. A. Soufen, F. D. Nascimento, A. C. F. Caires, *Bioorg. Med. Chem.* **2005**, *13*, 3047–3055.

[38] D. K. Nägler, A. C. Storer, F. C. V. Portaro, E. Carmona, L. Juliano, R. Ménard, *Biochemistry* **1997**, *36*, 12608–12615.

[39] M. W. Chang, R. K. Belew, K. S. Carroll, A. J. Olson, D. S. Goodsell, *J. Comput. Chem.* **2008**, *29*, 1753–1761.

[40] P. Bansode, P. Patil, P. Choudhari, M. Bhatia, A. Birajdar, I. Somasundaram, G. Rashinkar, *J. Mol. Liquids* **2019**, *290*, 111182.

[41] P. Schenker, P. Alfarano, P. Kolb, A. Caflisch, A. Baici, *Protein Sci.* **2008**, *17*, 2145–2155.

[42] G.-Z. Zeng, X.-L. Pan, N.-H. Tan, J. Xiong, Y.-M. Zhang, *Eur. J. Med. Chem.* **2006**, *41*, 1247–1252.

[43] M. Singh, N. Raghav, *Bioorg. Chem.* **2015**, *59*, 12–22.

[44] I. Sosič, B. Mirković, S. Turk, B. Štefane, J. Kos, S. Gobec, *Eur. J. Med. Chem.* **2011**, *46*, 4648–

4656.

[45] I. Sosič, A. Mitrović, H. Ćurić, D. Knez, H. Brodnik Žugelj, B. Štefane, J. Kos, S. Gobec, *Bioorg. Med. Chem. Lett.* **2018**, *28*, 1239–1247.

[46] P. Fuentes-Prior, G. S. Salvesen, *Biochem. J.* **2004**, *384*, 201–232.

[47] J. Schmitz, E. Gilberg, R. Löser, J. Bajorath, U. Bartz, M. Gütschow, *Bioorg. Med. Chem.* **2019**, *27*, 1–15.

[48] D. Watanabe, A. Yamamoto, K. Tomoo, K. Matsumoto, M. Murata, K. Kitamura, T. Ishida, *J. Mol. Biol*. **2006**, *362*, 979–993.

[49] B. Mirković, M. Renko, S. Turk, I. Sosič, Z. Jevnikar, N. Obermajer, D. Turk, S. Gobec, J. Kos, *ChemMedChem* **2011**, *6*, 1351–1356.

[50] Y. Wang, P. Pigeon, S. Top, J. Sanz García, C. Troufflard, I. Ciofini, M. J. McGlinchey, G. Jaouen, *Angew. Chem. Int. Ed.* **2019**, *58*, 8421–8425.

[51] P. Pigeon, S. Top, O. Zekri, E. A. Hillard, A. Vessières, M.-A. Plamont, O. Buriez, E. Labbé, M. Huché, S. Boutamine, C. Amatore, G. Jaouen, *J. Organomet. Chem.* **2009**, *694*, 895–901.

[52] M. Görmen, P. Pigeon, S. Top, E. A. Hillard, M. Huché, C. G. Hartinger, F. de Montigny, M.-A. Plamont, A. Vessières, G. Jaouen, *ChemMedChem* **2010**, *5*, 2039–2050.

[53] S. Top, A. Vessières, G. Leclercq, J. Quivy, J. Tang, J. Vaissermann, M. Huché, G. Jaouen, *Chem. Eur. J.* **2003**, *9*, 5223–5236.

[54] P. Pigeon, Y. Wang, S. Top, F. Najlaoui, M. C. Garcia Alvarez, J. Bignon, M. J. McGlinchey, G. Jaouen, *J. Med. Chem.* **2017**, *60*, 8358–8368.

[55] A. S. Bajkowski, A. Frankfater, *Anal. Biochem.* **1975**, *68*, 119–127.

[56] K. I. Hulkower, C. C. Butler, B. E. Linebaugh, J. L. Klaus, D. Keppler, V. L. Giranda, B. F. Sloane, *Eur. J. Biochem.* **2000**, *267*, 4165–4170.

[57] G. M. Morris, R. Huey, W. Lindstrom, M. F. Sanner, R. K. Belew, D. S. Goodsell, A. J. Olson, *J. Comput. Chem.* **2009**, *30*, 2785–2791.

[58] J. Gasteiger, M. Marsili, *Tetrahedron* **1980**, *36*, 3219–3228.

[59] F. L. Hirshfeld, *Theoret. Chim. Acta* **1977**, *44*, 129–138.

[60] U. C. Singh, P. A. Kollman, *J. Comput. Chem.* **1984**, *5*, 129–145.

[61] J. P. Ritchie, *J. Am. Chem. Soc.* **1985**, *107*, 1829–1837.

[62] J. P. Ritchie, S. M. Bachrach, *J. Comput. Chem.* **1987**, *8*, 499–509.

[63] B. H. Besler, K. M. Merz Jr., P. A. Kollman, *J. Comput. Chem.* **1990**, *11*, 431–439.

[64] H. Hu, Z. Lu, W. Yang, *J. Chem. Theory Comput.* **2007**, *3*, 1004–1013.

[65] G. M. Morris, D. S. Goodsell, R. S. Halliday, R. Huey, W. E. Hart, R. K. Belew, A. J. Olson, *J. Comput. Chem.* **1998**, *19*, 1639–1662.

Graphical abstract

Ferrocenyl indenes resulting from oxidation of ferrocifen mono- and diphenols act as moderate inhibitors of the lysosomal enzyme cathepsin B as highlighted by in vitro enzymatic assays. These experimental results are substantiated by molecular docking calculations that position the active complexes in the active site of the enzyme.

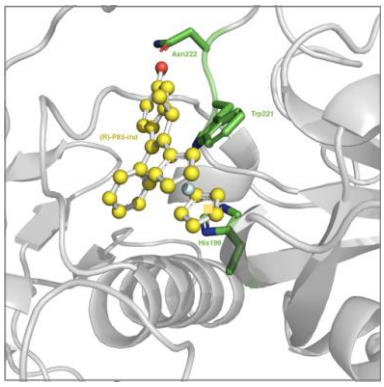

Supporting Information for:

Inhibition of cathepsin B by ferrocenyl indenes highlights a new pharmacological facet of ferrocifens.

Juan Sanz Garcia,[1] Marie Gaschard,[2] Isabelle Navizet,[1] Mehdi Sahihi,[1] Siden Top,[2] Yong Wang,[2,3] Pascal Pigeon,[2,3] Anne Vessières,[2] Michèle Salmain,[2*] and Gérard Jaouen[2,3*]

[1] Univ Gustave Eiffel, CNRS, Univ Paris-Est Créteil, MSME, UMR 8208, F-77454 Marne-la-Vallée Cedex 2, France

[2] Sorbonne Université, CNRS, Institut Parisien de Chimie Moléculaire, 4 place Jussieu 75005 Paris, France

[3] PSL Research University, Chimie ParisTech, 11 rue Pierre et Marie Curie, 75005 Paris, France

Table of Contents

Computational Details

Ligand Optimization

Gas-phase geometry optimizations of all the compounds studied in this work were carried out with the Gaussian 16 quantum package.[1] Density Functional Theory (DFT) was employed to perform these calculations using the standard hybrid functional B3LYP,[2,3] including Grimme's dispersion correction (D3-BJ),[4] with the diffuse-augmented polarization valence-double-ζ (6-31+G(d))[5] basis set with one set of *d* polarization functions,[6,7] a set of *s* and *p* diffuse functions for all atoms but the hydrogens atoms, and the double-ζ quality LANL2DZ[8] basis set with its associated effective core potential[9] (including 10 core electrons) for the iron atom. Subsequently, vibrational frequency calculations were performed at the same level of theory in order to confirm that all the structures found were minima. All the optimized structures can be found in the Supporting Information (Tables S1-S13).

Cathepsin B Model Preparation

In order to perform the protein-ligand docking experiments, the crystal structure of the Bovine Spleen cathepsin B (PDB ID: **2DC7**) from the Protein Data Bank (http://www.rcsb.org/pdb) was analyzed. The resolution and R-value observed for this X-ray crystallographic structure are 1.94 Å and 0.187, respectively. In order to complete the protein sequence missing gaps, the SWISS-MODEL server (https://swissmodel.expasy.org/) was used to model the Bovine Spleen cathepsin B using the Blast method. The obtained structure was used for a subsequent molecular dynamics (MD) simulation. The MD calculation was performed using the GROMACS 2018 package[10,11] together with the GROMOS 53a6 force field[12]. The protonation state of histidine residues which optimizes the hydrogen bonding conformation was determined by the pdb2gmx module of the GROMACS package. The cathepsin model was placed in the center of a cubic box with periodic boundary conditions in three dimensions. The minimum distance between the protein surface and the box was set to 1.0 nm. The box was filled with SPC water molecules[13], and the solvated system was neutralized by adding the appropriate amount of sodium ions. The system was minimized using the steepest descent algorithm and subsequently it was equilibrated for 1 ns in the NVT ensemble followed by a second equilibration of 1 ns in the NPT ensemble. Finally, a 50 ns MD simulation was carried out at 1 bar and 300 K. The Berendsen thermostat[14] and Parrinello-Rahman barostat[15,16] were used together with 1 nm cut-off for the van der Walls (vdW) and Coulomb interactions. The particle mesh Ewald (PME) method[17,18] was used for long range electrostatics and the leap-frog algorithm with a time step of 2 fs was used to integrate the equations of motion. The clustering analysis of the 50 ns MD trajectory was performed using the GMX Cluster module of the GROMACS package, and the best structure of the most populated cluster was selected for the subsequent docking calculations.

Analysis of the Docking Results

For each docking experiment, 10,000 runs leads to 10,000 poses. An unsupervised machine learning density-based clustering algorithm is used by AutoDock to classify the different poses by structure similarity. This clustering algorithm is based on the RMSD criteria of 2 Å. For each docking experiment, this algorithm leads to a different distribution of N clusters. In this study, N oscillates between *ca.* 50 and 400. Each cluster population corresponds to the number of poses inside the cluster. A cluster is defined as highly populated when it is built with at least 1000 poses **(10% of the total number of poses)**. In contrast, a cluster is defined as modestly populated when it is built with less than 100 poses **(1 % of the total number of poses)**. In each distribution, every cluster is represented by the best pose with the lowest binding energy.

Three different types of distributions will be considered:

1) **Well clustered distributions**. Distributions with a highly populated cluster and showing few clusters (**less than 50**) modestly populated will be considered as well **clustered distributions**.
2) **Dispersed distributions**. Distributions showing no highly populated cluster or showing an important amount of clusters (**more than 300**) modestly populated will be considered as **dispersed distributions**.
3) **Intermediate distributions**. Cases not falling in the previous "two extreme" type of distributions will be considered as **intermediate distributions**.

Following the recommendations of the AutoDock developers and their collaborators,[19] the best docked pose between the ligand and the protein was identified as the best pose of the most populated cluster. We call this pose the docked conformation.

Scheme S1. General Mechanism of the thioester formation and subsequent proteolysis cleavage (hydrolysis) of cysteine protease enzyme.[20,21]

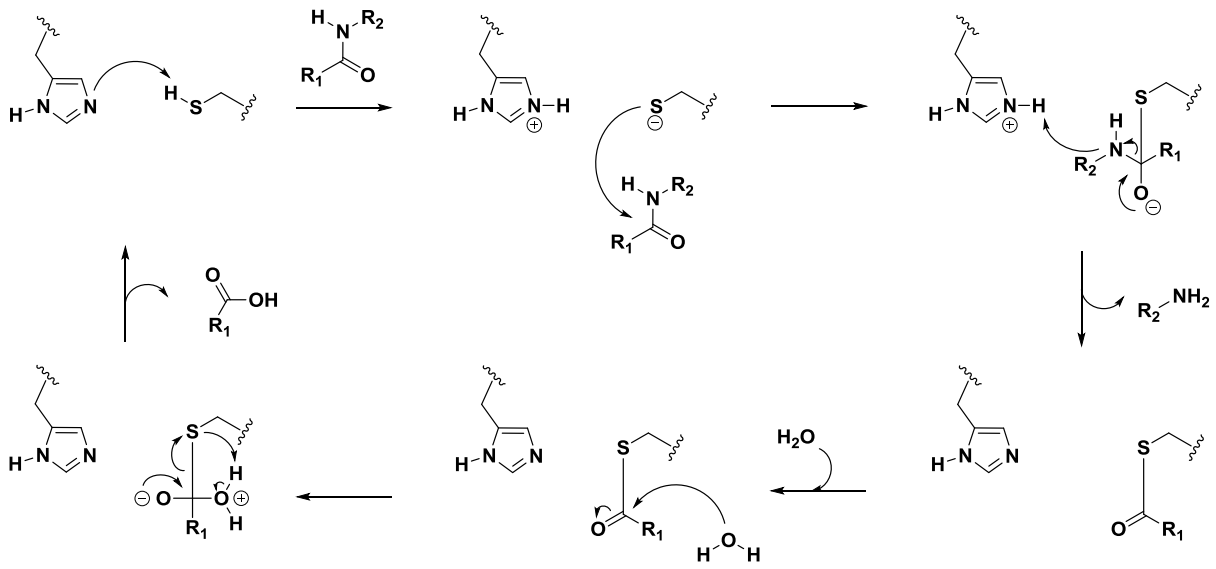

Table S1. Optimized Cartesian coordinates and energies of **(*R*)-P5-ind** at the B3LYP-D3-BJ/6-31+G* (Fe LANL2DZ) level of theory in vacuum.

C	6.950839124675	0.448343053728	1.117840603942
C	6.314454957115	1.186554492840	0.160179965010
C	6.455656928614	-0.998049021629	1.071387070694
H	6.053869785296	-1.292828035817	2.051345499683
C	7.550808963068	-2.004797560068	0.657726456741
H	7.138016042239	-3.018425624041	0.607432846845
H	7.939161365162	-1.746342455276	-0.333154191206
C	5.319063134496	0.351623714913	-0.523187696220
C	6.537657669708	2.600791228606	-0.207965983532
C	3.614287231834	-1.641079740023	-1.456203698603
C	7.731271175510	2.998272606606	-0.831841619641
C	7.952889554150	4.323308800333	-1.197068352399
C	6.967405679425	5.283420283041	-0.943654311387
C	5.764942655886	4.907293721548	-0.336815842380
C	5.555158725735	3.573535514336	0.019780617718
H	8.497219441650	2.252741531843	-1.019849300661
H	8.877078695404	4.629314585403	-1.677687506905
H	4.995308327346	5.651642473668	-0.140103061053
H	4.621758544934	3.286602595366	0.496333579927
C	3.567563803162	-0.357792168578	-2.014726937686
C	4.425403305009	0.647615888198	-1.552368144360
C	4.521225204881	-1.947893951043	-0.428765810984
C	5.359172123897	-0.944991453083	0.029466418038
H	4.539462204282	-2.955285726563	-0.022422255023
H	4.392232524366	1.639966601383	-1.993309885443
H	2.861830088615	-0.143565903093	-2.815503078343
Fe	9.973327702265	0.900472717552	2.063639079413
C	7.889942142326	0.897857825046	2.137675125778
C	8.441951910278	0.068934061145	3.180809728669
C	9.272472065042	0.869620975141	4.016460562026
C	9.250809603379	2.202452980987	3.505785283386
C	8.412620210737	2.224314584960	2.354183020162
C	11.902055421969	1.496833064646	1.594642290633
C	11.904647185688	0.142063456284	2.048664598740
C	11.068119123040	-0.618268193307	1.173931593914
C	10.548602679789	0.266988965791	0.178978317259
C	11.064146951552	1.574088662551	0.438812055630
H	12.408893882170	2.327260803286	2.067798283292
H	12.415501667190	-0.233675570314	2.925186392666
H	10.841263617349	-1.671536045169	1.268151341017
H	9.847148615829	0.002350987137	-0.600988298011
H	10.827651126190	2.474613601157	-0.111617481412
H	8.222415445553	3.087187965034	1.736186443508
H	9.810005102409	3.043095015986	3.894663057779
H	9.846584360669	0.518264093011	4.863390107357
H	8.266485254554	-0.989804839506	3.306531855871
H	8.386533510495	-2.002397649849	1.360903582211
O	2.788840846688	-2.656289673970	-1.877469387949
H	2.208695837977	-2.332689206602	-2.583816492627
O	7.236260036027	6.575460973088	-1.317202290025
H	6.484117404378	7.145640623317	-1.093861302059

Energies (a.u.)	
E	-1278.041211
Zero-point correction	0.407844
Sum of electronic and thermal enthalpies	-1277.608013
Sum of electronic and thermal free energies	-1277.687921

(*R*)-P5-ind Structure

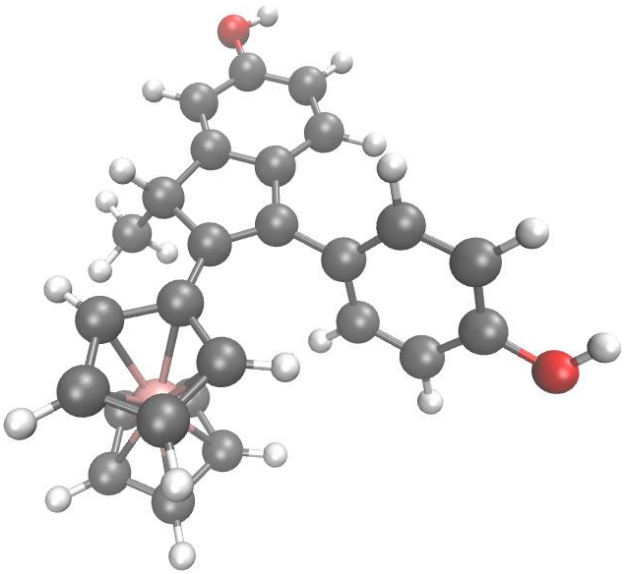

Table S2. Optimized Cartesian coordinates and energies of **(*S*)-P5-ind** at the B3LYP-D3-BJ/6-31+G* (Fe LANL2DZ) level of theory in vacuum.

C	6.795489808688	0.515490117156	1.395972997358
C	6.318741455411	1.193792297838	0.310725514081
C	6.247379961487	-0.910734093487	1.401645522322
C	5.497328631702	0.292453676639	-0.507058905958
C	6.593214187795	2.588531082990	-0.095236575488
C	4.072632449819	-1.805164345900	-1.655557647192
C	7.380366426410	2.856832357757	-1.227337150627
C	7.656604249157	4.162127385896	-1.627248760732
C	7.132388381793	5.233607651229	-0.896764660173
C	6.328974272993	4.989688007902	0.221673879738
C	6.062851131614	3.675671367142	0.611176616829
H	7.792185785538	2.026663981171	-1.794566411966
H	8.274421251335	4.366499586605	-2.496291461702
H	5.910504668400	5.820831053033	0.786681244363
H	5.441915454486	3.488940600877	1.482915553474
C	4.104332672355	-0.551939507692	-2.279657245256
C	4.816354582296	0.508001373075	-1.705191440835
C	4.749882577289	-2.025492232947	-0.445188532514
C	5.460032185939	-0.974685350289	0.111366690043
H	4.702955053486	-3.007784185564	0.016531819492
H	4.834324571337	1.480473447800	-2.189294138912
H	3.569147632386	-0.402046833212	-3.215763520791
Fe	9.805930572044	0.956337208403	2.024028555614
C	7.765632317532	0.940615994102	2.397900458542
C	8.455435214672	0.047534128887	3.296625194761
C	9.401306073627	0.796619087670	4.055013741077
C	9.313545205518	2.159855366956	3.639961016100
C	8.320880109858	2.252693785418	2.620982223708
C	11.596301404591	1.625589097966	1.222520811049
C	11.726865542958	0.266720004371	1.646130687992
C	10.768569548173	-0.513532917533	0.926720474315
C	10.047029506858	0.364141546087	0.059361075473
C	10.557480398490	1.686202368194	0.241219052294
H	12.155092745335	2.467807374082	1.608438175522
H	12.402618483891	-0.100037526849	2.407306237551
H	10.593166702854	-1.574385125426	1.046809706230
H	9.212370233407	0.087649285923	-0.571326834318
H	10.181621167183	2.580879056416	-0.236243402896
H	8.057980507727	3.149166011436	2.082685511624
H	9.925262640338	2.976018260994	4.000864608451
H	10.088928591335	0.394508802222	4.786923306557
H	8.315024660025	-1.022686555351	3.353319284442
O	3.387603018104	-2.872687632762	-2.185489650161
H	2.962927116012	-2.607482410397	-3.015870670594
O	7.435562168697	6.499320580286	-1.329319814416
H	7.015495221778	7.154019275019	-0.749954227085
C	5.362884559345	-1.210881911934	2.628733020046
H	5.922610440604	-1.090918335664	3.561298794765
H	4.508693389998	-0.525413634388	2.650639165031
H	4.977860924389	-2.235793934785	2.584903668058
H	7.079935942943	-1.629085727362	1.379823134718

Energies (a.u.)	
E	-1278.041876
Zero-point correction	0.407723
Sum of electronic and thermal enthalpies	-1277.608773
Sum of electronic and thermal free energies	-1277.688855

(*S*)-P5-ind Structure

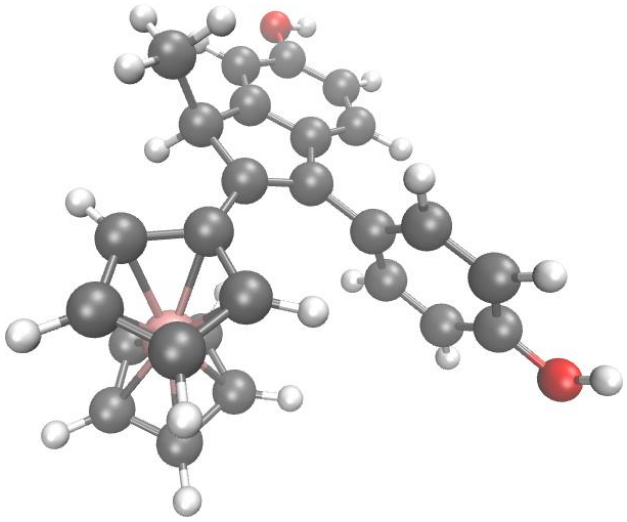

Table S3. Optimized Cartesian coordinates and energies of **(*R*)-P15-ind** at the B3LYP-D3-BJ/6-31+G* (Fe LANL2DZ) level of theory in vacuum.

C	6.972291327178	0.364398087593	1.173361519122
C	6.275975915977	1.098345006115	0.255053261391
C	6.565544459369	-1.106787690400	1.078000312924
C	5.319248976018	0.231053654186	-0.442795477274
C	6.411266498982	2.535772036888	-0.063210789144
C	3.716740366949	-1.823345495657	-1.421634401049
C	7.563406656774	3.020923222464	-0.707135254925
C	7.699756250183	4.366757812909	-1.022544583752
C	6.675524870027	5.271413137277	-0.701681351232
C	5.513754621433	4.806237074803	-0.072986351685
C	5.391424825173	3.445880608935	0.232202716361
H	8.361101844372	2.326268452393	-0.950195285732
H	8.589529644792	4.742957305649	-1.518520999884
H	4.706701163676	5.482117069683	0.184550163416
H	4.489954248522	3.091896397506	0.725424852560
C	3.582786862077	-0.525011109085	-1.928842119693
C	4.389216560020	0.511736462125	-1.443536669941
C	4.660797181961	-2.114013726083	-0.423341088971
C	5.447169692273	-1.080805117956	0.058398922782
H	4.746476897372	-3.133083325249	-0.056647897935
H	4.288525296340	1.516756950810	-1.843660654202
H	2.849128878794	-0.323377007109	-2.707540114617
Fe	9.977048223076	0.984277374383	2.076585491763
C	7.901723818259	0.832696898721	2.193465233574
C	8.533460797985	0.000873848177	3.187767749829
C	9.327054270674	0.821594802649	4.039908349221
C	9.201572977321	2.170232863607	3.588616997885
C	8.336317356757	2.182247334068	2.456981231512
C	11.849117523809	1.731673310446	1.595734165755
C	11.954204224869	0.360305686215	1.983021080813
C	11.148607725134	-0.413266425948	1.090983860628
C	10.545632830935	0.480513396497	0.152285742356
C	10.978482659436	1.806187509449	0.464111449105
H	12.310362289165	2.571538874566	2.097996736890
H	12.511658507020	-0.020491236876	2.828438345045
H	10.995112991792	-1.482818888497	1.138520663163
H	9.842844693128	0.205644085636	-0.622899158779
H	10.664879129917	2.713591660314	-0.033911463877
H	8.072432388393	3.054344047236	1.880158002112
H	9.711104227677	3.030565010758	4.001904939197
H	9.943982456066	0.475498320191	4.858425212926
H	8.434940876289	-1.071876089674	3.270767302973
O	2.943874016018	-2.869558487607	-1.867009552519
H	2.331265769089	-2.554318911640	-2.549290233415
O	6.902430344975	6.573407277624	-1.044974780826
C	5.899110927636	7.542528336658	-0.747640782956
H	4.962329299535	7.270622371621	-1.255874782844
H	5.708314689829	7.556525287185	0.335453568535
C	6.404442655978	8.895518030989	-1.223135384384
H	6.630265747843	8.829506004131	-2.296272736335
H	7.341597388731	9.140815913550	-0.711319224836
C	5.386099795917	10.009267717841	-0.973275460792
H	4.431000470463	9.749011446072	-1.465005199154
H	5.179818943197	10.082917143016	0.102154689694
N	5.933398555945	11.300190230812	-1.404652973735
H	6.083527295862	11.307210200689	-2.412475545297
H	5.286185869922	12.057148869586	-1.194912168094
C	7.712437602857	-2.025224053305	0.602977554008
H	8.063460410604	-1.702188278047	-0.382909176842
H	8.560822980510	-1.998935203828	1.290405418184
H	7.362582489288	-3.059980447982	0.517476161302
H	6.203167029837	-1.465037247077	2.052133159693

Energies (a.u.)	
E	-1451.339913
Zero-point correction	0.511273
Sum of electronic and thermal enthalpies	-1450.797814
Sum of electronic and thermal free energies	-1450.891638

(*R*)-P15-ind Structure

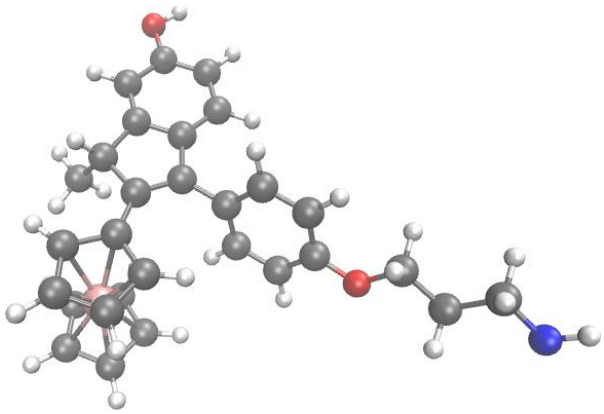

Table S4. Optimized Cartesian coordinates and energies of **(*S*)-P15-ind** at the B3LYP-D3-BJ/6-31+G* (Fe LANL2DZ) level of theory in vacuum.

C	6.728512816006	0.379591735665	1.359651167745
C	6.170151984395	1.024624521084	0.293106580890
C	6.329701210043	-1.095500152187	1.345018449035
C	5.427053914270	0.059089687196	-0.526804052329
C	6.300005400445	2.444730549933	-0.096718495604
C	4.187311576690	-2.148478340924	-1.683893744280
C	7.033703024394	2.801752368463	-1.242567776904
C	7.174126279364	4.130433792477	-1.624557448121
C	6.568526640194	5.146808430597	-0.869653816719
C	5.813486661871	4.811072523455	0.261181130677
C	5.685133731985	3.467875047474	0.631166213632
H	7.510235798374	2.022976009820	-1.831686972353
H	7.751283196060	4.406506576705	-2.501913358310
H	5.324238064846	5.573777841614	0.855687433155
H	5.100227852880	3.212579579295	1.510753541288
C	4.085700908860	-0.888684335099	-2.286993387395
C	4.704409981402	0.226052288054	-1.708212619243
C	4.907939304577	-2.321066514106	-0.491123433418
C	5.524923879943	-1.215093320729	0.069897240519
H	4.965049252888	-3.310135309508	-0.045301359242
H	4.618567693730	1.203204633895	-2.175264892531
H	3.518937056407	-0.776817726417	-3.209779325812
Fe	9.669921929373	1.210865074086	1.993379539025
C	7.654888108291	0.883430528352	2.367029103531
C	8.472275009361	0.048492679814	3.212782419335
C	9.309835834813	0.880364367606	4.011250138029
C	9.025523901903	2.238550042559	3.674705264987
C	8.020323487728	2.246206352632	2.663817796589
C	11.336520293964	2.178414004331	1.231450047115
C	11.668812991890	0.833323915406	1.582869821459
C	10.832034080093	-0.040882824710	0.821158413620
C	9.983907456752	0.765231459721	0.000195244199
C	10.294491005928	2.136779482762	0.252674352649
H	11.767002294212	3.072335131716	1.662830771108
H	12.395758563418	0.530934932580	2.324962248017
H	10.815821053698	-1.120871964042	0.884338469258
H	9.196659261996	0.401919667360	-0.647004949384
H	9.786990308604	2.989309721356	-0.177735491697
H	7.626306271727	3.124611758651	2.178397070175
H	9.518548633891	3.111863476739	4.080792464245
H	10.054546118945	0.539624716556	4.718045625116
H	8.484723099837	-1.032401786402	3.208149289993
O	3.595785864026	-3.268649290302	-2.218446742631
H	3.130256251678	-3.032335797823	-3.035522493902
O	6.766586915971	6.420773348770	-1.318986642261
C	6.180629517131	7.499669675151	-0.592983295383
H	5.087895495494	7.376968393304	-0.568631436137
H	6.548457546443	7.490234396322	0.443551925464
C	6.568605961446	8.793832973442	-1.290546742199
H	6.228720913154	8.746684995710	-2.334198766867
H	7.659822573726	8.889728367010	-1.311277689283
C	5.966843542030	10.020216144924	-0.602231770127
H	4.867884074839	9.911483464339	-0.555659639277
H	6.325037145444	10.071691505630	0.433917469344
N	6.405357123183	11.245365067528	-1.279520191223
H	6.043264763262	11.278073679896	-2.231414340076
H	6.054432654520	12.071150247907	-0.799121670051
C	5.513628740815	-1.511836700021	2.584933759949
H	6.083220253310	-1.353755769161	3.505859416917
H	4.593969244384	-0.919566281375	2.644030814716
H	5.235723463425	-2.570155089710	2.526517653984
H	7.231548739669	-1.722828195370	1.287619747000

Energies (a.u.)

E	-1451.340634
Zero-point correction	0.511052
Sum of electronic and thermal enthalpies	-1450.798660
Sum of electronic and thermal free energies	-1450.893638

(*S*)-P15-ind Structure

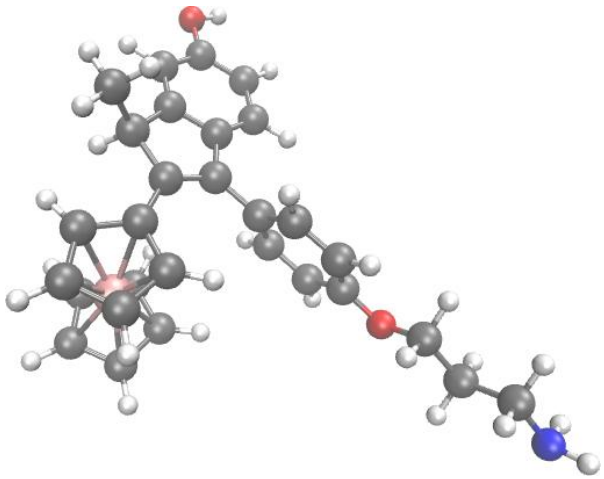

Table S5. Optimized Cartesian coordinates and energies of **(*R*)-P85-ind** at the B3LYP-D3-BJ/6-31+G* (Fe LANL2DZ) level of theory in vacuum.

C	6.948948487920	0.448382028476	1.120979850283
C	6.321426431441	1.183101102514	0.155842798192
C	6.449824195178	-0.996934994984	1.077136696881
H	6.037133336160	-1.284857337432	2.054616098437
C	7.545509655668	-2.009691940161	0.680182177954
H	7.129240064048	-3.021955585486	0.631757064123
H	7.944408816961	-1.758673204740	-0.308370215507
C	5.330892124399	0.348772965591	-0.533922203089
C	6.546489289421	2.598292473979	-0.211965052920
C	3.629553296586	-1.642668965621	-1.473738742216
C	7.719283756487	2.977921842865	-0.882443469193
C	7.934655477864	4.308881731912	-1.243093971777
C	6.975748005871	5.280996328882	-0.941117102051
C	5.797656979493	4.910811750898	-0.285904797536
C	5.581930540195	3.577137104129	0.069876824015
H	8.463721916424	2.220223819029	-1.106711183530
H	8.849594861197	4.588120859719	-1.759437878001
H	7.143806060371	6.318334207733	-1.217806364530
H	5.047112832246	5.660613960125	-0.049698830728
H	4.669114169166	3.288669557688	0.584261525835
C	3.589290578983	-0.360790228267	-2.036112194459
C	4.445357342209	0.644387034596	-1.570157121456
C	4.527152293272	-1.948235180975	-0.437693564200
C	5.363799340475	-0.945896610924	0.024032662967
H	4.538936444658	-2.954078106909	-0.027325351097
H	4.415626659505	1.636398534684	-2.012073886531
H	2.889452885102	-0.147244879839	-2.842176564737
Fe	9.966860697792	0.901529001796	2.063364678821
C	7.885032698548	0.902822399955	2.141195736122
C	8.436208717072	0.081035068299	3.190202967604
C	9.269455998017	0.886918350854	4.018075864631
C	9.249361532418	2.215812077545	3.497041715221
C	8.409864110853	2.230250575933	2.346394136173
C	11.893773262879	1.493734995029	1.583036394209
C	11.898141670133	0.142950224058	2.048911082142
C	11.058757772559	-0.625127893034	1.183721161709
C	10.535599444272	0.251390810034	0.182971137380
C	11.051617011146	1.560808599304	0.429531679765
H	12.401946156106	2.328193150612	2.047627472101
H	12.412019206119	-0.225076467641	2.926931593074
H	10.832307088192	-1.677525817164	1.288048000989
H	9.830646630759	-0.019616753663	-0.591543026103
H	10.810759757982	2.456279056518	-0.127198986184
H	8.220609669760	3.088299128319	1.721255111561
H	9.810290467880	3.058453149020	3.878989355953
H	9.843996625948	0.541459194728	4.867124601946
H	8.258819144411	-0.976350708039	3.324401491777
H	8.374371228670	-2.006548399170	1.391378780063
O	2.805812981992	-2.657533605405	-1.898654693997
H	2.230420085194	-2.334529815367	-2.609163300088

Energies (a.u.)

E	-1202.818623
Zero-point correction	0.403894
Sum of electronic and thermal enthalpies	-1202.390576
Sum of electronic and thermal free energies	-1202.468105

(*R*)-P85-ind Structure

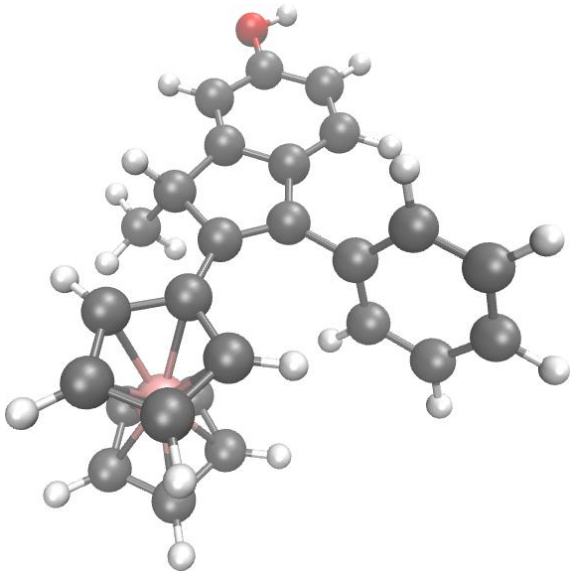

Table S6. Optimized Cartesian coordinates and energies of **(*S*)-P85-ind** at the B3LYP-D3-BJ/6-31+G* (Fe LANL2DZ) level of theory in vacuum.

C	6.808582163917	0.515443065820	1.396987092454
C	6.334577635491	1.199103761583	0.314262332095
C	6.251300262386	-0.907340467466	1.398987618002
C	5.505914111087	0.306171426353	-0.505243197651
C	6.617126883251	2.593180144837	-0.090847905374
C	4.065038759118	-1.778693580045	-1.656486084935
C	7.411323409924	2.849814159837	-1.219420486541
C	7.685567792104	4.160193583966	-1.615973384656
C	7.159023223666	5.235864933893	-0.894504724492
C	6.350834227199	4.991354789888	0.219810482468
C	6.079831519938	3.679685653956	0.615466794515
H	7.823073725415	2.013748468619	-1.778217537151
H	8.311079179048	4.341181816722	-2.486344539408
H	7.372173312226	6.256224754822	-1.201520196867
H	5.930772593308	5.821976111691	0.781047235346
H	5.454624883022	3.486670645023	1.483006379597
C	4.103698542470	-0.523926435505	-2.277124953461
C	4.823966950682	0.529664864238	-1.701384096688
C	4.743509967924	-2.006921744453	-0.448299652437
C	5.461508329422	-0.962376688377	0.109930468232
H	4.691205887888	-2.990171827436	0.010757909624
H	4.847407796415	1.503143884012	-2.183142534106
H	3.567336657971	-0.367738210399	-3.211500728413
Fe	9.821272086593	0.938078393719	2.032726046285
C	7.780069340270	0.932692870802	2.400660208646
C	8.462746508786	0.034207902071	3.299456851041
C	9.409708548785	0.777368791344	4.062203283572
C	9.329851706518	2.141778403025	3.649358987911
C	8.341001717536	2.241584769083	2.627540304785
C	11.618092923234	1.599346534949	1.239695341552
C	11.739957672578	0.238913504240	1.660876660957
C	10.780411580321	-0.534849836482	0.936158808627
C	10.066768933324	0.348325309380	0.067873250901
C	10.583326864694	1.667378494232	0.254554661737
H	12.179542515527	2.437817239179	1.629894655402
H	12.410713741909	-0.132927161086	2.423995673930
H	10.599094402468	-1.595031605474	1.053347919051
H	9.233374358295	0.077505677575	-0.566911749917
H	10.212758899549	2.564970470879	-0.221497073400
H	8.082839686686	3.140884128109	2.091465285625
H	9.944170557480	2.954363900009	4.013828488500
H	10.093142107867	0.370648659525	4.795480082364
H	8.316847891008	-1.035401333228	3.353704143596
O	3.371897971963	-2.840106639041	-2.187818644343
H	2.945787411807	-2.569503953860	-3.015723863058
C	5.366093894154	-1.204179550616	2.626452698526
H	5.927579901999	-1.090632555102	3.558699142432
H	4.516863323211	-0.512713550425	2.651046778341
H	4.973813117136	-2.226202498653	2.580200933992
H	7.078945172427	-1.631211565736	1.374298852790

Energies (a.u.)	
E	-1202.819302
Zero-point correction	0.403705
Sum of electronic and thermal enthalpies	-1202.391384
Sum of electronic and thermal free energies	-1202.469768

(*S*)-P85-ind Structure

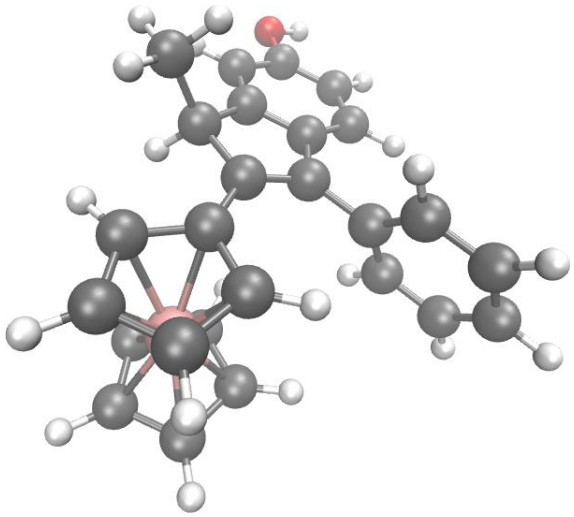

Table S7. Optimized Cartesian coordinates and energies of **(*R*)-P722-ind** at the B3LYP-D3-BJ/6-31+G* (Fe LANL2DZ) level of theory in vacuum.

C	6.705662024309	0.617390102866	1.351461812346
C	6.248487042098	1.214948120958	0.211610034637
C	6.122725620984	-0.791499094498	1.464496995422
H	5.632202187831	-0.936322519554	2.437290779450
C	7.248120898138	-1.842502053937	1.307230543440
H	7.617472468021	-1.811423321264	0.275428817194
C	5.267014692185	0.337916835145	-0.440333224387
C	6.633095942323	2.523279692385	-0.356745647742
C	3.459016305822	-1.635764939106	-1.203415481022
C	7.935748671704	2.740326834887	-0.825665121293
C	8.308295305680	3.963130731114	-1.383980219327
C	7.368695948552	4.994657681494	-1.485352524507
C	6.060113837174	4.794848415643	-1.033974418884
C	5.701144157440	3.566443629482	-0.482990565291
H	8.666053408930	1.942258360181	-0.738938824567
H	9.325512562108	4.112577883132	-1.742276131439
H	5.342606826395	5.604961431947	-1.119721997306
H	4.685223210175	3.415543374820	-0.128330741483
C	3.603384173477	-0.479020357058	-1.977695236481
C	4.511506568412	0.516823979241	-1.598514639966
C	4.229442101827	-1.829204459192	-0.044726343806
C	5.130890993485	-0.842852216103	0.321565461143
H	4.084529841620	-2.737621473891	0.531422775800
H	4.617779327095	1.415778193121	-2.199036002309
H	3.002214005974	-0.352142741132	-2.876245687221
Fe	9.622328583984	1.026031112267	2.642725500227
C	7.550661812084	1.164161362254	2.405568610910
C	7.889583590658	0.483837582559	3.632564875931
C	8.661012124850	1.362151471037	4.446184587081
C	8.819034435727	2.591610652896	3.737724734655
C	8.149461450959	2.473119007031	2.486097351929
C	11.634072170667	1.433900667710	2.353489764442
C	11.477918148053	0.213515619863	3.079800898731
C	10.720421138713	-0.689443148772	2.271274822989
C	10.408992107725	-0.026226596954	1.042616114867
C	10.973517627834	1.285916449319	1.094204656336
H	12.126074157102	2.328471322397	2.711435737461
H	11.827114176601	0.021879616650	4.085573110559
H	10.392738577407	-1.674801155890	2.572951436338
H	9.809714378568	-0.427501018319	0.236274369701
H	10.882930481954	2.049738260197	0.333794589378
H	8.111059235334	3.233189936383	1.722038872284
H	9.387277904614	3.450316365249	4.069942122631
H	9.088274190306	1.118508692954	5.409606266580
H	7.628783918128	-0.532911782732	3.892151921057
H	8.076686135808	-1.567393446451	1.960791392283
O	2.568372921870	-2.630881250970	-1.524002406008
H	2.098880677703	-2.399352510137	-2.340163442253
C	6.819602484671	-3.270808253321	1.650882373912
H	6.352797792811	-3.305156897977	2.640220243770
H	6.131654911454	-3.681090245165	0.910404966477
N	7.979728249225	-4.157908023261	1.683354277047
C	8.873457220285	-4.187535752177	2.747600837749
C	8.350834323710	-4.982931654913	0.619879977283
C	9.638035609385	-5.700956930623	1.009003730581
H	10.402687478068	-5.482532503683	0.257282293938
H	9.459326761539	-6.780441926486	0.983327358601
C	9.986174374721	-5.171275133845	2.409432835689
H	10.944279651462	-4.643306580086	2.449412215650
H	10.015198796858	-5.950224281553	3.177700623658
O	8.759219151023	-3.519196101169	3.759895059092
O	7.731012329239	-5.086935586121	-0.419652400359
O	7.670230513883	6.220304987047	-2.021573014811
H	8.599352723254	6.237920414107	-2.299378898788

Energies (a.u.)	
E	-1676.864747
Zero-point correction	0.510261
Sum of electronic and thermal enthalpies	-1676.321784
Sum of electronic and thermal free energies	-1676.420877

(*R*)-P722-ind Structure

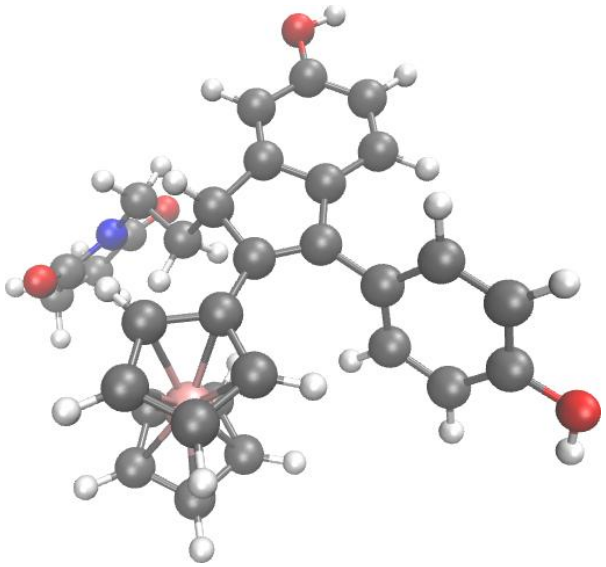

Table S8. Optimized Cartesian coordinates and energies of **(*S*)-P722-ind** at the B3LYP-D3-BJ/6-31+G* (Fe LANL2DZ) level of theory in vacuum.

C	6.585338247657	0.843974748401	1.593817098163
C	6.299099574984	1.314433030799	0.345109020546
C	5.946638886662	-0.528758641613	1.792330750967
H	6.721998318870	-1.265793778925	2.048527017915
C	4.906148405182	-0.501116675066	2.933880409322
H	5.366126480104	-0.034114054322	3.808870591007
C	5.538930611726	0.300253451930	-0.395992144553
C	6.723035708821	2.588436179154	-0.273112740555
C	4.201188447971	-1.945540349802	-1.351132192609
C	7.673370078941	2.592044124902	-1.303443929999
C	8.094629613180	3.784631386135	-1.893879208939
C	7.555439710710	5.000801357706	-1.462027656613
C	6.592084113011	5.017207726127	-0.448090925433
C	6.183270217411	3.818967312248	0.133092367792
H	8.098986389200	1.650104021795	-1.638438298070
H	8.841379060846	3.766938426227	-2.685925848679
H	6.176633588803	5.968162801620	-0.129395594006
H	5.439314709771	3.832364512752	0.924770200069
C	4.374862934507	-0.828586961576	-2.176230662121
C	5.048118737350	0.303356675048	-1.701157472653
C	4.687090071201	-1.951786006795	-0.033123474443
C	5.346519787747	-0.825886147839	0.433817739091
H	4.541682786845	-2.841530458952	0.571223507476
H	5.186639963587	1.167605854894	-2.344718511509
H	3.986953693977	-0.843000194611	-3.193236907832
Fe	9.496871164595	1.182258936773	2.584234488715
C	7.441028252017	1.412786057197	2.627356506992
C	7.895750972137	0.701212530799	3.798961745997
C	8.805176522305	1.532757605119	4.513527025011
C	8.928807409171	2.764265688954	3.801832871430
C	8.101761322646	2.694782865549	2.643185620690
C	11.442008051987	1.503685872149	1.947679283036
C	11.360909118550	0.274214013789	2.672162340371
C	10.426796140726	-0.573971647553	1.999378308276
C	9.932345045973	0.131822796478	0.858852069110
C	10.558046817696	1.416099242009	0.826383634683
H	12.034331090697	2.365900645375	2.223879253517
H	11.881440859797	0.042399818636	3.591828942140
H	10.118072627154	-1.559920623059	2.320494185381
H	9.166028988352	-0.217219639407	0.178993696286
H	10.352230443658	2.202716048049	0.113063348095
H	8.015460862553	3.459952392482	1.888284820484
H	9.573272532165	3.591855058807	4.067162438614
H	9.334748624664	1.259366790376	5.416219177920
H	7.626522169708	-0.307878590830	4.078846299087
H	4.055662446813	0.122954161547	2.636417697860
O	3.560801740801	-3.084150448500	-1.776861652266
H	3.260752811130	-2.967994457542	-2.691517153930
C	4.413531839659	-1.896904887723	3.335851447565
H	3.658367644025	-2.275905110219	2.645756299782
H	5.251761614521	-2.599368792618	3.376815969490
N	3.806851236486	-1.880209675680	4.662722653912
C	2.433999588919	-1.790059365733	4.890958011021
C	4.567300230375	-1.892872453499	5.827907869742
C	3.616885177329	-1.826217752486	7.016528818290
H	3.870376274457	-0.948757776327	7.619648315090
H	3.776493002043	-2.707172333173	7.646097282894
C	2.210236211795	-1.760131551297	6.398956543429
H	1.664130650133	-0.846735168478	6.654187627846
H	1.572285076743	-2.605140038899	6.676068598108
O	1.590742559243	-1.747505771075	4.017009742822
O	5.783521454830	-1.948616525219	5.851650069277
O	7.927224241753	6.207248279262	-1.997930030606
H	8.594097323334	6.068633185730	-2.688465690498

Energies (a.u.)

E	-1676.863345
Zero-point correction	0.510038
Sum of electronic and thermal enthalpies	-1676.320501
Sum of electronic and thermal free energies	-1676.420978

(*S*)-P722-ind Structure

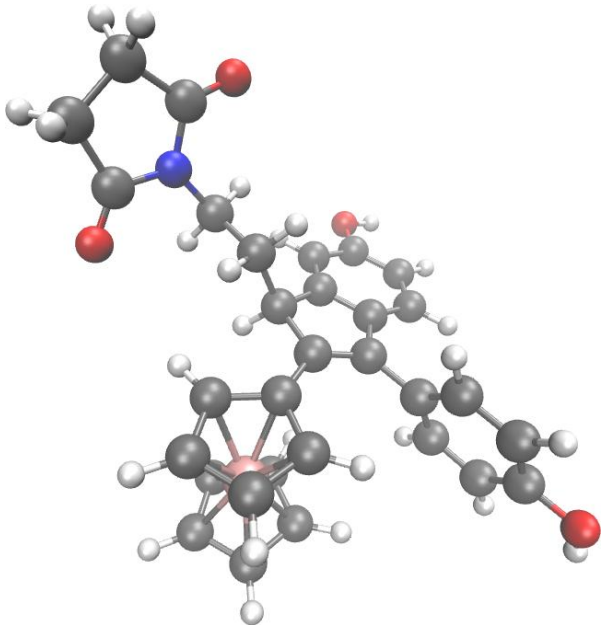

Table S9. Optimized Cartesian coordinates and energies of **P15** at the B3LYP-D3-BJ/6-31+G* (Fe LANL2DZ) level of theory in vacuum.

C	6.942044258077	0.696597023296	1.393783673412
C	6.246108877325	1.133241546972	0.308404971635
C	5.490462490638	0.197413751875	-0.573681654725
C	6.137483448714	2.564844422851	-0.078973547091
C	4.066058278784	-1.517502004750	-2.300732057591
C	6.333469854079	2.969185567835	-1.412831930254
C	6.235603716519	4.304056216667	-1.785864409306
C	5.912042851254	5.279495800474	-0.830416954274
C	5.680153790319	4.895349682793	0.496825470364
C	5.792500861534	3.549790029333	0.854729500698
H	6.574954512874	2.221525414323	-2.163472134190
H	6.401903562354	4.615809013612	-2.812612671611
H	5.412130534704	5.623758144827	1.253253347962
H	5.618023546697	3.260803279083	1.886866082331
C	3.403603830535	-0.477542388678	-1.640270914824
C	4.116849271399	0.372522095952	-0.794923642520
C	5.440337215313	-1.696397265299	-2.116092830875
H	5.946324205717	-2.494761974591	-2.650232487897
H	3.599933441422	1.188501184313	-0.297183934556
H	2.335429126757	-0.328256221955	-1.788943054983
Fe	9.892126377996	1.150334232822	2.364475947172
C	7.864176416383	1.559975448296	2.152256476035
C	8.216508555097	1.400352660930	3.539789028846
C	9.195713835068	2.380410429430	3.879612611979
C	9.472552484780	3.148949383397	2.707425042195
C	8.666611669149	2.642320543546	1.647424145681
C	11.901104230908	1.001736187594	1.873456777967
C	11.616563295668	0.200651837940	3.022228248867
C	10.630050822417	-0.765782479203	2.653028758887
C	10.307316888407	-0.562560445620	1.275111633828
C	11.091023979386	0.530306904438	0.793491544549
H	12.578251369042	1.844807070316	1.838477973750
H	12.041236805915	0.330495065465	4.008768996805
H	10.181251260704	-1.498630234027	3.310379297503
H	9.563775789063	-1.107718275820	0.709238927458
H	11.046970916848	0.953725419091	-0.201026066287
H	8.676078403920	2.990178690583	0.625463939792
H	10.204805454292	3.941017463849	2.623518663441
H	9.674669835795	2.490866075066	4.843469212581
H	7.822509332366	0.649331134690	4.210119385034
O	3.424059825493	-2.384018717583	-3.149229846602
H	2.483089036286	-2.154818150324	-3.200370925724
O	5.835986427514	6.563830355846	-1.289953567702
C	5.518045828500	7.600535983743	-0.364446072124
H	4.531550254209	7.407063452963	0.082053912593
H	6.261958441072	7.614019878842	0.445622490784
C	5.523302135587	8.918728974994	-1.122532955584
H	4.805048875937	8.851204782213	-1.951165358485
H	6.511204671431	9.086290146980	-1.565693597328
C	5.167073233174	10.101481142794	-0.220410523807
H	4.183713592020	9.919510082027	0.250358169618
H	5.899762728556	10.175571526977	0.593359706812
N	5.228029955805	11.354406657279	-0.981390814334
H	4.521250744351	11.362465654204	-1.715358707482
H	5.041273268737	12.153797406961	-0.379715098371
C	5.487447287539	-0.790426696644	2.832996045221
H	5.523040503562	-0.061170834311	3.650686891239
H	4.590504195990	-0.582879523247	2.239322257138
H	5.384213782235	-1.790656331161	3.271664530014
C	6.745927304233	-0.705852022618	1.949875005143
H	7.627016379292	-0.994407856829	2.529853862018
H	6.649790806583	-1.435741264417	1.143238933382
C	6.136060985404	-0.843246982247	-1.262392749525
H	7.207149578274	-0.974938178158	-1.133183214682

Energies (a.u.)	
E	-1452.532441
Zero-point correction	0.532761
Sum of electronic and thermal enthalpies	-1451.967393
Sum of electronic and thermal free energies	-1452.067983

P15 Structure

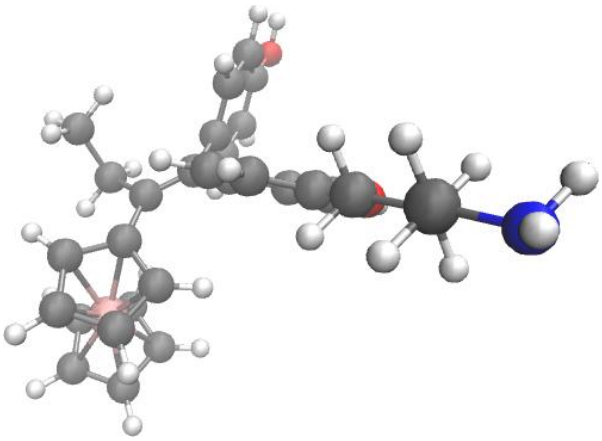

Table S10. Optimized Cartesian coordinates and energies of **P85** at the B3LYP-D3-BJ/6-31+G* (Fe LANL2DZ) level of theory in vacuum.

C	6.838536248060	0.343956105567	1.202816400023
C	6.156368158920	0.373019464478	0.025756787381
C	5.353663264080	-0.515534381012	3.060308253646
H	5.232934171609	-1.293045198868	3.824651622604
H	5.396415208947	0.456239810936	3.565678241783
C	5.385240821852	-0.803249041263	-0.470915629504
C	6.077410099706	1.572569346177	-0.852940470760
C	3.932742470882	-2.998118768444	-1.482305780845
C	6.296560772683	1.460000688401	-2.235831388633
C	6.210714855205	2.577576045882	-3.067949010017
C	5.879071325101	3.826712063776	-2.534454005497
C	5.630219183296	3.945955242835	-1.163238726102
C	5.726748593065	2.829654481219	-0.332813847212
H	6.541174875895	0.487881027973	-2.655426012313
H	6.397699097388	2.472166049822	-4.133573750601
H	5.805593957427	4.696472599171	-3.181835835867
H	5.358066263777	4.909711816812	-0.740517563962
H	5.538016656142	2.924809436352	0.732363570092
C	3.287023103513	-1.781807731701	-1.236896180927
C	4.014103129741	-0.697684468319	-0.745045282366
C	5.304391581645	-3.120170069822	-1.240266077357
C	6.014211178006	-2.029934882365	-0.742216481797
H	5.797270096135	-4.063727740118	-1.453460882458
H	7.083282156050	-2.123105888421	-0.569851846371
H	3.509663901303	0.248942785657	-0.571062059697
H	2.221082491046	-1.679294718686	-1.433184242433
Fe	9.790037507599	1.067997089940	1.971175595427
C	7.771343826254	1.407595881180	1.613010770449
C	8.117848870656	1.744260662720	2.970191691422
C	9.111888694316	2.766625263871	2.948214845953
C	9.404044645535	3.066067879147	1.582216246078
C	8.592288266660	2.229282234033	0.763699180197
C	11.797098311665	0.726175966411	1.579061016865
C	11.497295276698	0.385716900506	2.934202240920
C	10.495380763942	-0.633864199396	2.921911133737
C	10.178503361299	-0.924468397604	1.558374854585
C	10.981280819341	-0.083442536708	0.728399895282
H	12.488216416887	1.492633085238	1.254439920528
H	11.922542130978	0.848443735210	3.814815715148
H	10.033383910978	-1.081268093568	3.791929400173
H	9.426984817524	-1.622807585853	1.215205309161
H	10.946067600849	-0.037065498830	-0.351841044994
H	8.611170424244	2.192309185888	-0.315058700902
H	10.149237858909	3.766567186321	1.229449662624
H	9.590217019291	3.204653963009	3.814169721979
H	7.708732879493	1.286514540970	3.859960732274
H	4.463102980825	-0.521495472766	2.422532083609
C	6.617957308079	-0.767139696944	2.218251298675
H	6.513959033867	-1.734145030688	1.721602253204
H	7.491666963827	-0.842795104445	2.871499941326
O	3.276842498650	-4.099838993023	-1.970384857359
H	2.339125790160	-3.890714560660	-2.102930297173

Energies (a.u.)

E	-1204.011265
Zero-point correction	0.425555
Sum of electronic and thermal enthalpies	-1203.560235
Sum of electronic and thermal free energies	-1203.641963

P85 Structure

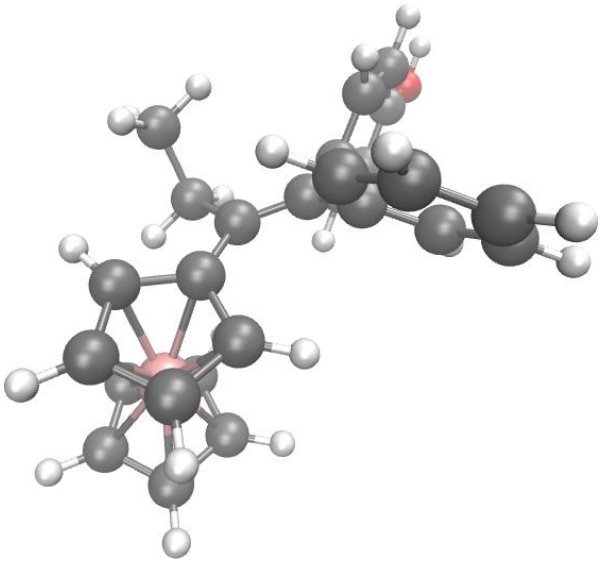

Table S11. Optimized Cartesian coordinates and energies of **P85-QM** at the B3LYP-D3-BJ/6-31+G* (Fe LANL2DZ) level of theory in vacuum.

C	6.394879769494	0.833484825220	1.827443147146
C	6.027783447067	0.577507366703	0.409605427790
C	5.548125113788	0.569893292560	2.846601112327
H	5.892141870717	0.828600574572	3.847758299047
C	4.168231846697	-0.011603689971	2.766133617790
H	3.464422790622	0.596198046954	3.349311259106
H	3.799853942493	-0.083783431341	1.740086230442
C	5.759964864810	-0.697392205922	-0.042502557600
C	5.990163143862	1.762102628320	-0.471129937244
C	5.229660656515	-3.394537649184	-0.974342717532
O	5.008975882318	-4.544678254419	-1.373514123253
C	6.628425646747	1.762061121677	-1.724721543671
C	6.632922587124	2.907957320606	-2.519428560622
C	5.995078729790	4.071376267930	-2.077730549453
C	5.361468872207	4.084939293557	-0.830606598502
C	5.370350552803	2.944726971357	-0.029071056405
H	7.151605121988	0.870118222198	-2.054072968902
H	7.142006842376	2.895666597725	-3.479233222167
H	5.999419684337	4.963974210265	-2.697041161679
H	4.869126364612	4.987523204488	-0.479417154167
H	4.899282288840	2.959548693233	0.949350326377
C	4.908706363080	-2.209616820576	-1.784765666622
C	5.166676256161	-0.953758507564	-1.347926828796
C	5.824079178176	-3.125053936722	0.344427752521
C	6.056235647743	-1.863867822412	0.777117434352
H	6.083093997699	-3.991155943208	0.946818766094
H	6.521367197187	-1.694902218092	1.742336336258
H	4.881035950431	-0.102772419501	-1.957134527327
H	4.432715423525	-2.391769726920	-2.744004752515
Fe	9.575174373323	0.736597327810	1.402557564255
C	7.731321062459	1.406012019353	2.109183004584
C	8.568172836328	0.987637826509	3.198363570832
C	9.756801931045	1.775212782560	3.188056392597
C	9.669384523813	2.684516726730	2.090886624041
C	8.432882441628	2.453935774471	1.416801951769
C	11.301482559878	0.412145317594	0.307572994332
C	11.156557515887	-0.597865904649	1.308409119794
C	9.926215751593	-1.284397728243	1.067596482526
C	9.313748595829	-0.700673246623	-0.082905018791
C	10.159722959932	0.350339368775	-0.550051434975
H	12.109545548159	1.128373892273	0.240049791329
H	11.837759729068	-0.781460393138	2.128595587698
H	9.515243731168	-2.086845309976	1.665324575103
H	8.363120924513	-0.989028229229	-0.505197434429
H	9.952515085067	1.011510470597	-1.380947323379
H	8.092859848317	2.973085695410	0.534258905352
H	10.429009644661	3.393280617785	1.788990281269
H	10.597102811890	1.665807132228	3.860494927617
H	8.346580141933	0.175553543869	3.877745647184
H	4.144149130064	-1.022072959662	3.198550611928

Energies (a.u.)

E	-1202.780195
Zero-point correction	0.402250
Sum of electronic and thermal enthalpies	-1202.353108
Sum of electronic and thermal free energies	-1202.432507

P85-QM Structure

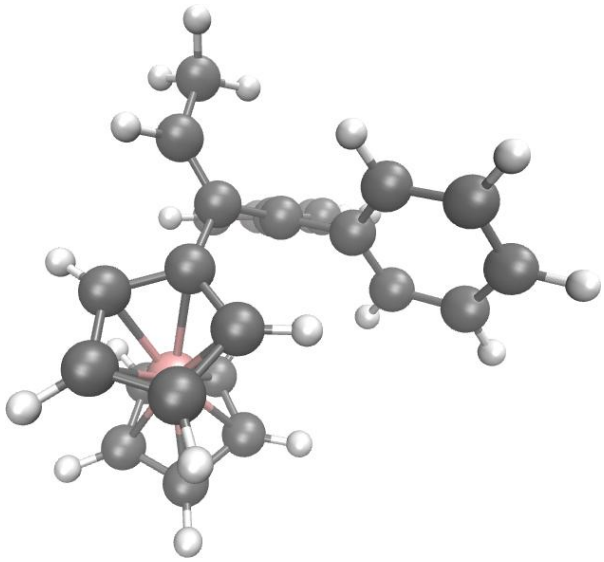

Table S12. Optimized Cartesian coordinates and energies of **(*R*)-P85-ind** at the B3LYP-D3-BJ/6-31+G* (Fe LANL2DZ) level of theory in vacuum.

C	6.944005228261	0.455527737270	1.098250752596
C	6.326411621272	1.193822748867	0.128866998823
C	6.440433829322	-0.988188644633	1.045090588655
H	6.020182587154	-1.278755166761	2.018723137452
C	7.537586392789	-2.000906782455	0.652674469240
H	7.121263926202	-3.013035746103	0.597144265383
H	7.943445540141	-1.746610804494	-0.332196101003
C	5.340081204417	0.364803667258	-0.571493443136
C	6.560150631166	2.608868090448	-0.233749628929
C	3.626170857597	-1.633222232223	-1.536025104281
C	7.746038405548	2.987843976959	-0.881231598788
C	7.969626993494	4.318615251590	-1.237379273327
C	7.005963135198	5.291660169144	-0.953965624806
C	5.814997486547	4.922239158336	-0.322029571348
C	5.591188178018	3.588643015461	0.029061289547
H	8.493780322219	2.229400886684	-1.091262022579
H	8.894619085891	4.597022695973	-1.736025699937
H	7.180236719541	6.328896449261	-1.227281120305
H	5.060433446807	5.672593143014	-0.100674323905
H	4.667856533576	3.300624863556	0.524550867223
C	3.608703381374	-0.339705322222	-2.089427912617
C	4.462336233234	0.659858575800	-1.616175161058
C	4.525763734484	-1.927110271869	-0.489354292868
C	5.362953466898	-0.930196834677	-0.017443069249
H	4.553637695639	-2.931150980759	-0.068982391842
H	4.437905733537	1.652494920188	-2.057709898574
H	2.922772359294	-0.121993758920	-2.905288842866
Fe	9.955813225394	0.898324241560	2.076809468938
C	7.870991872101	0.903761289407	2.129277862546
C	8.409028349805	0.076712662454	3.180910068956
C	9.235011586830	0.877002396849	4.021919786672
C	9.223835102360	2.208016045202	3.506114726008
C	8.397366178613	2.228674210325	2.345819559598
C	11.889976933261	1.486356802032	1.620181115221
C	11.884863693478	0.133198676053	2.079264835594
C	11.052125546192	-0.627605589976	1.201247789925
C	10.542540994968	0.255571372661	0.199362868309
C	11.060337491297	1.561994986755	0.458132928391
H	12.395895880829	2.316853410451	2.094256458523
H	12.388172249506	-0.240975596028	2.960825274228
H	10.820558687208	-1.679626376971	1.298069286515
H	9.844744574362	-0.008944245803	-0.583842731722
H	10.828089443692	2.460978987838	-0.096600295875
H	8.217717716325	3.089635564433	1.721821147876
H	9.782361864422	3.047987024754	3.897429870233
H	9.799033264440	0.526552597423	4.876004013764
H	8.228525084967	-0.981064137746	3.307945770735
H	8.361660481257	-2.001413487500	1.369619361547
N	2.803738331213	-2.641581596105	-2.061403489187
H	2.589678092342	-3.395449797745	-1.419276543318
H	1.967843585517	-2.309926055017	-2.528040280979

Energies (a.u.)	
E	-1182.955976
Zero-point correction	0.416525
Sum of electronic and thermal enthalpies	-1182.515013
Sum of electronic and thermal free energies	-1182.593028

(*R*)-P85-ind Structure

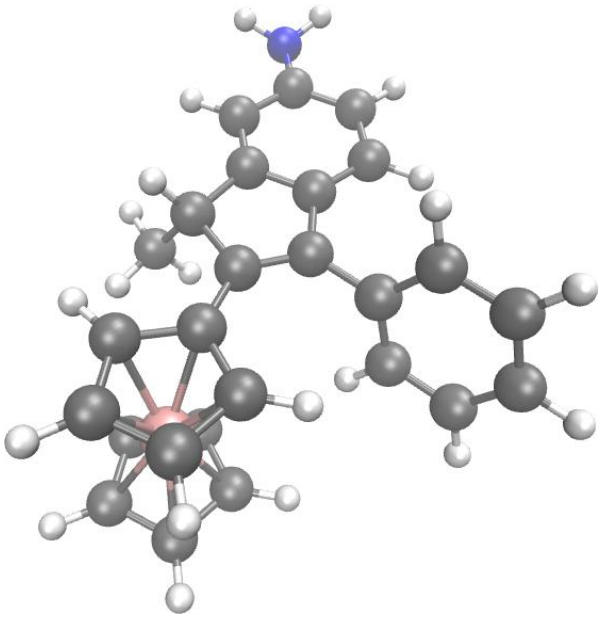

Table S13. Optimized Cartesian coordinates and energies of **(*S*)-P85-ind** at the B3LYP-D3-BJ/6-31+G* (Fe LANL2DZ) level of theory in vacuum.

C	6.790134562524	0.532147880412	1.387945902148
C	6.329579365357	1.217429670003	0.299975615910
C	6.221789679104	-0.886579136484	1.385273961573
C	5.500434568306	0.330912008735	-0.524621324974
C	6.627840107424	2.608138303167	-0.105027013297
C	4.035519665276	-1.757507946070	-1.689731347048
C	7.423540924419	2.855527317447	-1.234661281403
C	7.713112462588	4.162553136881	-1.631328055430
C	7.200509857241	5.244514856940	-0.909188613545
C	6.390628794745	5.009512465509	0.205954578532
C	6.104456025378	3.701119506568	0.601775027251
H	7.823707149876	2.014585567470	-1.794503890508
H	8.339518686977	4.336003029864	-2.502614658824
H	7.425491170477	6.262294366738	-1.216435045165
H	5.981009375033	5.845070233578	0.767667215044
H	5.477713457104	3.515430739931	1.469815680238
C	4.099134059421	-0.492195610558	-2.301854945479
C	4.824553603628	0.553657245451	-1.725792147597
C	4.715565388125	-1.972890721979	-0.472402718902
C	5.440422677206	-0.935592770835	0.090066891383
H	4.672676365442	-2.951417592749	0.003208111863
H	4.856674069641	1.526215919062	-2.209538181323
H	3.575194364733	-0.331685698969	-3.241702017718
Fe	9.805932552624	0.929010436486	2.039986934504
C	7.760955271749	0.940254682626	2.395999602501
C	8.431687190678	0.035177918844	3.297142399401
C	9.381417153324	0.769038407453	4.066017004448
C	9.315360638296	2.134524313274	3.654428524790
C	8.332406869074	2.243674945735	2.627526497236
C	11.610249518964	1.578119819885	1.253786073851
C	11.721216426486	0.216726907316	1.675087626083
C	10.758944342615	-0.550141002852	0.946531999120
C	10.054656305306	0.338031334225	0.075696898210
C	10.579552729987	1.653405962813	0.264831676608
H	12.176009982303	2.412646502883	1.646248024701
H	12.386664062993	-0.159983407942	2.440491740216
H	10.569752266559	-1.609066664188	1.062797731470
H	9.221371003364	0.073405211094	-0.561828964899
H	10.216505216912	2.553540567650	-0.212235525364
H	8.085430960417	3.145665157931	2.090707484502
H	9.934642952763	2.941559808457	4.022889503675
H	10.057217906488	0.355493277239	4.802589392920
H	8.276666654343	-1.033299062004	3.348806998802
N	3.356803992294	-2.815674370318	-2.313738576851
H	3.027250588982	-3.539905686772	-1.686316204577
H	2.629498477375	-2.532680447019	-2.959961031863
H	7.044420498143	-1.616508033220	1.366504872103
C	5.326923766846	-1.176094137362	2.607146295782
H	5.882604805135	-1.065066705282	3.543301633199
H	4.482160236024	-0.478874866840	2.624996406648
H	4.928066759930	-2.195884290222	2.560372290056

Energies (a.u.)	
E	-1182.956682
Zero-point correction	0.416451
Sum of electronic and thermal enthalpies	-1182.515795
Sum of electronic and thermal free energies	-1182.593702

(*S*)-P85-ind Structure

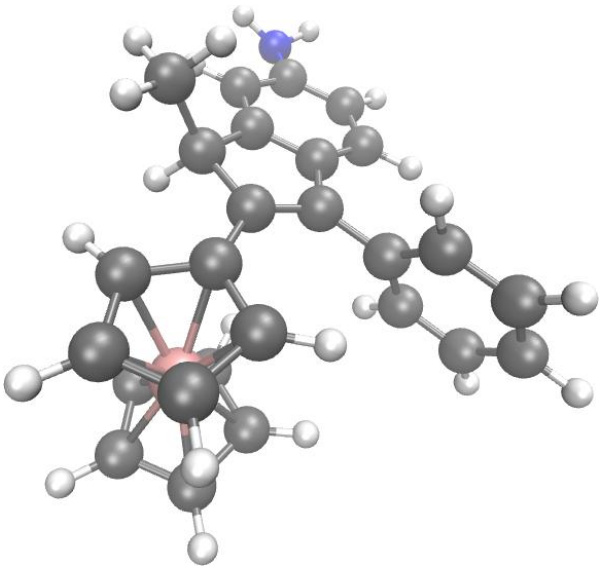

Figure S1. Docking cluster distribution and best docked conformation for the **(*R*)-P5-ind** – Cathepsin B complex.

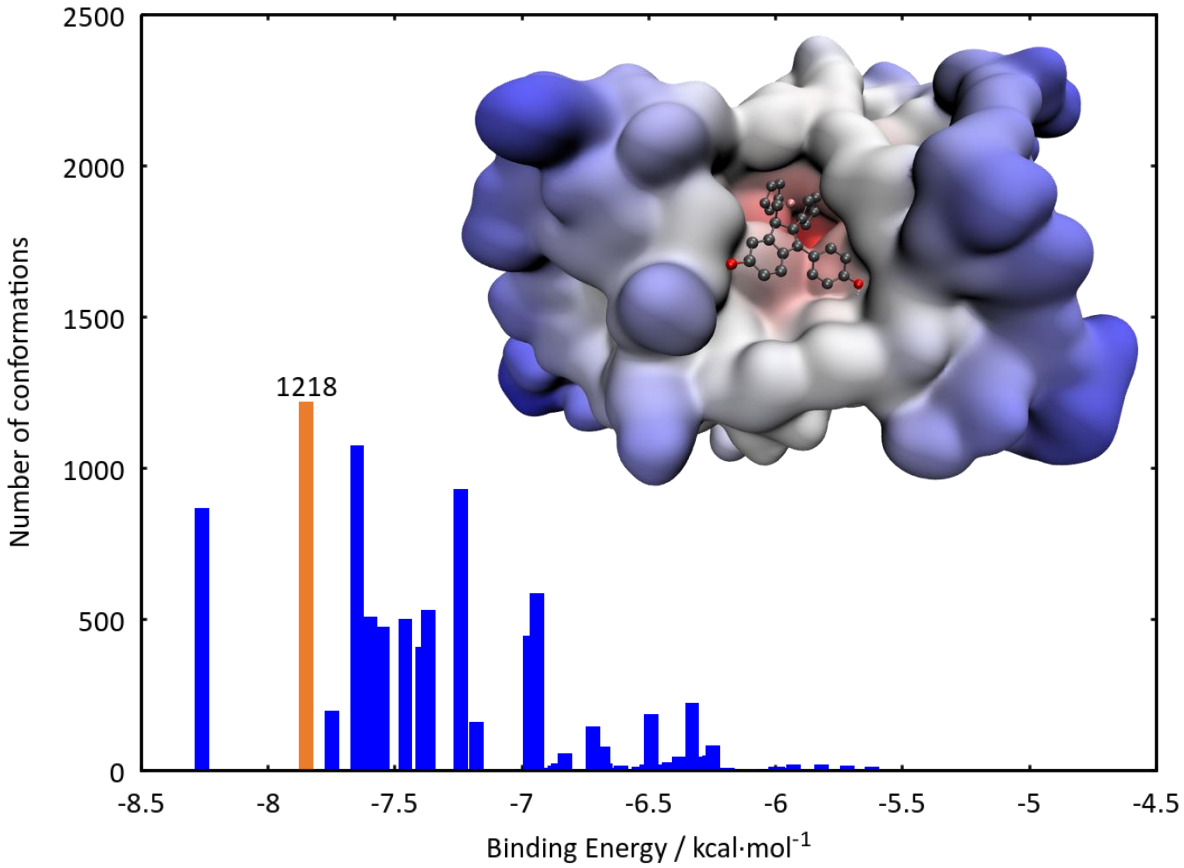

N.B. This **clustered distribution** is considered to be somewhere **intermediate** between a well clustered distribution and a dispersed one. It shows **75 clusters containing less than 100 poses** (1 % of the total number of poses), with a total of **10.23 % of the total number of poses classified into these low populated clusters**.

Figure S2. Docking cluster distribution and best docked conformation for the **(*S*)-P5-ind** – Cathepsin B complex.

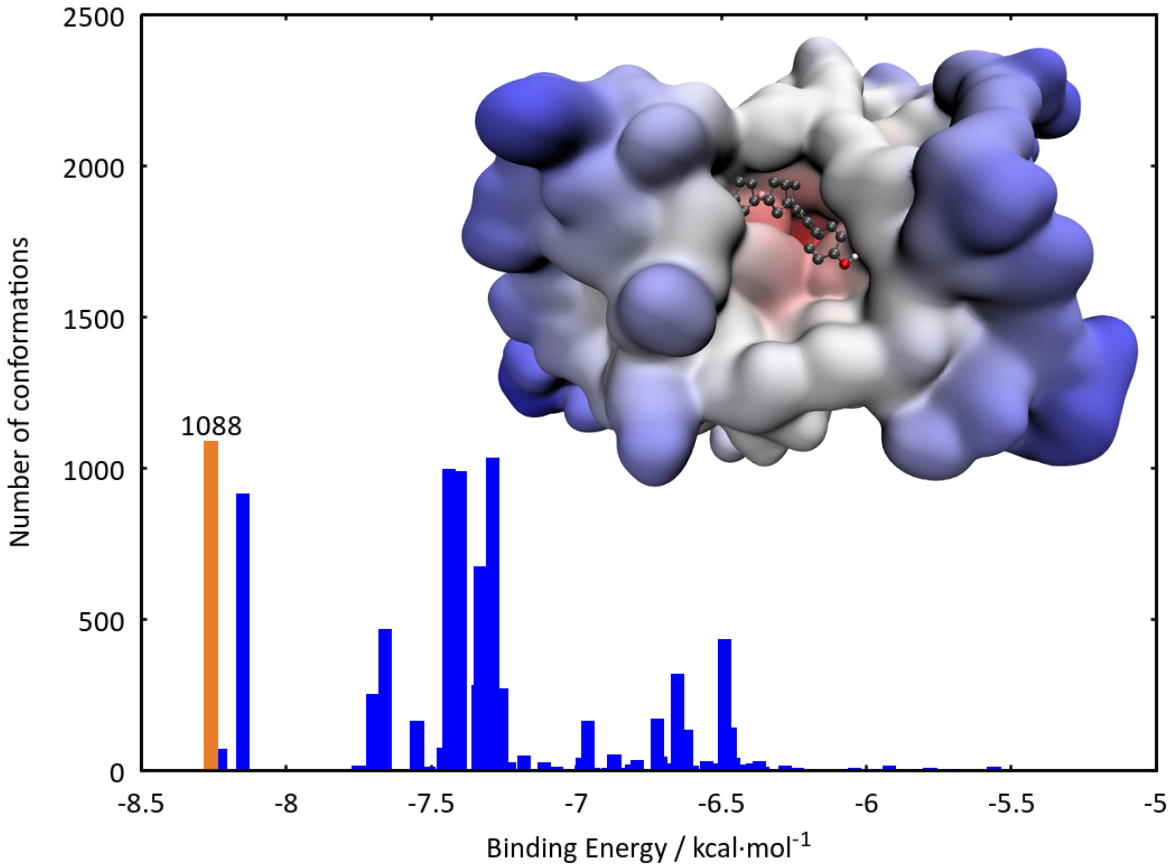

N.B. This **clustered distribution** is considered to be somewhere **intermediate** between a well clustered distribution and a dispersed one. It shows **84 clusters containing less than 100 poses** (1 % of the total number of poses), with a total of **9.65 % of the total number of poses classified into these low populated clusters**.

Figure S3. Docking cluster distribution and best docked conformation for the **(*R*)-P15-ind** – Cathepsin B complex.

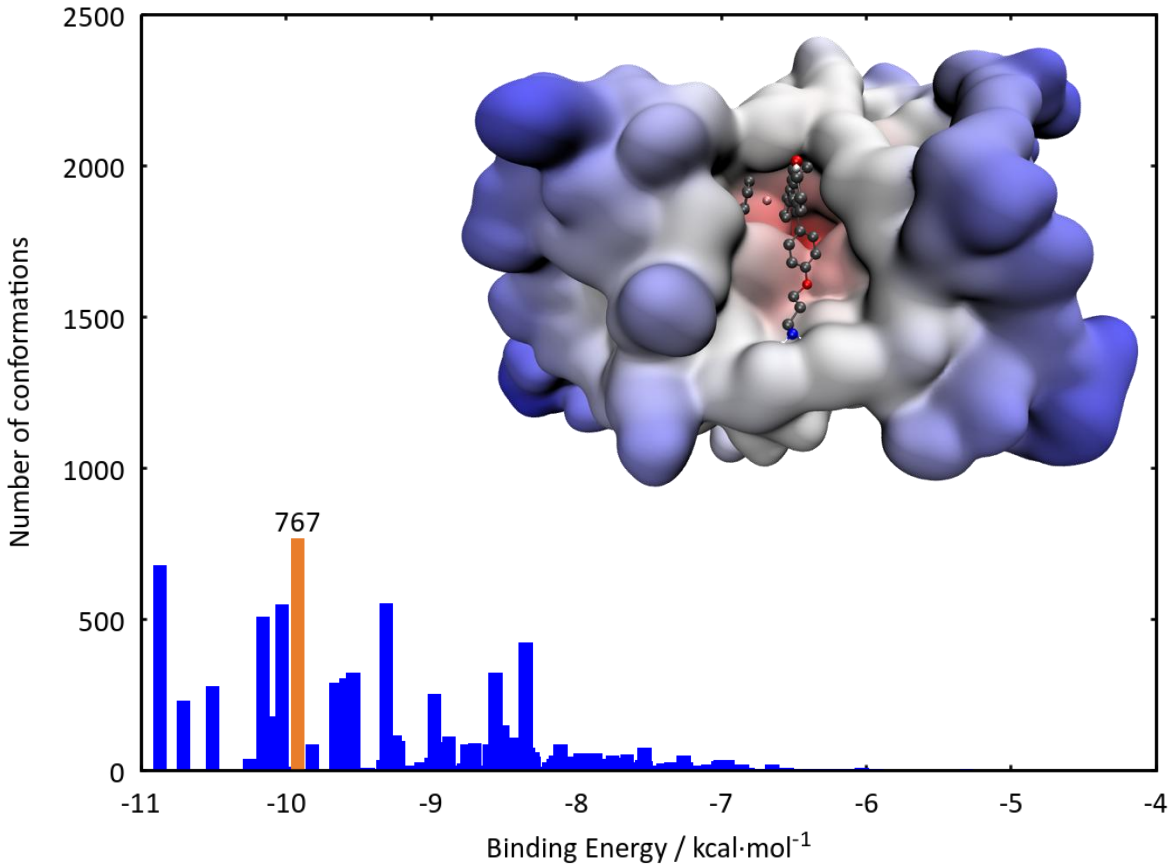

N.B. This **clustered distribution** is considered to be a **dispersed** distribution. It shows **385 clusters containing less than 100 poses** (1 % of the total number of poses), with a total of **38.55 % of the total number of poses classified into these low populated clusters**.

Figure S4. Docking cluster distribution and best docked conformation for the **(*S*)-P15-ind** – Cathepsin B complex.

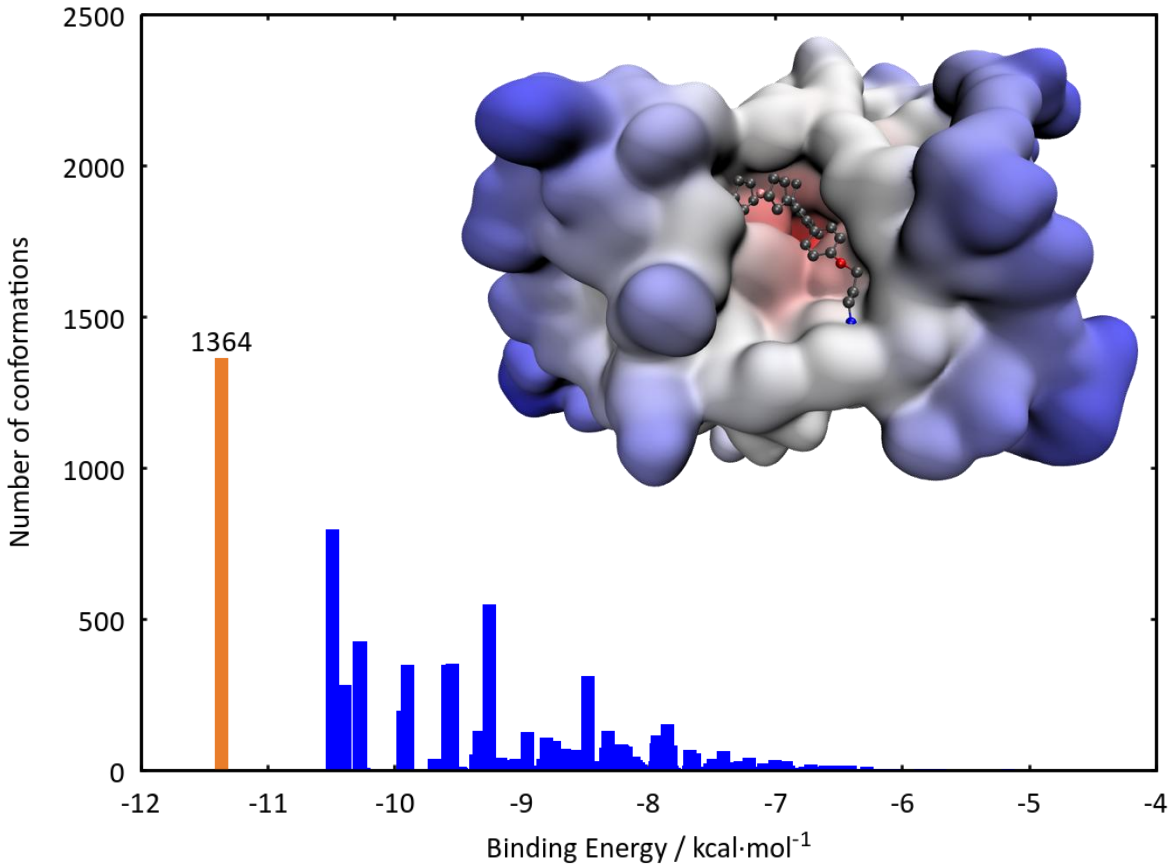

N.B. This **clustered distribution** is considered to be a **dispersed** distribution. It shows **360 clusters containing less than 100 poses** (1 % of the total number of poses), with a total of **34.25 % of the total number of poses classified into these low populated clusters**.

Figure S5. Docking cluster distribution and best docked conformation for the **(*R*)-P85-ind** – Cathepsin B complex.

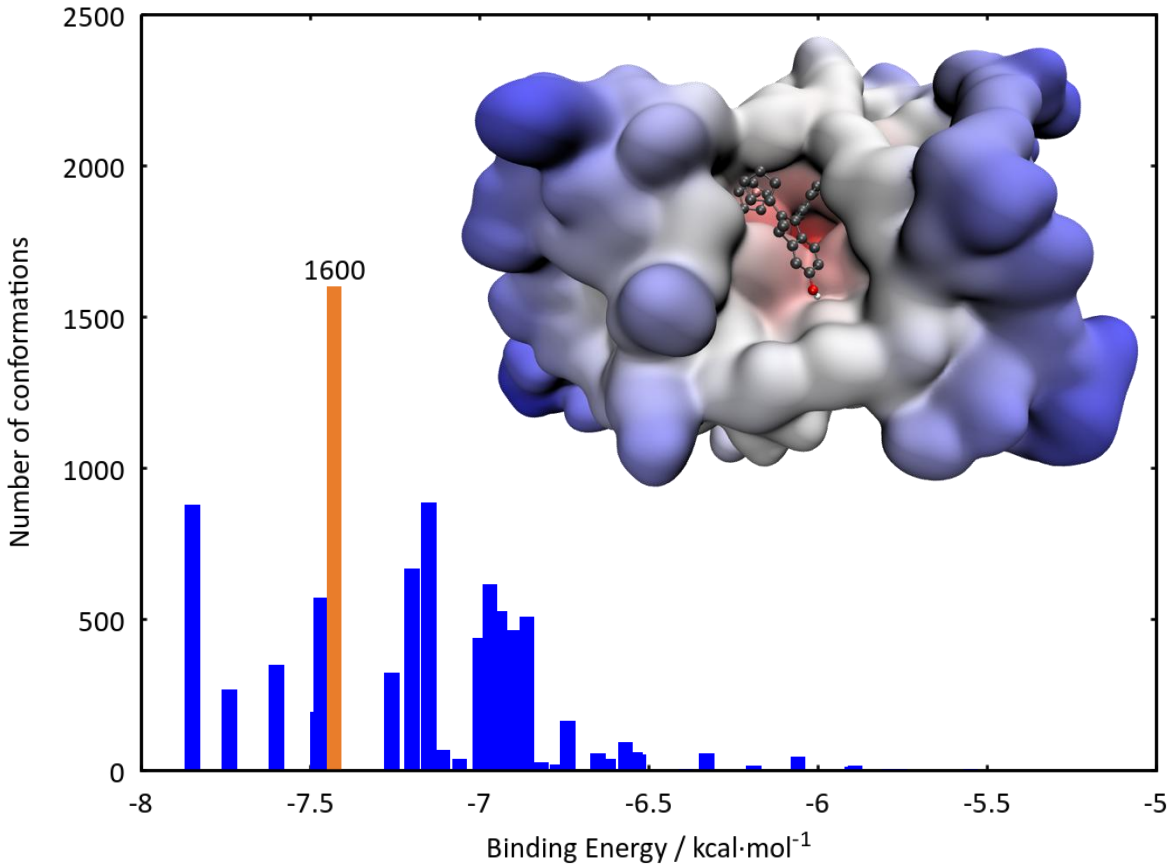

N.B. This **clustered distribution** is considered to be a **well clustered** distribution. It shows only **34 clusters containing less than 100 poses** (1 % of the total number of poses), with a total of **7.02 % of the total number of poses classified into these low populated clusters**.

Figure S6. Docking cluster distribution and best docked conformation for the **(*S*)-P85-ind** – Cathepsin B complex.

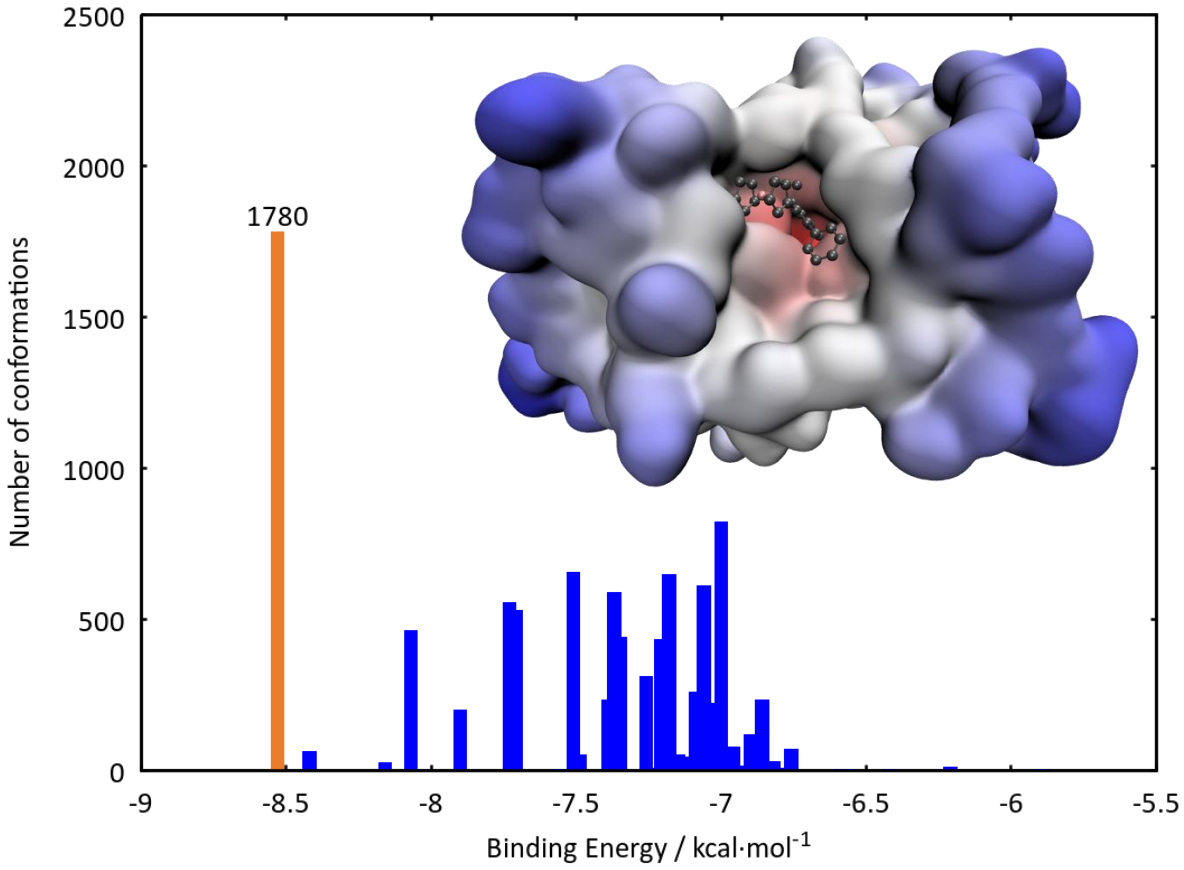

N.B. This **clustered distribution** is considered to be a **well clustered** distribution. It shows **40 clusters containing less than 100 poses** (1 % of the total number of poses), with a total of **7.55 % of the total number of poses classified into these low populated clusters**.

Figure S7. Docking cluster distribution and best docked conformation for the **(*R*)-P722-ind** – Cathepsin B complex.

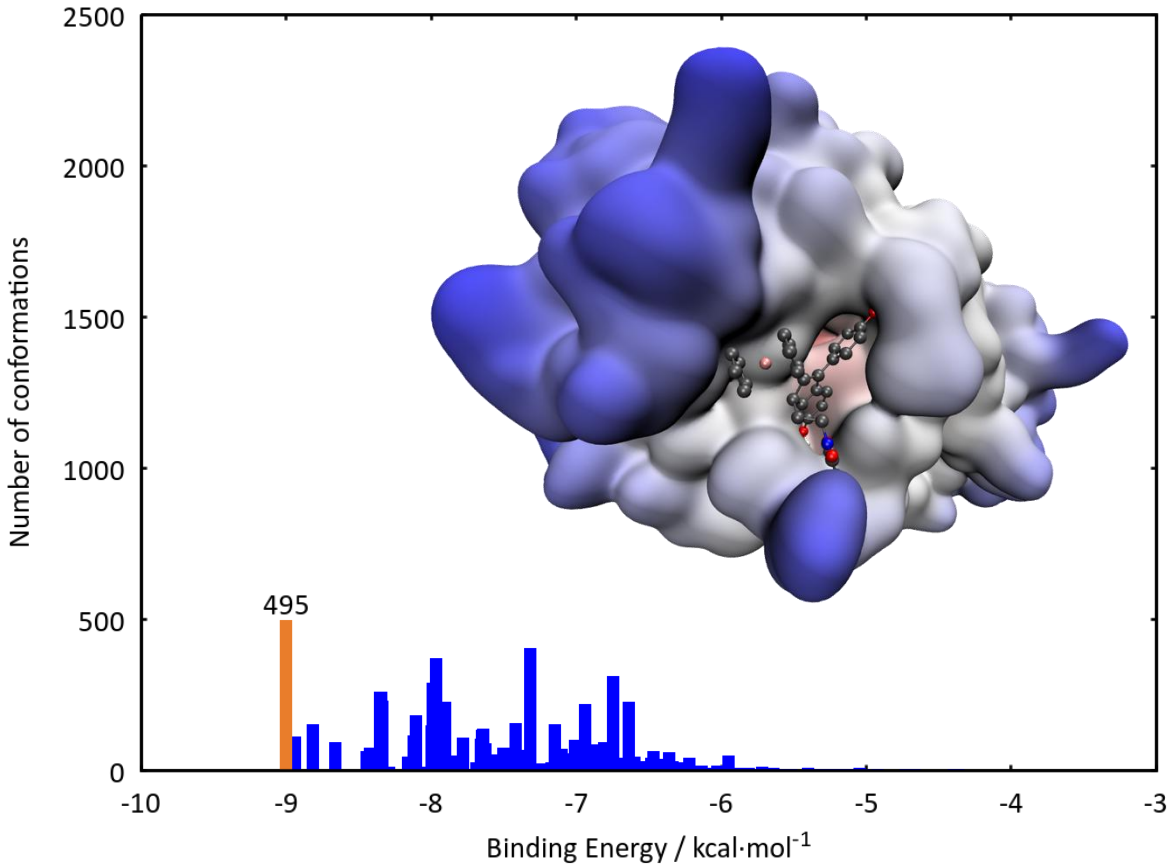

N.B. This **clustered distribution** is considered to be a **dispersed** distribution. It shows **437 clusters containing less than 100 poses** (1 % of the total number of poses), with a total of **49.99 % of the total number of poses classified into these low populated clusters**.

Figure S8. Docking cluster distribution and best docked conformation for the **(*S*)-P722-ind** – Cathepsin B complex.

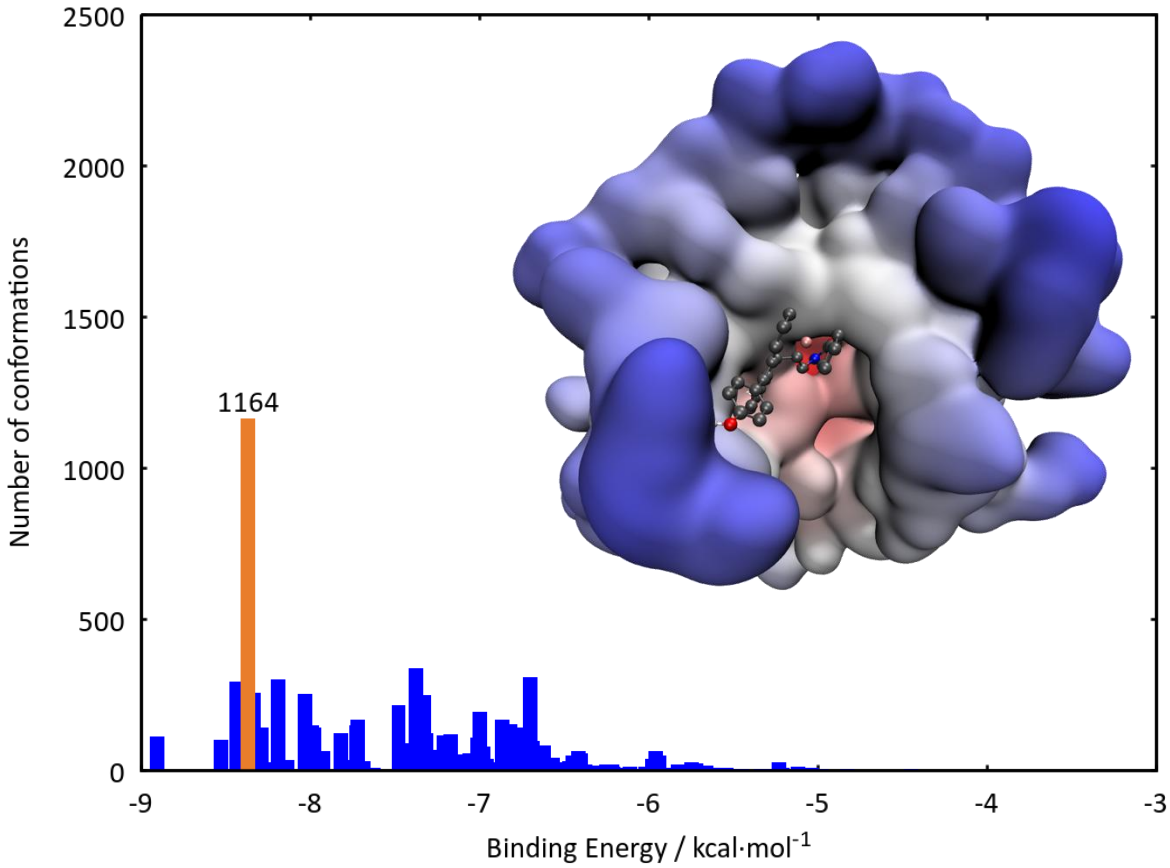

N.B. This **clustered distribution** is considered to be a **dispersed** distribution. It shows **370 clusters containing less than 100 poses** (1 % of the total number of poses), with a total of **44.18 % of the total number of poses classified into these low populated clusters**.

Figure S9. Docking cluster distribution and best docked conformation for the **P15** – Cathepsin B complex.

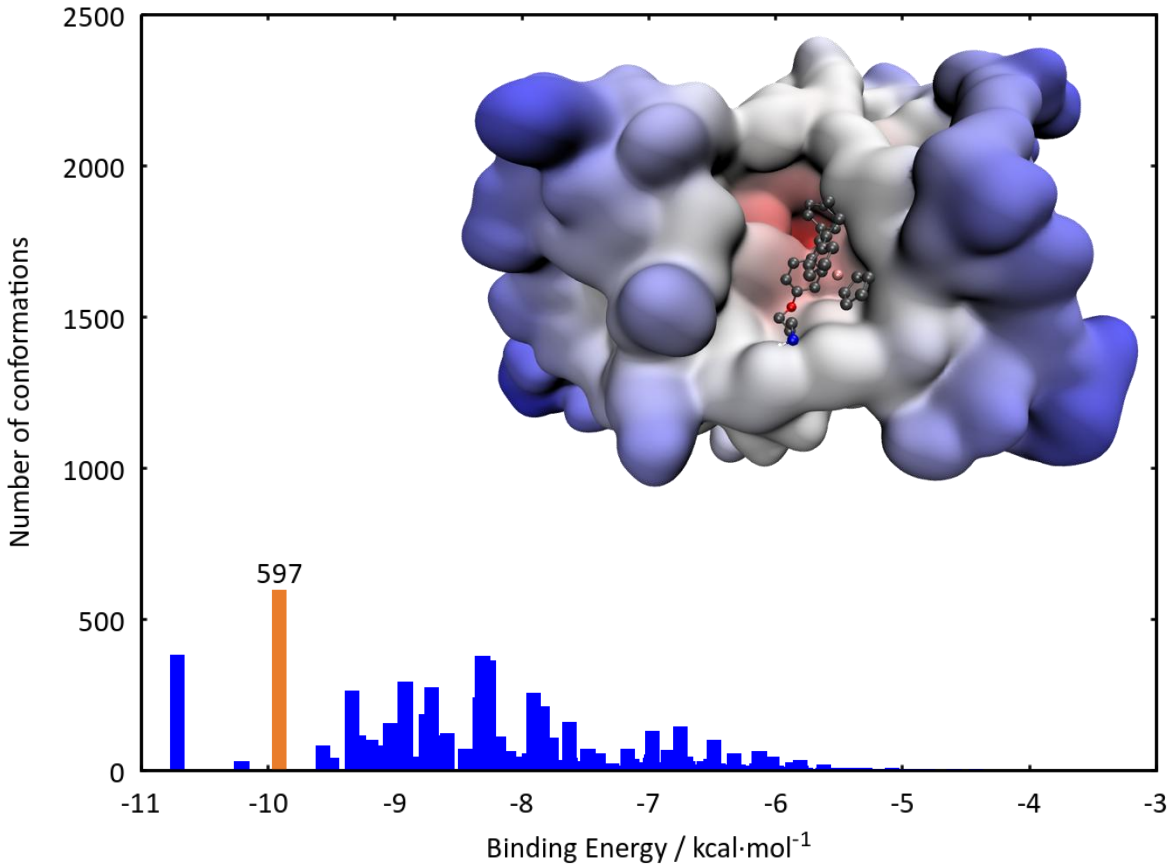

N.B. This **clustered distribution** is considered to be a **dispersed** distribution. It shows **618 clusters containing less than 100 poses** (1 % of the total number of poses), with a total of **49.62 % of the total number of poses classified into these low populated clusters**.

Figure S10. Docking cluster distribution and best docked conformation for the **P85** – Cathepsin B complex.

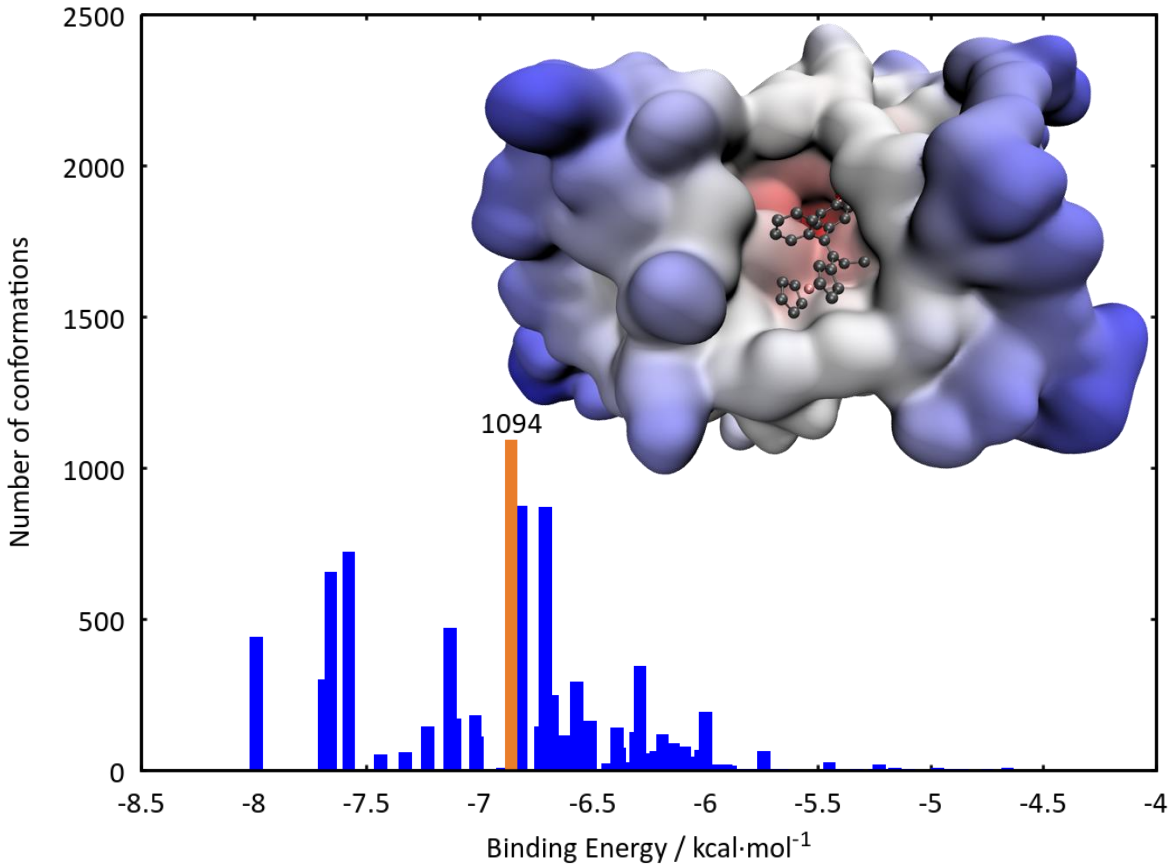

N.B. This **clustered distribution** is considered to be somewhere **intermediate** between a well clustered distribution and a dispersed one. It shows **96 clusters containing less than 100 poses** (1 % of the total number of poses), with a total of **15.06 % of the total number of poses classified into these low populated clusters**.

Figure S11. Docking cluster distribution and best docked conformation for the **P85-QM** – Cathepsin B complex.

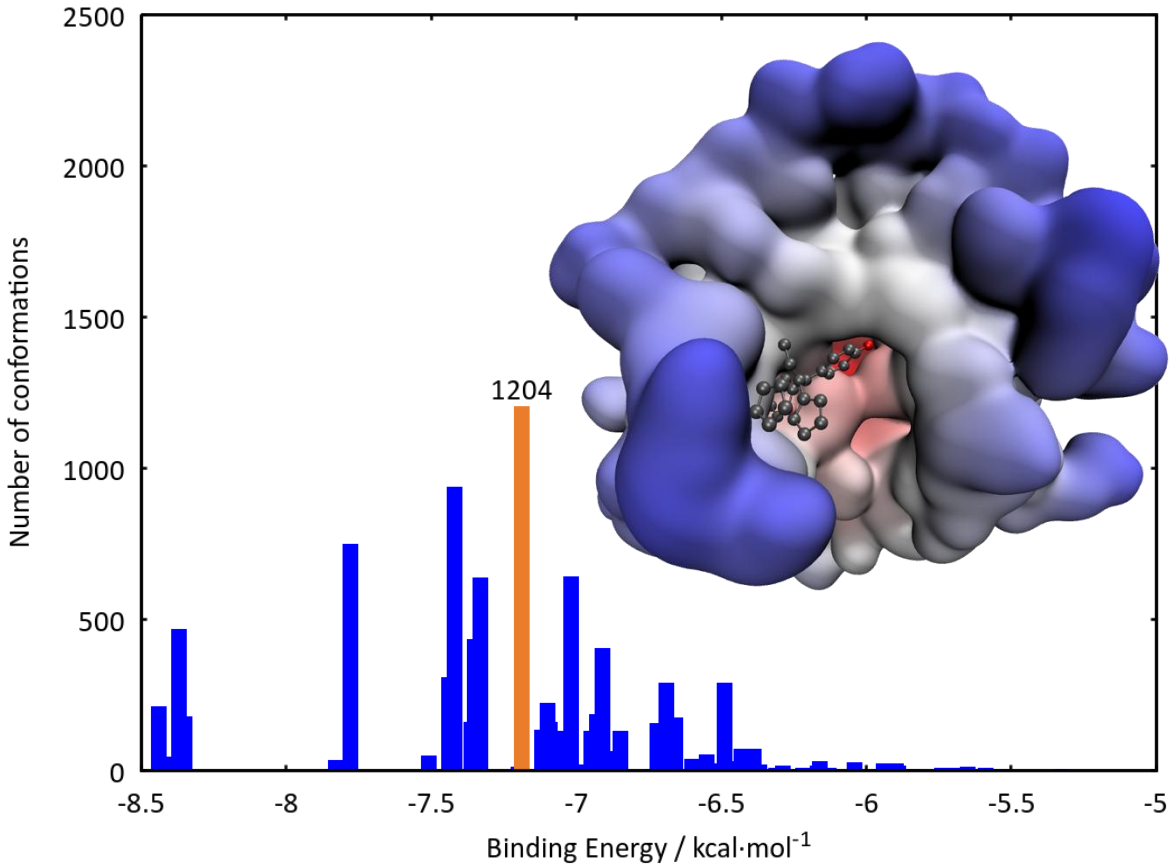

N.B. This **clustered distribution** is considered to be somewhere **intermediate** between a well clustered distribution and a dispersed one. It shows **91 clusters containing less than 100 poses** (1 % of the total number of poses), with a total of **13.46 % of the total number of poses classified into these low populated clusters**.

Figure S12. Docking cluster distribution and best docked conformation for the **(*R*)-P35-ind** – Cathepsin B complex.

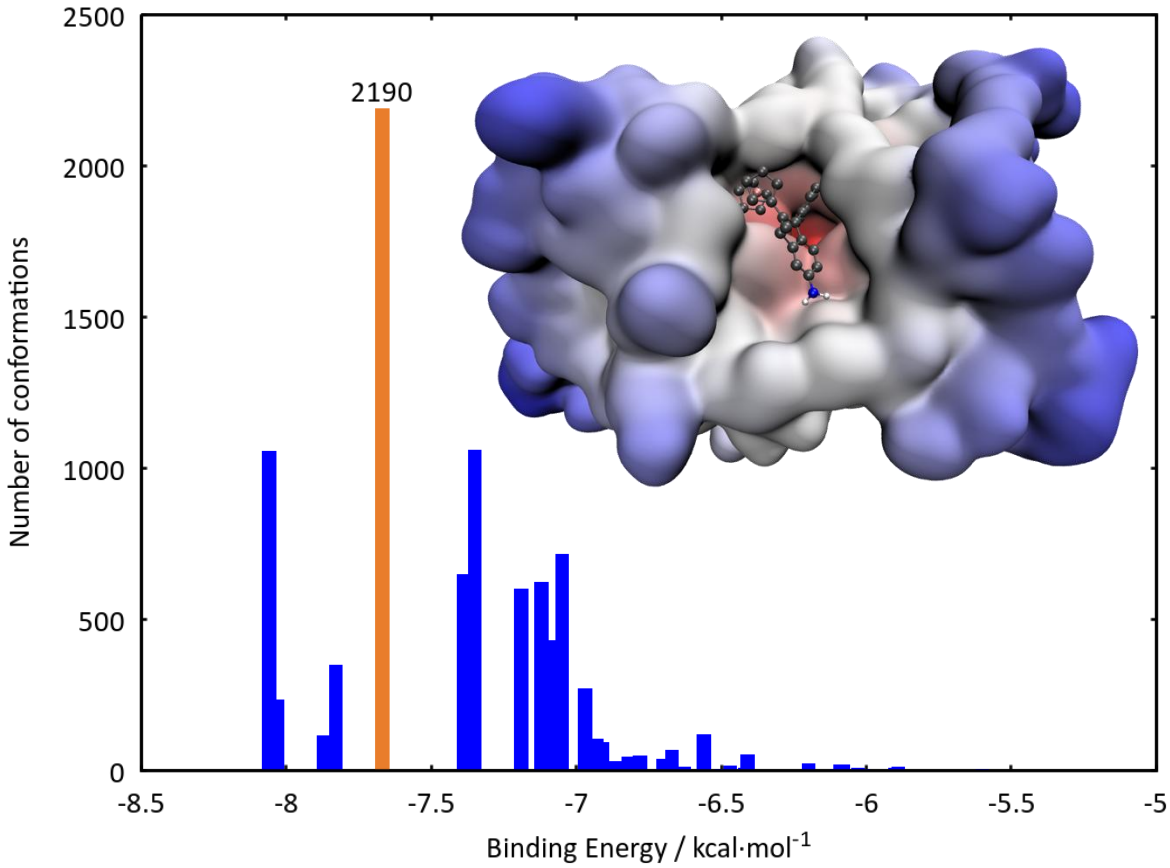

N.B. This **clustered distribution** is considered to be a **well clustered** distribution. It shows only **38 clusters containing less than 100 poses** (1 % of the total number of poses), with a total of **9.33 % of the total number of poses classified into these low populated clusters**.

Figure S13. Docking cluster distribution and best docked conformation for the **(*S*)-P35-ind** – Cathepsin B complex.

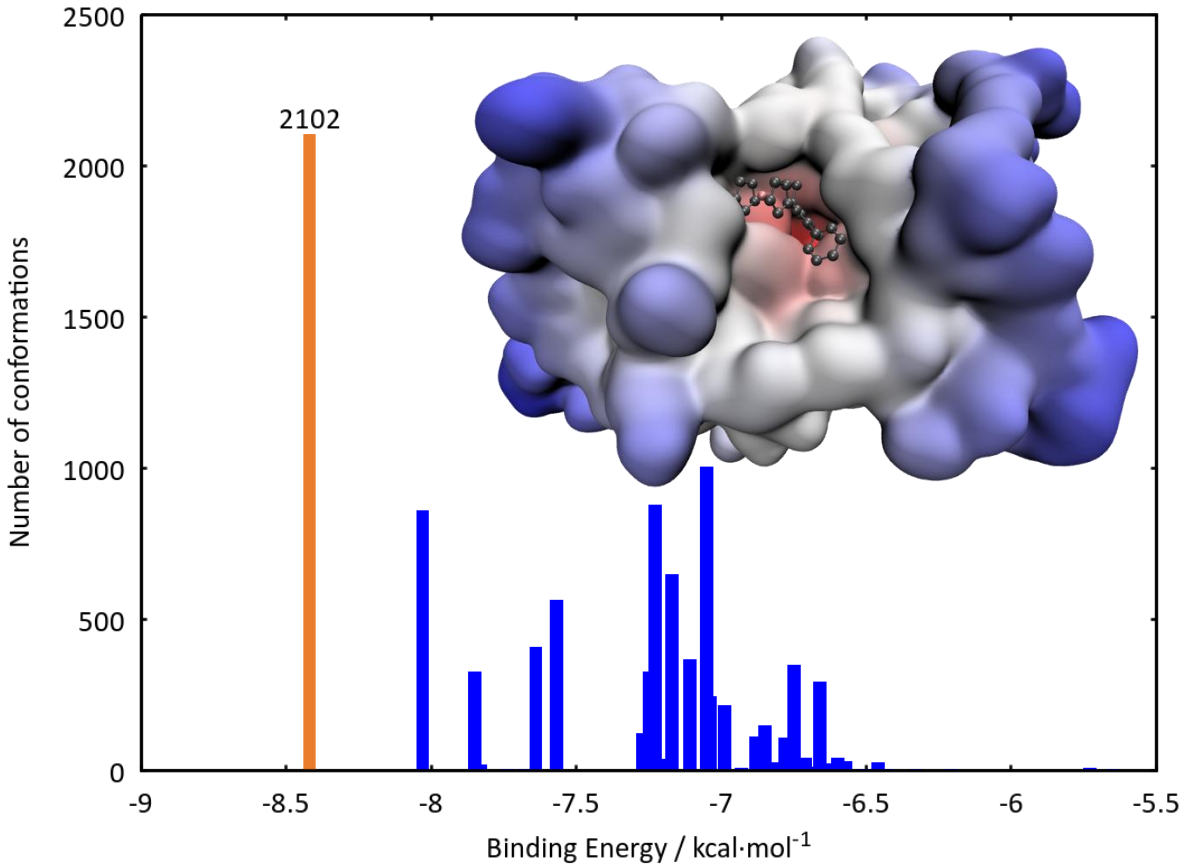

N.B. This **clustered distribution** is considered to be a **well clustered** distribution. It shows **44 clusters containing less than 100 poses** (1 % of the total number of poses), with a total of **6.29 % of the total number of poses classified into these low populated clusters**.

Figure S14. H-bonds (green dashed lines, distances in Å) and hydrophobic interactions (red arcs) between **(*R*)-P5-ind** and cathepsin B.

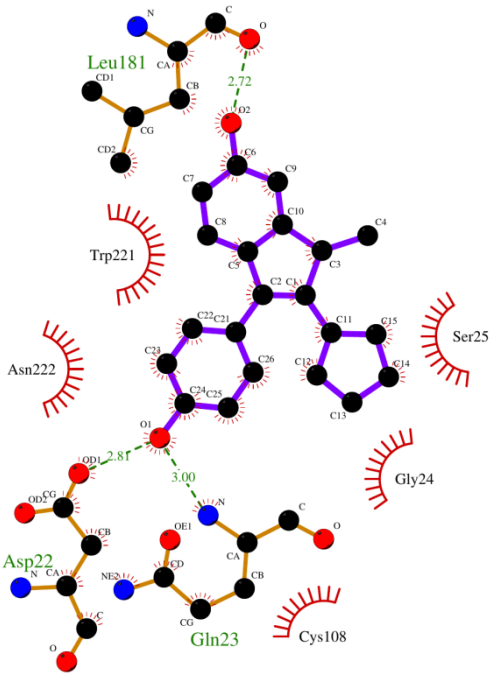

Figure S15. Other interactions (distances in Å) between **(*R*)-P5-ind** and cathepsin B.

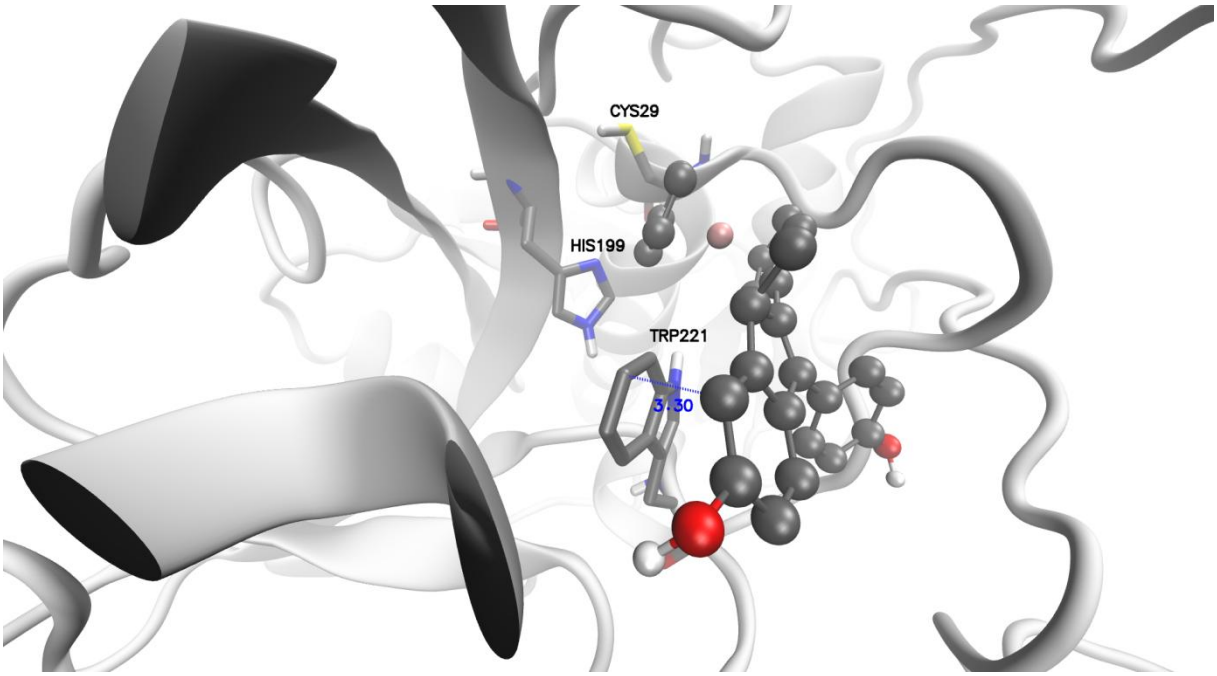

Figure S16. H-bonds (green dashed lines, distances in Å) and hydrophobic interactions (red arcs) between **(*S*)-P5-ind** and cathepsin B.

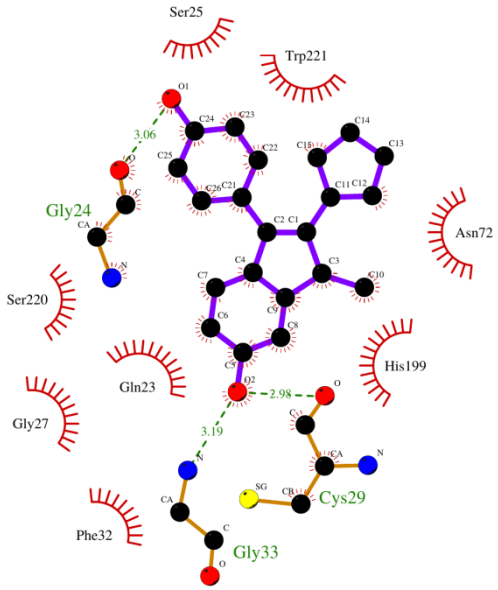

Figure S17. Other interactions (distances in Å) between **(*S*)-P5-ind** and cathepsin B.

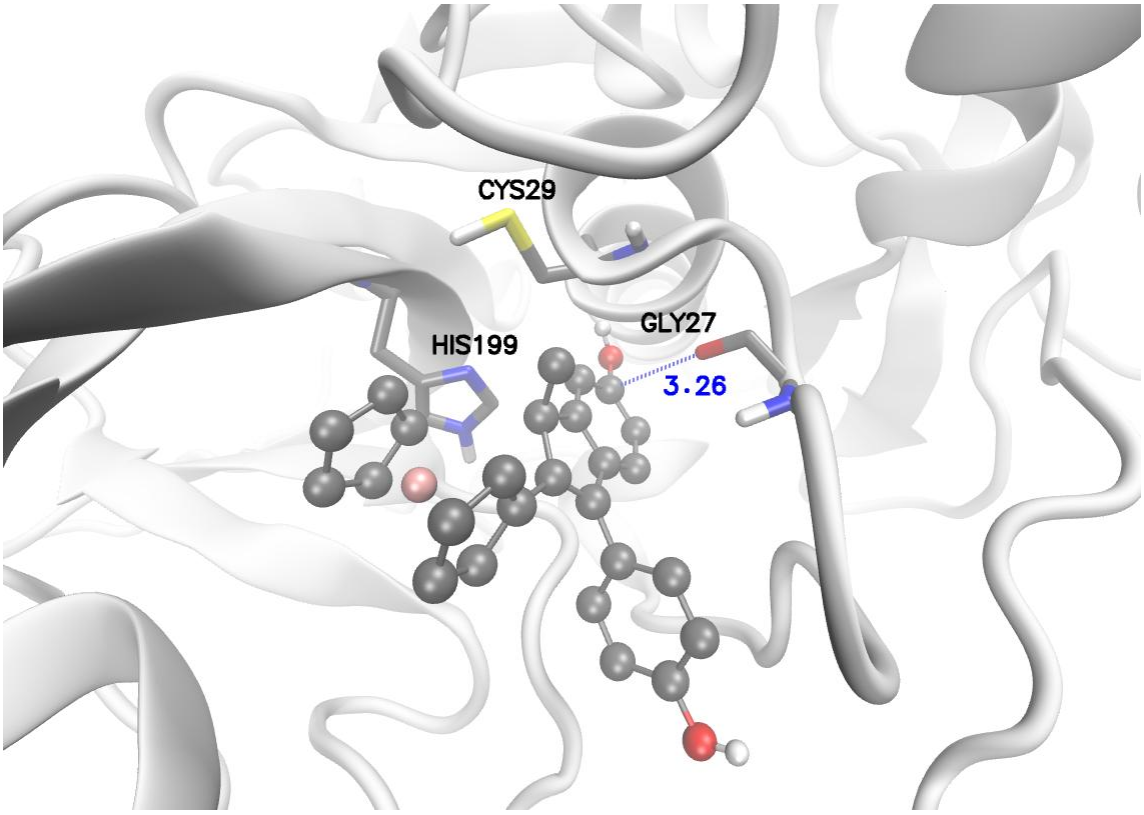

Figure S18. H-bonds (green dashed lines, distances in Å) and hydrophobic interactions (red arcs) between **(*R*)-P15-ind** and cathepsin B.

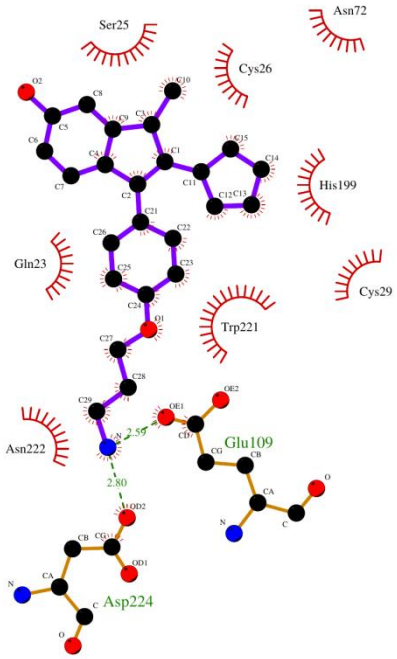

Figure S19. Other interactions (distances in Å) between **(*R*)-P15-ind** and cathepsin B.

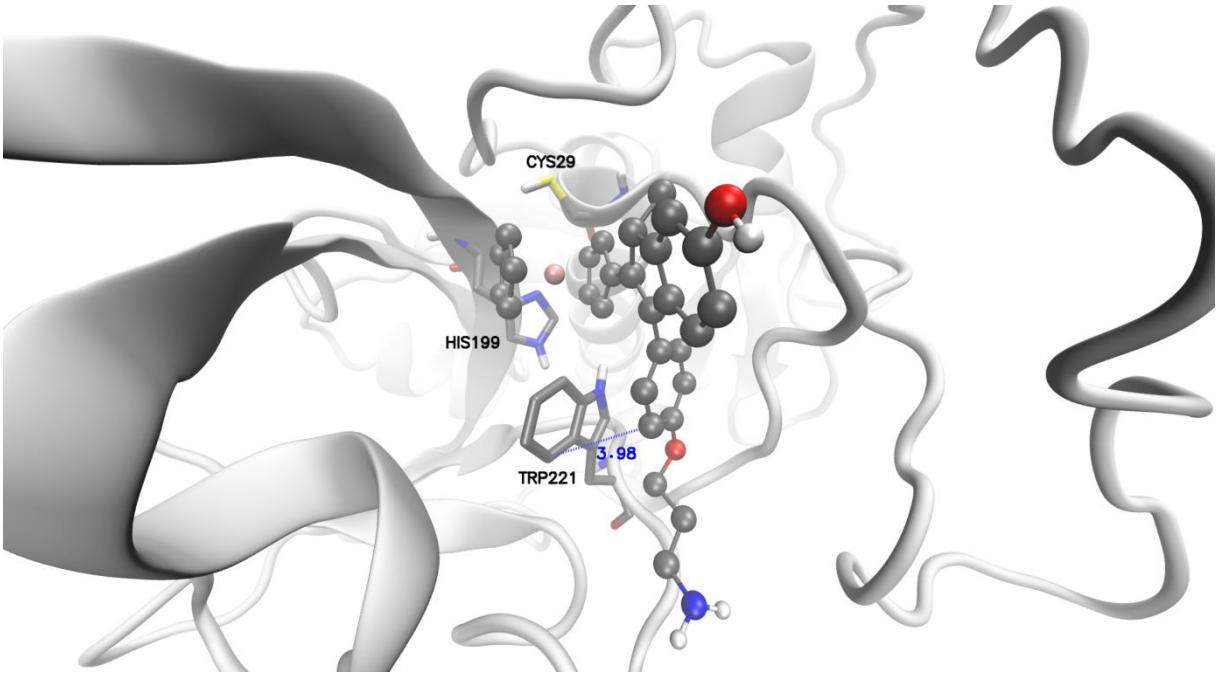

Figure S20. H-bonds (green dashed lines, distances in Å) and hydrophobic interactions (red arcs) between **(*S*)-P15-ind** and cathepsin B.

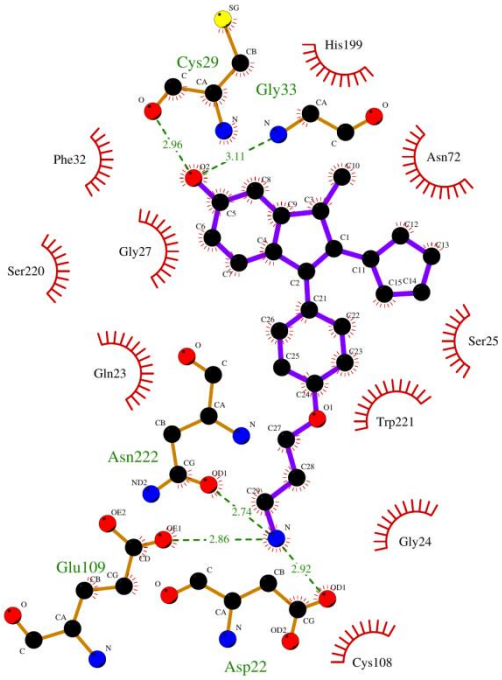

Figure S21. Other interactions (distances in Å) between **(*S*)-P15-ind** and cathepsin B.

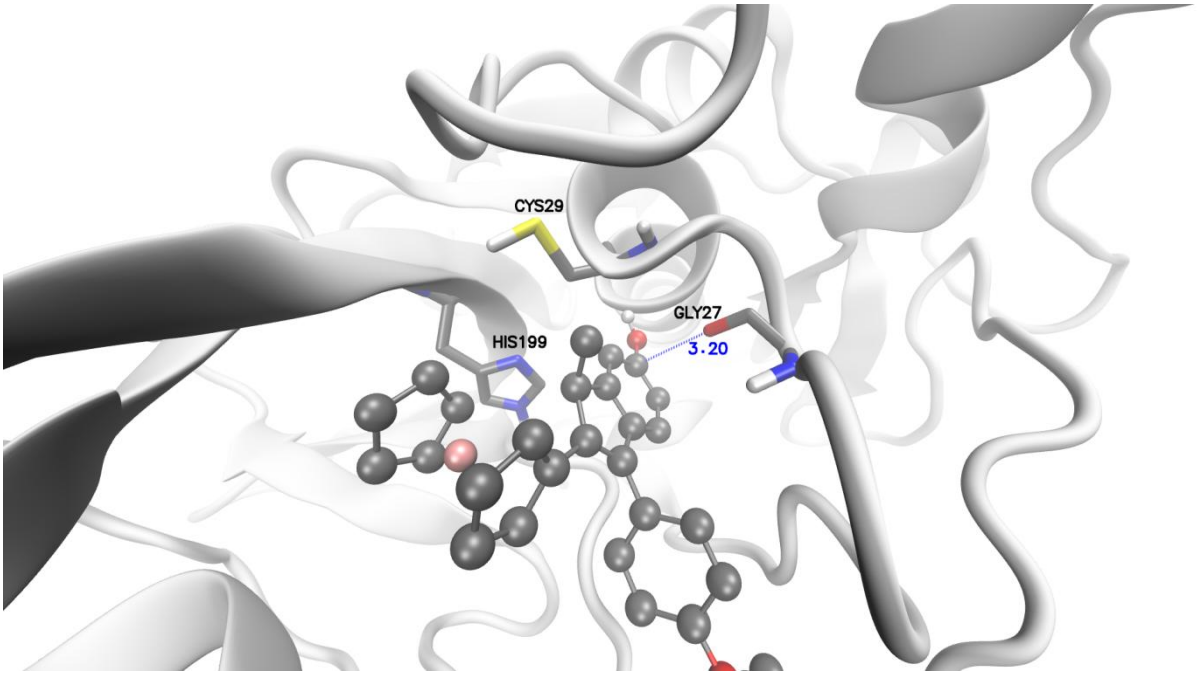

Figure S22. H-bonds (green dashed lines, distances in Å) and hydrophobic interactions (red arcs) between **(*R*)-P85-ind** and cathepsin B.

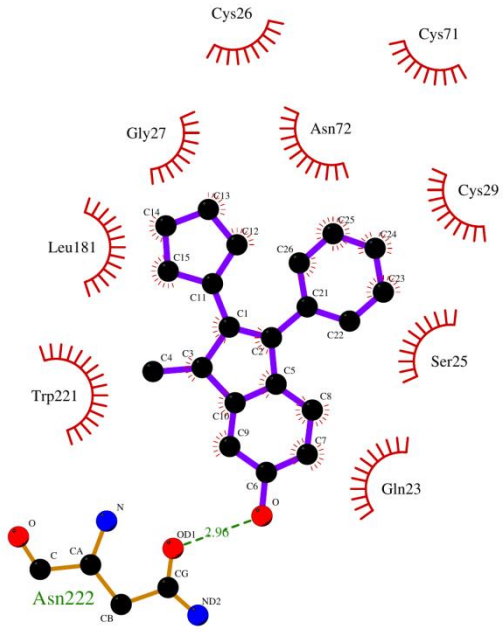

Figure S23. Other interactions (distances in Å) between **(*R*)-P85-ind** and cathepsin B.

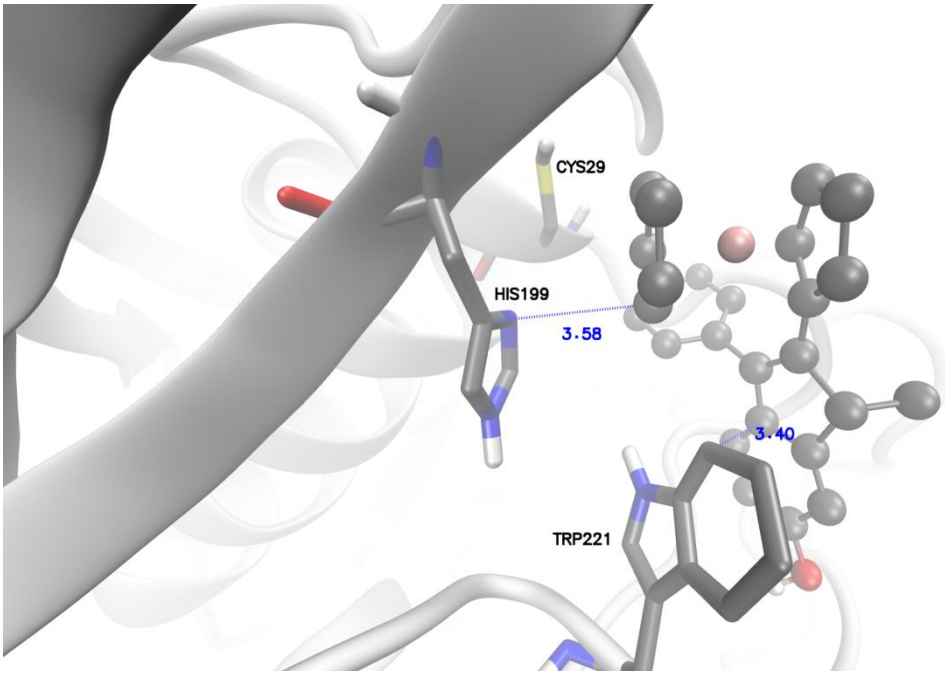

Figure S24. H-bonds (green dashed lines, distances in Å) and hydrophobic interactions (red arcs) between **(*S*)-P85-ind** and cathepsin B.

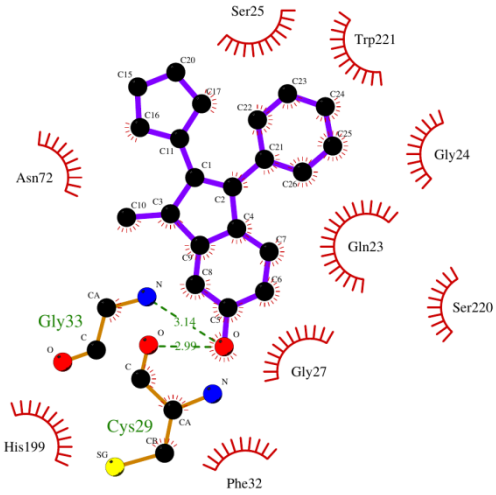

Figure S25. Other interactions (distances in Å) between **(*S*)-P85-ind** and cathepsin B.

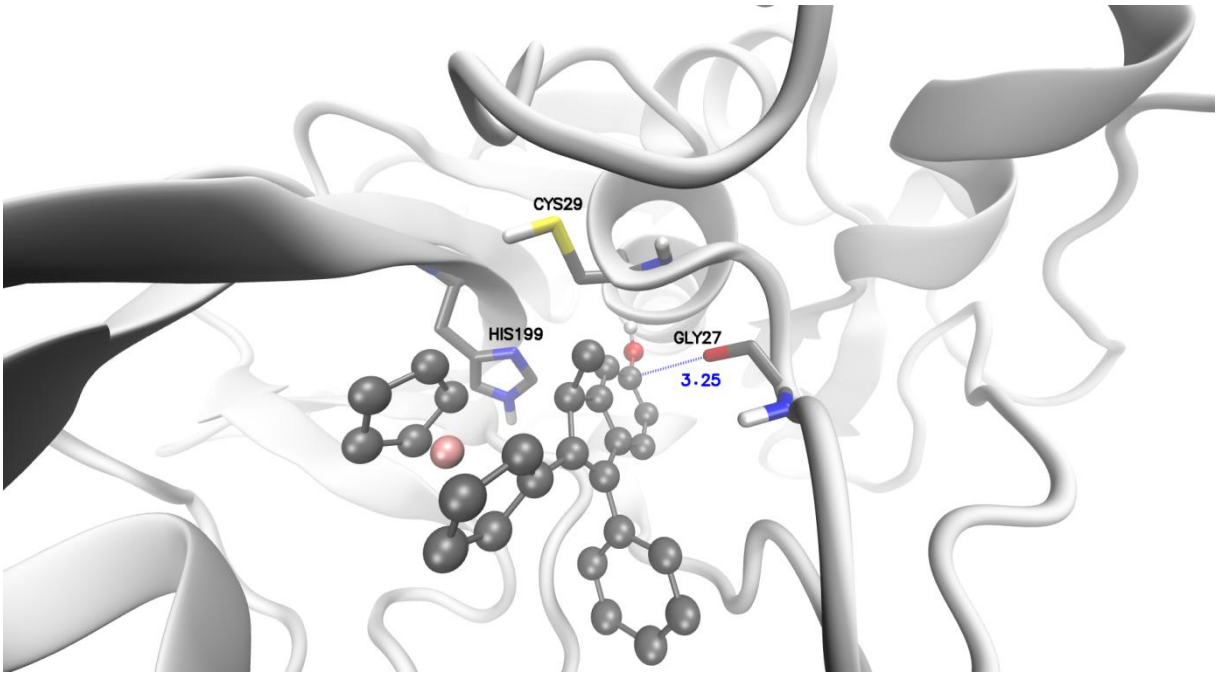

Figure S26. H-bonds (green dashed lines, distances in Å) and hydrophobic interactions (red arcs) between **(*R*)-P722-ind** and cathepsin B.

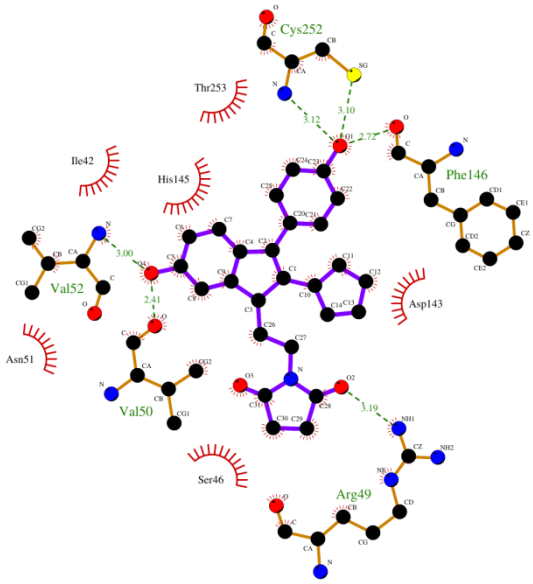

Figure S27. H-bonds (green dashed lines, distances in Å) and hydrophobic interactions (red arcs) between **(*S*)-P722-ind** and cathepsin B.

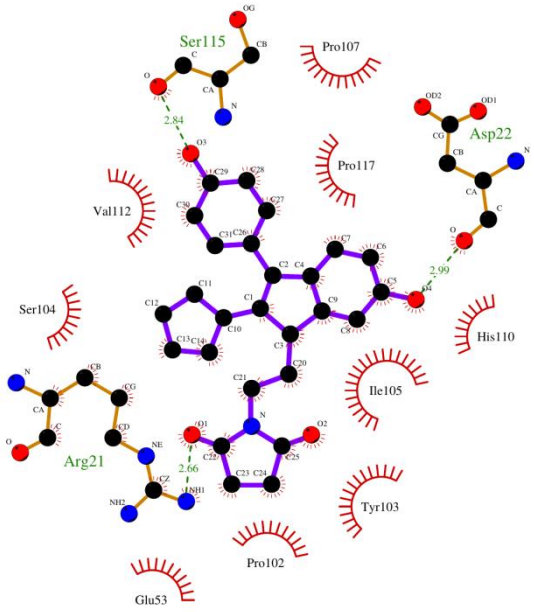

Figure S28. H-bonds (green dashed lines, distances in Å) and hydrophobic interactions (red arcs) between **P15** and cathepsin B.

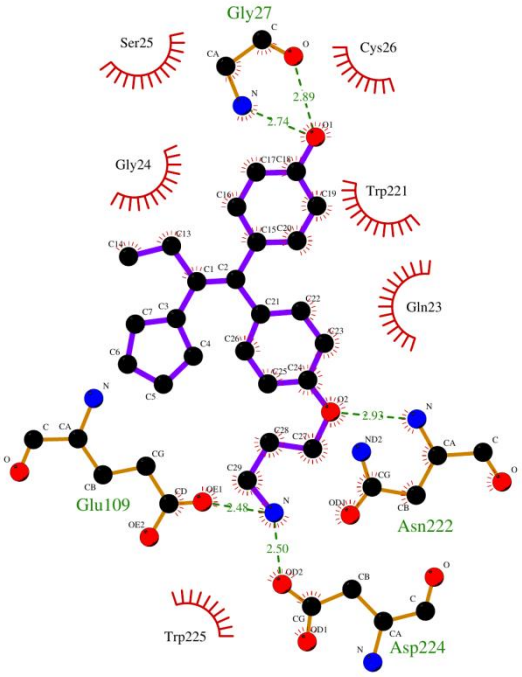

Figure S29. Other interactions (distances in Å) between **P15** and cathepsin B.

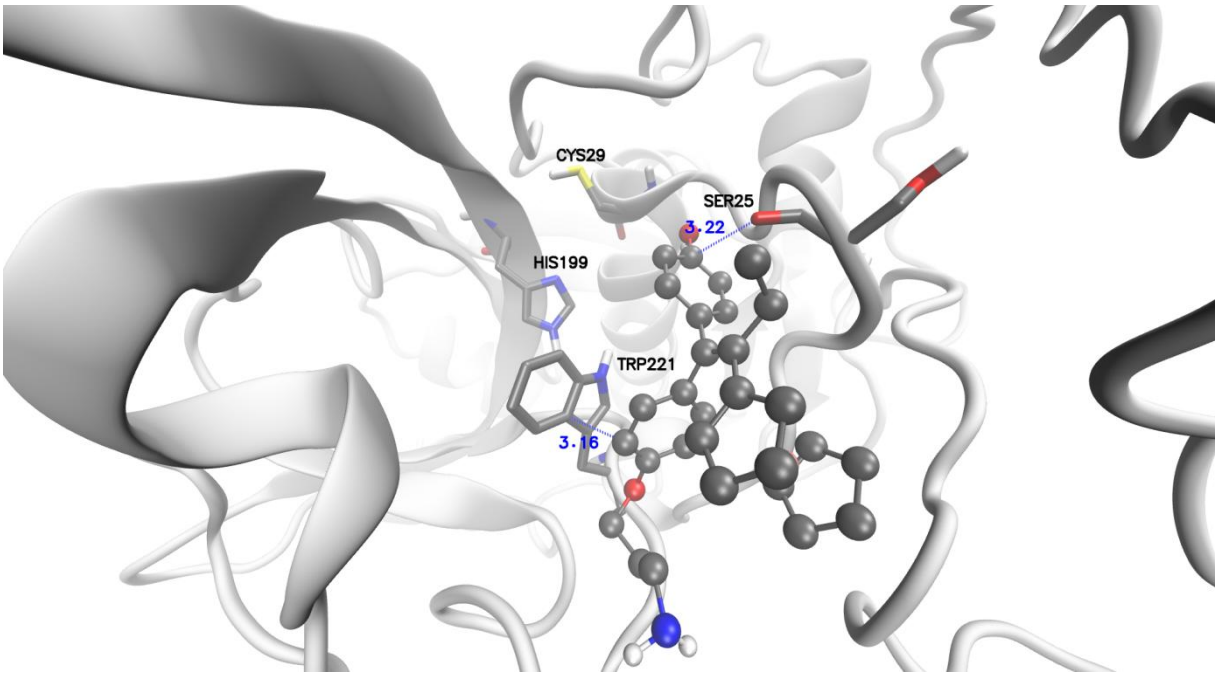

Figure S30. H-bonds (green dashed lines, distances in Å) and hydrophobic interactions (red arcs) between **P85** and cathepsin B.

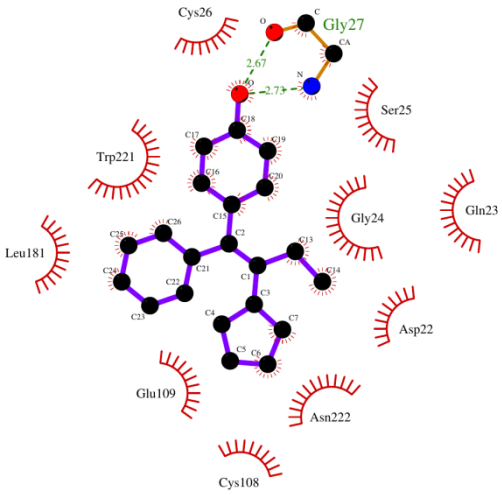

Figure S31. Other interactions (distances in Å) between **P85** and cathepsin B.

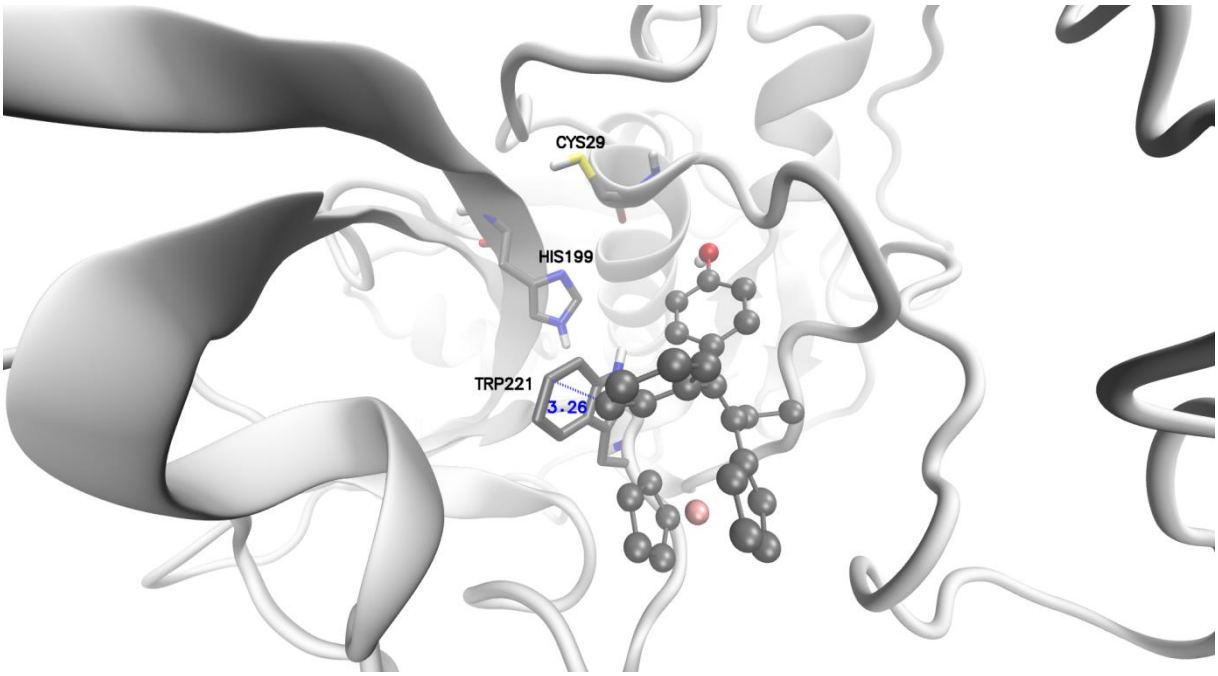

Figure S32. H-bonds (green dashed lines, distances in Å) and hydrophobic interactions (red arcs) between **P85-QM** and cathepsin B.

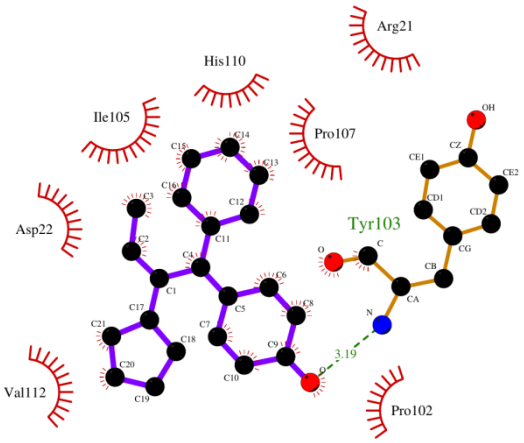

Figure S33. H-bonds (green dashed lines, distances in Å) and hydrophobic interactions (red arcs) between **(*R*)-P35-ind** and cathepsin B.

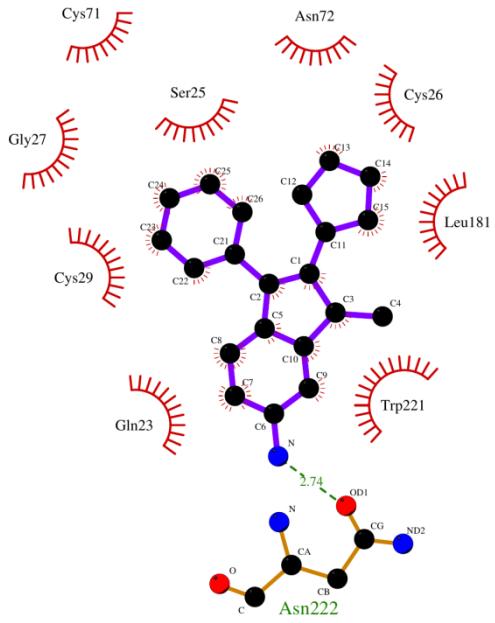

Figure S34. Other interactions (distances in Å) between **(*R*)-P35-ind** and cathepsin B.

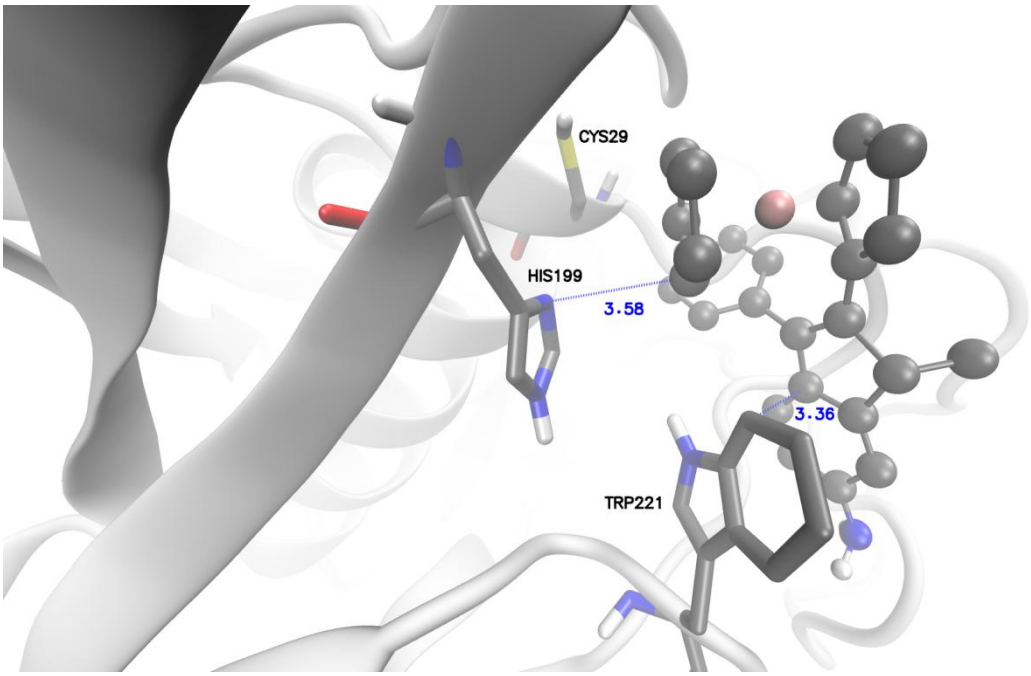

Figure S35. H-bonds (green dashed lines, distances in Å) and hydrophobic interactions (red arcs) between **(*S*)-P35-ind** and cathepsin B.

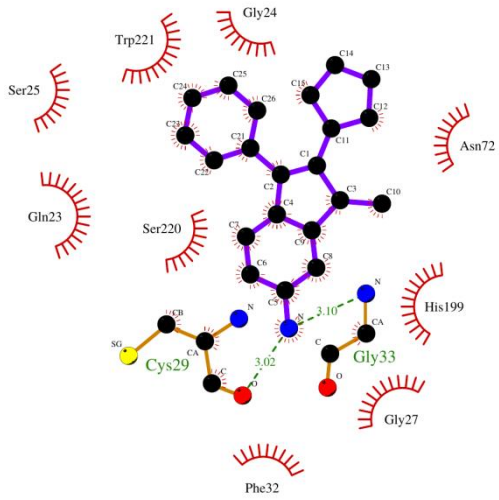

Figure S36. Other interactions (distances in Å) between **(*S*)-P35-ind** and cathepsin B.

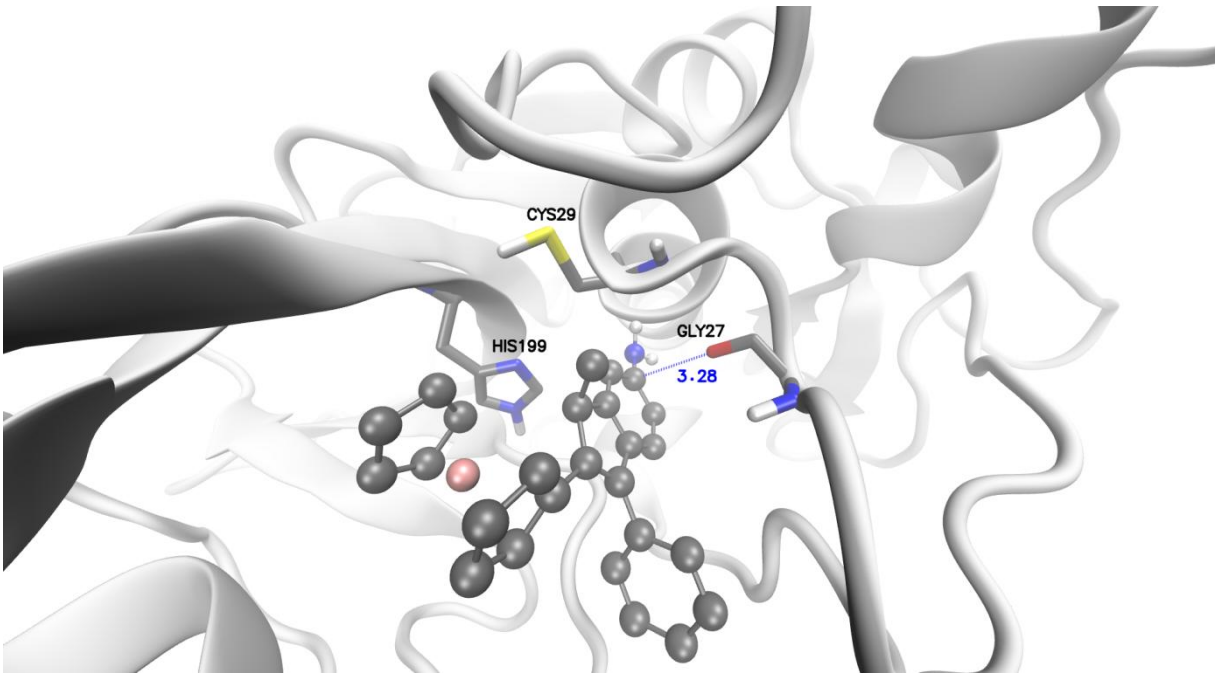

Figure S37. Docked conformations of **(*R*)- P35-ind** (in blue) *vs.* **(*R*)-P85-ind** (in red) (left) and **(*S*)- P35-ind** (in blue) *vs.* **(*S*)-P85-ind** (in red) (right) inside the cathepsin B main binding site (the "non-polar" hydrogen atoms are not represented).

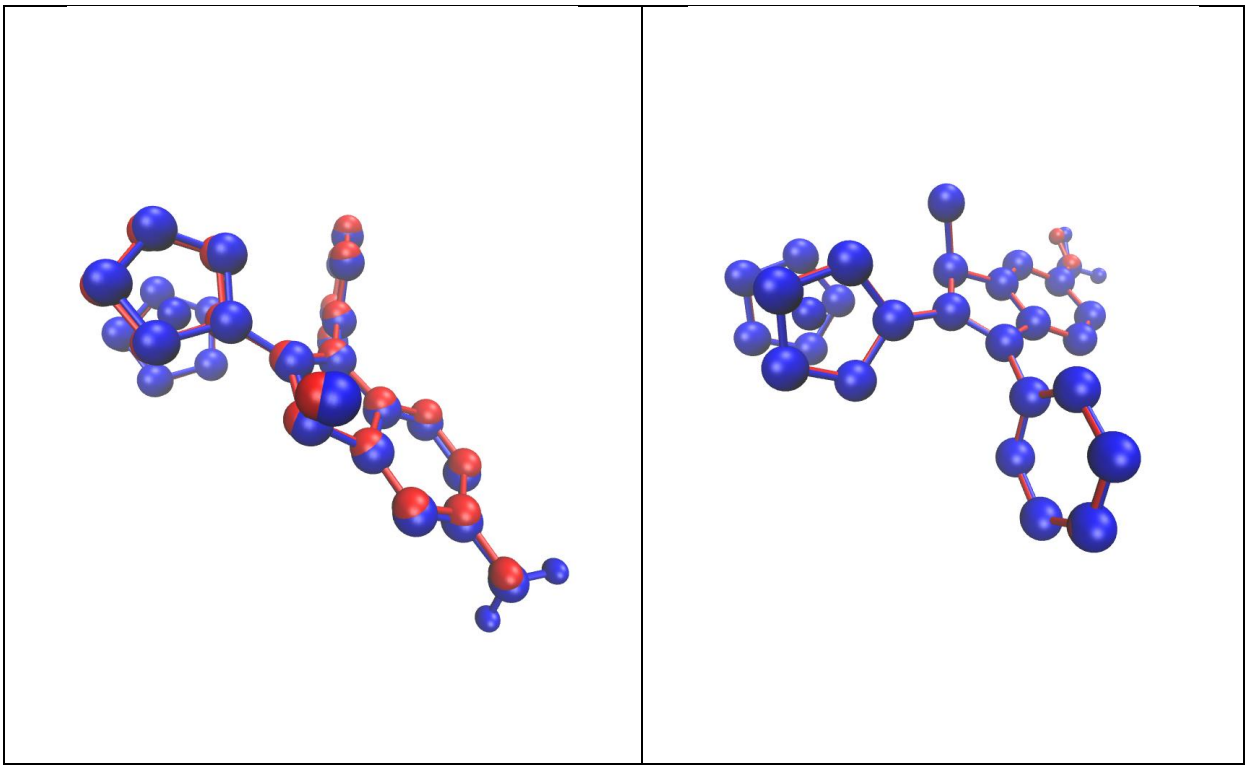

Figure S38. Inhibition curves of cathepsin B by (A) **P85-ind** and (B) **P5-ind**. Substrate = Z-Lys-ONp

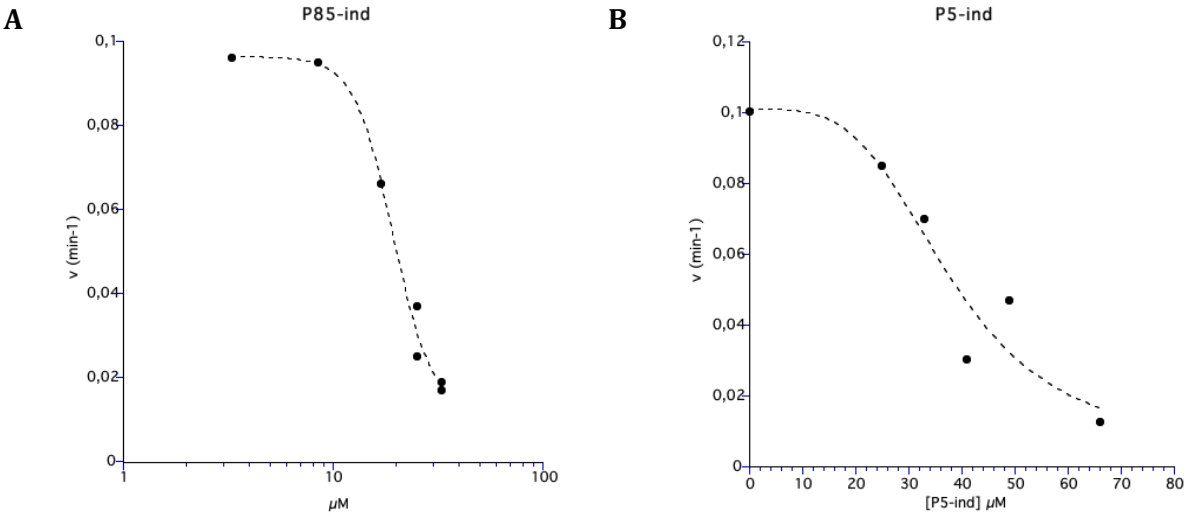

Figure S39. Inhibition curves of cathepsin B by (A) **P85-ind** and (B) **P5-ind**. Substrate = Z-Arg-Arg-AMC

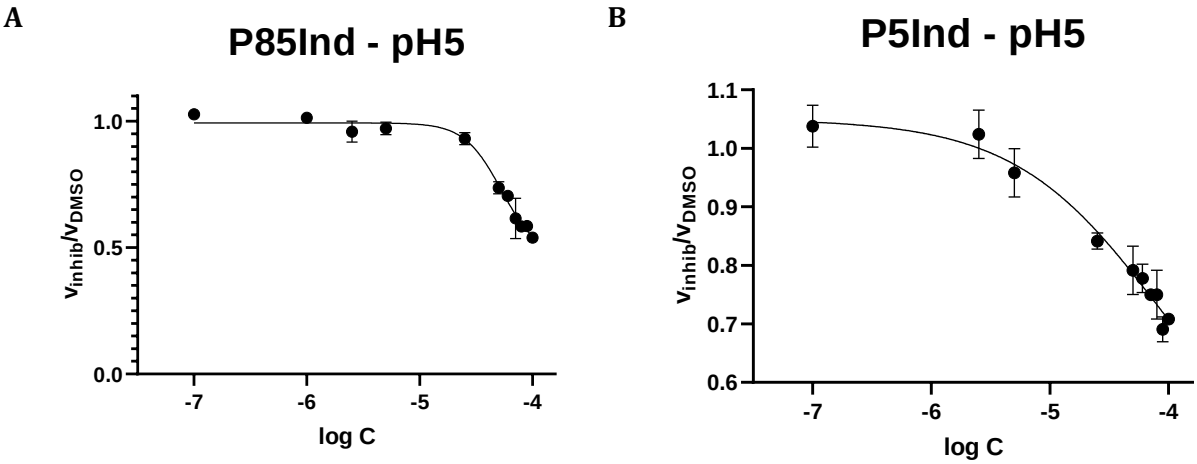

Figure S40. ^{1}H NMR spectrum of **P722-ind** in acetone-d_6

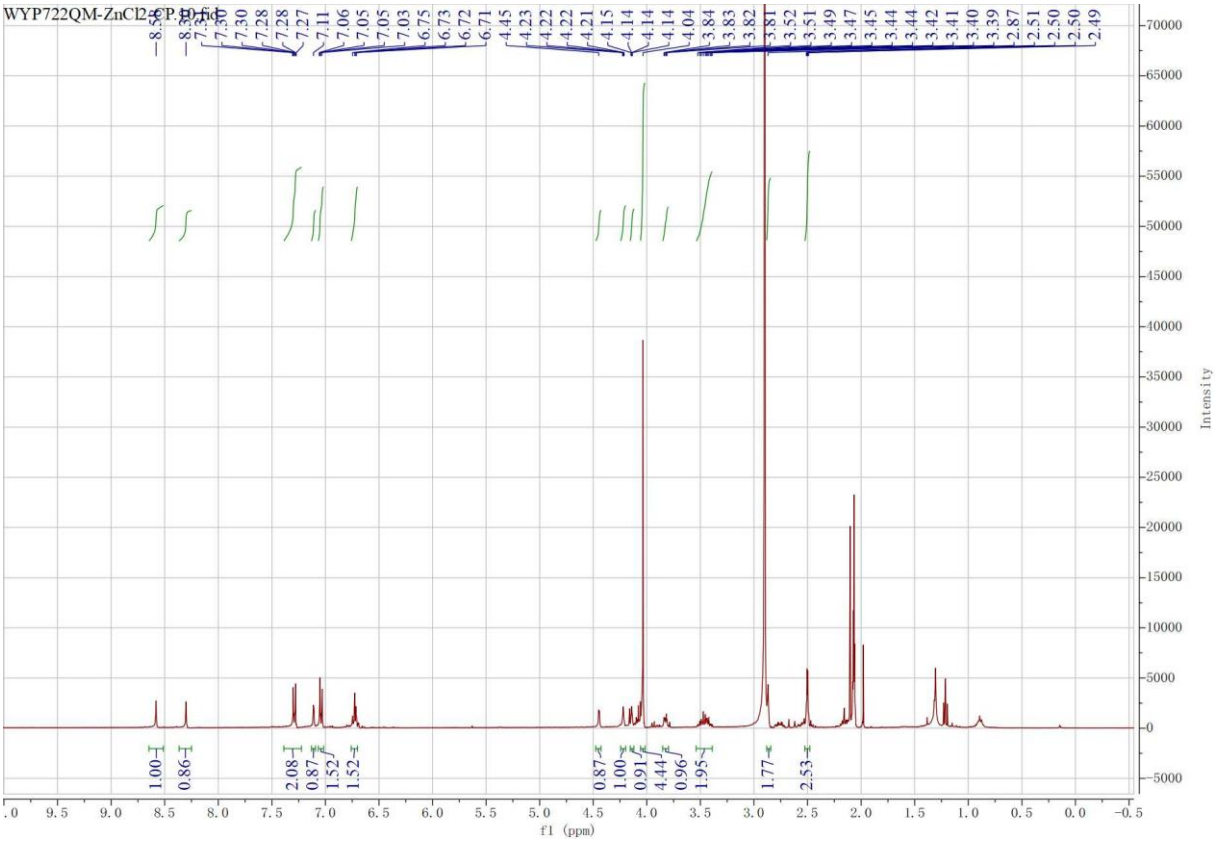

Figure S41. Two-dimensional NMR spectrum (COSY) of racemic **P722-Ind** in acetone-d_6 (MestReNova V14). This spectrum was recorded 6-7 h after sample preparation. Small signals at the base of the main peaks are indicative of the beginning of compound degradation.

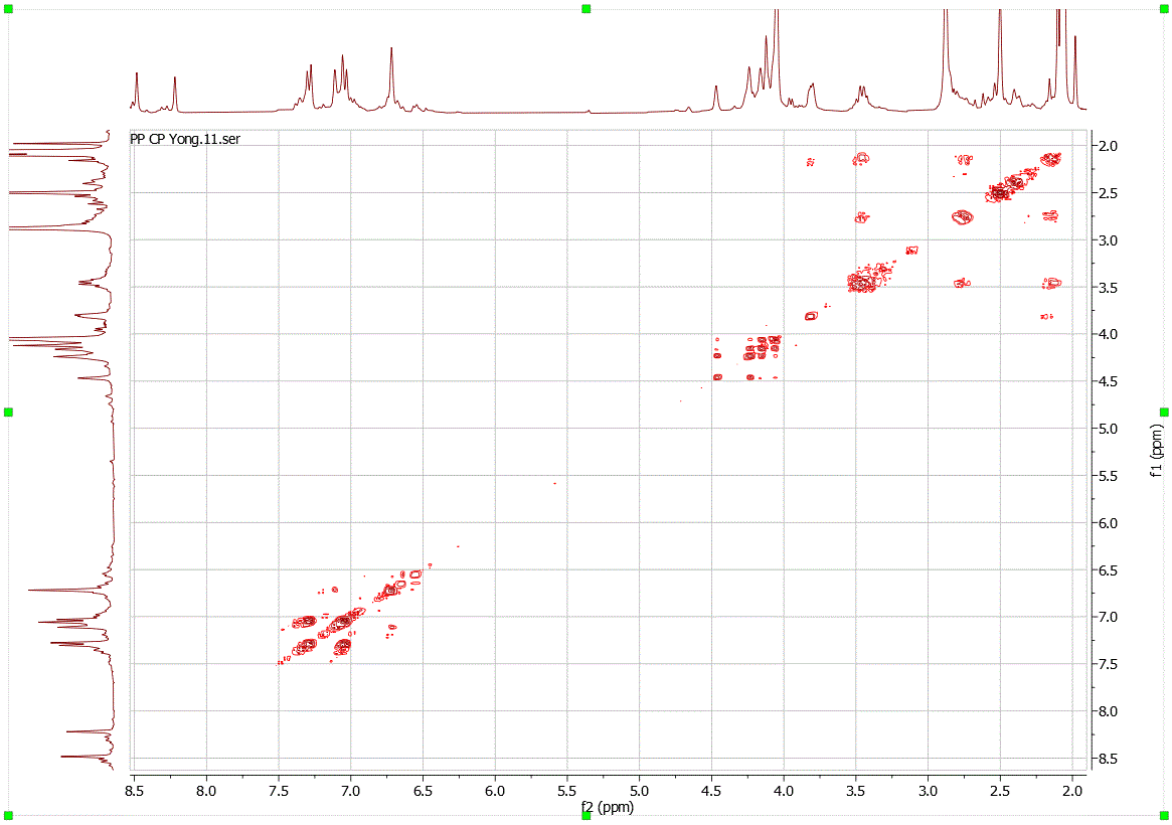

Figure S42. ^{13}C NMR spectrum of **P722-ind** in acetone-d_6

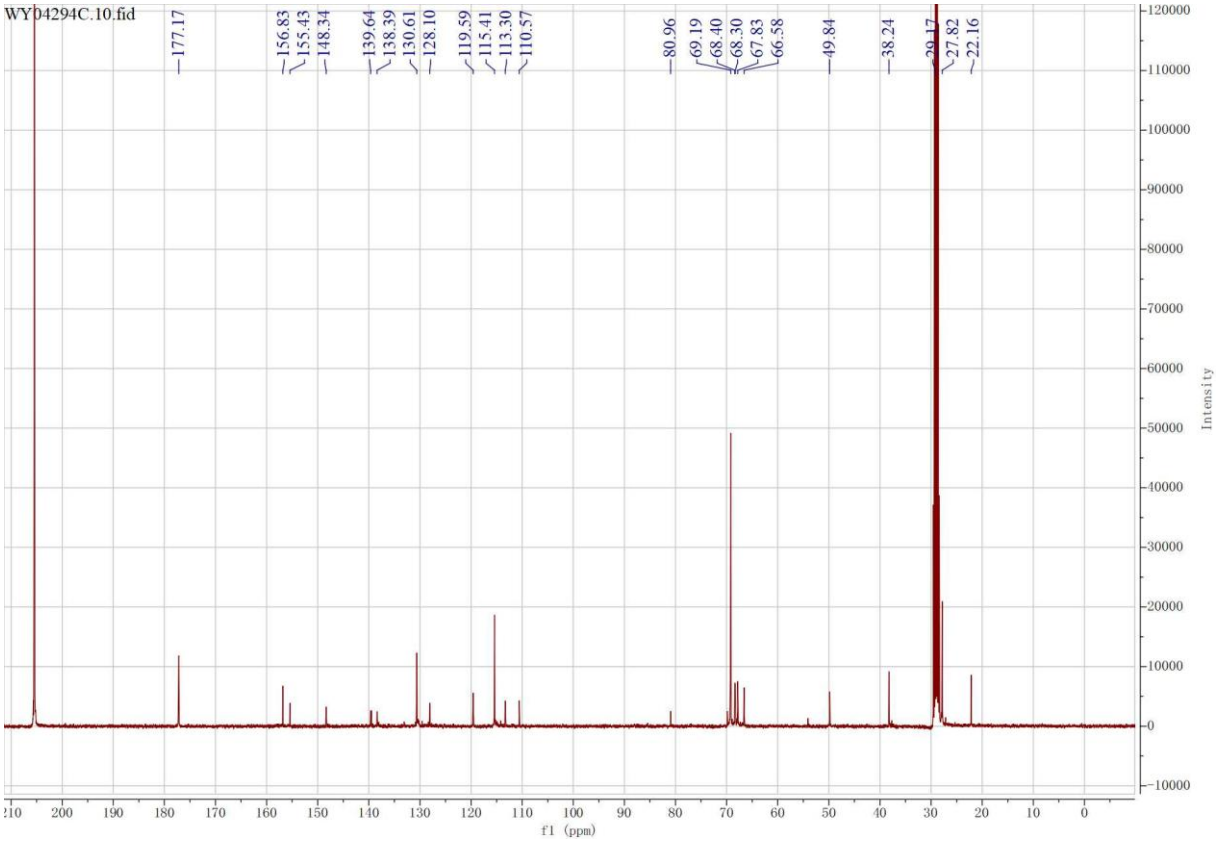

References

(1) Frisch M. J., et al. *Gaussian 16*; Gaussian, Inc.: Wallingford, CT, 2017.

(2) Lee, C.; Yang, W.; Parr, R. G. Development of the Colle-Salvetti Correlation-Energy Formula into a Functional of the Electron Density. *Physical Review B* **1988**, *37* (2), 785.

(3) Becke, A. D. Density-Functional Thermochemistry. III. The Role of Exact Exchange. *The Journal of Chemical Physics* **1993**, *98* (7), 5648. https://doi.org/10.1063/1.464913.

(4) Grimme, S.; Ehrlich, S.; Goerigk, L. Effect of the Damping Function in Dispersion Corrected Density Functional Theory. *J. Comput. Chem.* **2011**, *32* (7), 1456–1465. https://doi.org/10.1002/jcc.21759.

(5) Hehre, W. J.; Ditchfield, R.; Pople, J. A. Self—Consistent Molecular Orbital Methods. XII. Further Extensions of Gaussian—Type Basis Sets for Use in Molecular Orbital Studies of Organic Molecules. *The Journal of Chemical Physics* **1972**, *56* (5), 2257–2261. https://doi.org/10.1063/1.1677527.

(6) Hariharan, P. C.; Pople, J. A. The Influence of Polarization Functions on Molecular Orbital Hydrogenation Energies. *Theoret. Chim. Acta* **1973**, *28* (3), 213–222. https://doi.org/10.1007/BF00533485.

(7) Francl, M. M.; Pietro, W. J.; Hehre, W. J.; Binkley, J. S.; Gordon, M. S.; DeFrees, D. J.; Pople, J. A. Self-consistent Molecular Orbital Methods. XXIII. A Polarization-type Basis Set for Second-row Elements. *The Journal of Chemical Physics* **1982**, *77* (7), 3654–3665. https://doi.org/10.1063/1.444267.

(8) Dunning, T. H.; Hay, P. J. *Modern Theoretical Chemistry*; Schaefer, H. F., Ed.; Plenum: New York, 1977.

(9) Hay, P. J.; Wadt, W. R. *Ab Initio* Effective Core Potentials for Molecular Calculations. Potentials for K to Au Including the Outermost Core Orbitals. *The Journal of Chemical Physics* **1985**, *82* (1), 299–310. https://doi.org/10.1063/1.448975.

(10) Berendsen, H. J. C.; van der Spoel, D.; van Drunen, R. GROMACS: A Message-Passing Parallel Molecular Dynamics Implementation. *Computer Physics Communications* **1995**, *91* (1–3), 43–56. https://doi.org/10.1016/0010-4655(95)00042-E.

(11) Abraham, M. J.; Murtola, T.; Schulz, R.; Páll, S.; Smith, J. C.; Hess, B.; Lindahl, E. GROMACS: High Performance Molecular Simulations through Multi-Level Parallelism from Laptops to Supercomputers. *SoftwareX* **2015**, *1–2*, 19–25. https://doi.org/10.1016/j.softx.2015.06.001.

(12) Oostenbrink, C.; Villa, A.; Mark, A. E.; Van Gunsteren, W. F. A Biomolecular Force Field Based on the Free Enthalpy of Hydration and Solvation: The GROMOS Force-Field Parameter Sets 53A5 and 53A6. *Journal of Computational Chemistry* **2004**, *25* (13), 1656–1676. https://doi.org/10.1002/jcc.20090.

(13) Berendsen, H. J. C.; Postma, J. P. M.; Van Gunsteren, W. F.; Hermans, J. Intermolecular Forces; Pullman, B., Ed.; Reidel: Dordrecht: The Netherlands, 1981; pp 331–342.

(14) Lemak, A. S.; Balabaev, N. K. On The Berendsen Thermostat. *Molecular Simulation* **1994**, *13* (3), 177–187. https://doi.org/10.1080/08927029408021981.

(15) Rahman, A.; Stillinger, F. H. Molecular Dynamics Study of Liquid Water. *The Journal of Chemical Physics* **1971**, *55* (7), 3336–3359. https://doi.org/10.1063/1.1676585.

(16) Parrinello, M.; Rahman, A. Polymorphic Transitions in Single Crystals: A New Molecular Dynamics Method. *Journal of Applied Physics* **1981**, *52* (12), 7182–7190. https://doi.org/10.1063/1.328693.

(17) Darden, T.; York, D.; Pedersen, L. Particle Mesh Ewald: An $N \cdot \log(N)$ Method for Ewald Sums in Large Systems. *The Journal of Chemical Physics* **1993**, *98* (12), 10089–10092. https://doi.org/10.1063/1.464397.

(18) Essmann, U.; Perera, L.; Berkowitz, M. L.; Darden, T.; Lee, H.; Pedersen, L. G. A Smooth Particle Mesh Ewald Method. *The Journal of Chemical Physics* **1995**, *103* (19), 8577–8593. https://doi.org/10.1063/1.470117.

(19) Chang, M. W.; Belew, R. K.; Carroll, K. S.; Olson, A. J.; Goodsell, D. S. Empirical Entropic Contributions in Computational Docking: Evaluation in APS Reductase Complexes. *Journal of Computational Chemistry* **2008**, *29* (11), 1753–1761. https://doi.org/10.1002/jcc.20936.
(20) Fuentes-Prior, P.; S. Salvesen, G. The Protein Structures That Shape Caspase Activity, Specificity, Activation and Inhibition. *Biochem. J.* **2004**, *2* (384), 201–232.
(21) Domsalla, A.; Melzig, M. F. Occurrence and Properties of Proteases in Plant Latices. *Planta Med.* **2008**, *74* (07), 699–711. https://doi.org/10.1055/s-2008-1074530.